Control Design of Active Magnetic Bearings for Rotors Subjected to Destabilising Seal Forces - Theory & Experiment

Lauridsen, Jonas Skjødt; Santos, Ilmar

Publication date:
2017

Document Version
Publisher's PDF, also known as Version of record

Control Design of Active Magnetic Bearings for Rotors Subjected to Destabilising Seal Forces

Theory & Experiment

Jonas Lauridsen

Technical University of Denmark
Kgs. Lyngby, Denmark, 2017

English title of the thesis:
Control Design of Active Magnetic Bearings for Rotors Subjected to Destabilising Seal Forces
– Theory & Experiment

Afhandlingens danske titel:
Reguleringsdesign af Aktive Magnetiske Lejer for Rotorer Udsat for Destabiliserende Tætningskræfter
– Teori og Eksperiment

PhD Student:
Jonas Lauridsen
jonlau@mek.dtu.dk
ORCID: 0000-0002-9345-8541

Supervisor:
Ilmar Ferreira Santos
ifs@mek.dtu.dk
ORCID: 0000-0002-8441-5523

Technical University of Denmark
Department of Mechanical Engineering
Section of Solid Mechanics
Nils Koppels Allé, Building 404
DK-2800 Kgs. Lyngby
Denmark
Phone: (+45) 45 25 25 25
Email: info@mek.dtu.dk
www.mek.dtu.dk

DCAMM Special Report no.: S225
ISBN: 87–7475–490–4 978–87–7475–490–9

Summary (English)

The use of Active Magnetic Bearings (AMBs) in industrial applications has increased over recent decades as the technology has grown more mature, further aided by advancements and decreasing prices of the electronic components. AMBs are well suited to turbo-machinery applications offering several advantages over traditional types of bearings, including: no mechanical contact, no lubrication, low maintenance, low vibration level, high rotational speed and low energy consumption. These advantages make AMBs especially useful in challenging environments, for instance in subsea turbomachinery applications for oil and gas production, where reliability, low maintenance and high speed are of great importance.

Annular seals are a key component in turbomachinery. They prevent internal flow leakage from high pressure to low pressure regions and improve the overall machine efficiency; in many applications, however, they also affect the system rotor-dynamic properties significantly. For this reason, the seal characteristics must be included in the rotor-dynamic stability analysis. Unfortunately, in many cases the seal forces are hard to model due to complex geometries of the seal and multiphase fluids. At present, there is no generally accepted method for determination of dynamic seal forces. Therefore, large uncertainties must be expected when modelling dynamic seal forces and consequently also in rotor-dynamic stability analysis.

This thesis focuses on i) closed loop identification of uncertain AMB parameters, ii) closed loop identification of unknown stiffness and damping coefficients of a dynamic seal model and iii) the design of AMB controllers to handle dynamic seal forces. Controllers that can guarantee stability and performance in the presence of uncertain seal forces are of special interest. The main original contribution of the thesis is the framework for design of model based controllers for AMB systems subjected to uncertain and changing dynamic seal forces. An identification method has been developed, and experimentally validated, to obtain precise models of Linear Fractional Transformation (LFT) form for synthesising $\mathscr{H}_\infty$, μ and Linear Parameter Varying (LPV) controllers. The seal parameters and AMB dynamics are identified on-site without any need of special equipment.

A perturbed model of the combined AMB, rotor and seal system is constructed using Finite Element Methods (FEM), modal reduction and LFT. It describes the dynamic behaviour due to parametric uncertainties/changes of the damping and stiffness coefficients of the seal and the uncertainties in the stiffness of the AMBs. Using different types of excitation signals, i.e. stepped sine, impulse and Pseudo Random Binary Sequence (PRBS), and optimisation in the time domain, the above mentioned parameters are

identified. Inserting the identified parameters in the known model structure results in accurate models, which - when simulated - fit experimental data well. The perturbed model is further used for the robust controller synthesis to describe the uncertainties in seal forces and for LPV control synthesis, to compensate for known changes in seal forces due to changes in operating conditions.

A rotor dynamic test facility with a rigid rotor, two radial AMBs and one annular test seal is used for i) closed loop identification of parameters in the AMB-rotor model, ii) identification of dynamic seal forces, iii) implementation of AMB controllers to compensate for dynamic seal forces. The stability and performance of the designed controllers are examined and compared to a reference decentralised PID controller. Controllers based on identified nominal seal models are shown to provide good compensation for the destabilising dynamic seal forces. Furthermore, significant performance improvement is shown when using a robust controller, which can handle changes in operational pressures better, in comparison to a nominal model based controller. Simulations using both type of model based controllers match experiments well.

Resumé (Dansk)

Anvendelsen af aktive magnetlejer (AMB) er steget over de seneste årtier efterhånden som teknologien er modnet og de elektriske komponenter er blevet billigere og bedre. AMB'erne er velegnet til blandet andet turbo-maskiner grundet deres mange fordele som ingen mekanisk kontakt, intet smøringsbehov, lave vedligeholdelsesomkoster, små vibrationer, høj rotationshastighed og lavt energiforbrug. Disse fordele gør AMB'er særdeles brugbare til udfordrende applikationer som f.eks. undersøisk turbomaskiner for olie- og gas produktion, hvor pålidelighed, lav vedligehold og høj hastighed er afgørende.

Tætninger er en nøglekomponent i turbomaskiner. De forhindrer intern flow-lækage fra højtryks til lavtryksområder for at forbedre den overordnede effektivitet. I mange applikationer påvirker de dog også de rotor-dynamiske egenskaber markant. Af den grund skal de inkluderes i den rotor-dynamiske stabilitetsanalyse. Tætningskræfterne er i mange tilfælde svære at modellere grundet blandt andet komplekse geometrier af tætningerne og multifase-flow. I øjeblikket findes der ingen generel accepteret metode til at bestemme dynamiske tætningskræfter. Store usikkerheder må derfor forventes ved modellering af dynamisk tætningskræfter og som følge deraf også i den rotor-dynamiske stabilitets-analyse.

Denne afhandling har fokus på i) lukket-sløjfe identifikation af usikre AMB-parametre, ii) lukket-sløjfe identifikation af ukendte stivheds- and dæmpningskoefficienter af en dynamisk tætningsmodel og iii) design af AMB-regulatorer til at håndtering af usikre tætningskræfter. Regulatorer der kan garantere stabilitet og performance mod usikre tætningskræfter er i hovedfokus.

Hovedbidraget består i et framework til design af modelbaseret regulatorer for AMB-systemer udsat for usikre og skiftende dynamiske tætningskræfter. En identifikationsmetode er blevet udviklet og eksperimentelt valideret til at opnå præcise modeller på LFT (Linear Fractional Transformation) form for design af $\mathscr{H}_\infty$, μ and LPV (Linear Parameter Varying) regulatorer. Tætningsparametrene er identificeret on-site uden brug af specialudstyr.

En perturberet model af det kombinerede AMB-rotor-tætningssystem er konstrueret ved brug af Finite Element Metoden (FEM), modal-reduktion og Linear Fractional Transformation (LFT). Den beskriver den dynamiske respons ved parametriske usikkerheder/ændringer af stivheds- og dæmpningskoefficienter af tætninger og usikkerheden i stivhederne af AMB'erme. Ved brug af forskellige typer excitations-signaler, dvs. stepped sinus og Pseudo Random Binary Signal (PRBS), og optimering i tidsdomæne, er de ovennævnte parametre identificeret. Indsættelse af de identificerede parametre i den

kendte modelstruktur resulterer i præcise modeller, som simuleret, stemmer overens med eksperimentel data. Den perturberede model er yderligere anvendt til at beskrive usikkerheder i tætningskræfterne til robust regulatorfremstilling og for Linear Parameter Varierende (LPV) regulatorfremstilling, til at kompensere for kendte ændringer i tætningsdynamikken som funktion af operationsbetingelserne.

Et rotor dynamisk test-facilitet bestående af en stiv rotor, to radielle AMB'er og en turbomaskine-tætning, er anvendt til i) lukket sløjfe identifikation af parametre i AMB-rotormodellen, ii) identifikation af dynamiske tætningskræfter, iii) implementering af AMB-regulatorer til kompensering for dynamiske tætningskræfter. Stabilitet og ydelse af de designede regulatorer er evalueret og sammenlignet i forhold til en decentraliseret PID referenceregulator. Regulatorer baseret på identificerede nominelle tætningsmodeller yder god kompensation for destabiliserende tætningskræfter. Yderligere kan en betydelig forbedring i performance ses for robuste regulatorer, der kan kompensere for ændringer i operationstryk bedre, sammenlignet med en nominel modelbaseret regulator. Simuleringer ved brug af begge typer regulatorer matcher eksperimentielle resultater.

Preface

This thesis is submitted as partial fulfilment of the requirements for obtaining the Danish PhD degree. The thesis is a summary of the work undertaken and a collection of three journal papers and two conference papers written during the PhD project between December 2013 and May 2017. The work has been carried out primarily at the Section of Solid Mechanics (FAM), Department of Mechanical Engineering (MEK), Technical University of Denmark (DTU). The work was funded by Siemens Turbomachinary Equipment GmbH and DTU.

This project was supervised by Ilmar F. Santos. His passion for the work he is doing, his drive and energy have been a strong motivation and inspiration for my PhD work.

Thanks to my closest collagues at DTU Mechanical and Electrical Engineering, Andreas J. Voigt, Alejandro V. Cerda, Bo B. Nielsen, Søren Enemark, Nikolaj A. Dagnæs-Hansen, Sebastian von Osmanski, Lukas R. S. Theisen, André Sekunda, Jorge A. G. Salazar, Alejandro de M. Tejada, Cesar A. L. L. da Fonseca, Geraldo F. de S. Rebouças, Christian Kim Christiansen, Christian Mandrup-Poulsen, Fabián G.P. Vásquez, Hannibal T. Overgaard, Simon D. Larsen, Mikael M. Eronen and Thomas T. Paulsen for hours spent at the office exchanging ideas and knowledge, and for having a lot of fun. A special thanks goes to Jon S. Larsen employed at Siemens Turbomachinery Equipment A/S for initiating and seeking money for this project and thus making this PhD possible.

A part of the research project was carried out at the University of Bath, UK. In this regard I thank especially professor Patrick Keogh and Chris Lusty for being met with open arms and for hours of technical discussions.

I would also like to thanks the masters students whom I have co-supervised during the PhD project: Kasper Gade, Mikkel Grauballe, Kasper Dyhr, Frank Skovsgaard and Ari Lamhauge.

Finally, I wish to thank my family and friends their patience and support.

For my father

Publications

Publication P1

Lauridsen, J. S., A. K. Sekunda, I. F. Santos and H. Niemann (2015). 'Identifying parameters in active magnetic bearing system using LFT formulation and Youla factorization'. *2015 IEEE Conference on Control Applications (CCA)*. IEEE, pp. 430–435. (Publication P1, Chap. 2 at page 13).

Publication P2

Voigt, A. J., J. S. Lauridsen, C. M. Poulsen, K. K. Nielsen and I. F. Santos (2016). 'Identification of Parameters in Active Magnetic Bearing Systems'. *Proceedings of ISMB15*. (Publication P2, Chap. 3 at page 21).

Publication P3

Lauridsen, J. S. and I. F. Santos (2017b). 'Design of Robust AMB Controllers for Rotors Subjected to Varying and Uncertain Seal Forces'. *JSME Advances in Magnetic Bearing Technology (accepted)*. (Publication P3, Chap. 4 at page 31).

Publication P4

Lauridsen, J. S. and I. F. Santos (2017c). 'On-site Identification of Dynamic Annular Seal Forces in Turbo Machinery Using Active Magnetic Bearings - An Experimental Investigation'. *ASME Journal of Engineering for Gas Turbines and Power (submitted)*. (Publication P4, Chap. 5 at page 45).

Publication P5

Lauridsen, J. S. and I. F. Santos (2017a). 'Design of Robust Active Magnetic Bearing Controllers for Rotors Subjected to Seal Forces'. *ASME Journal of Dynamic Systems, Measurement, and Control (accepted)*. (Publication P5, Chap. 6 at page 57).

Contents

Abbreviations and nomenclature

This nomenclature covers the thesis summary. The nomenclatures of the appended publications may differ.

Abbreviations

ACT	Actuator
ADC	Analog to Digital Converter
AMB	Active Magnetic Bearing
CFD	Computational Fluid Dynamics
CCS	Cross Coupled Stiffness
DOF	Degrees Of Freedom
DTU	The Technical University of Denmark
EM	Electromagnet
FE	Finite Element
FEM	Finite Element Method
FEMM	Finite Element Method Magnetics
FFT	Fast Fourier Transform
FRF	Frequency Response Function
LFT	Linear Fractional Transformation
LPV	Linear Parameter Varying
LQR	Linear-Quadratic Regulator
LTI	Linear Time Invariant
MIMO	Multiple Input Multiple Output
SISO	Single Input Single Output
SVD	Singular Value Decomposition
PRBS	Pseudo Random Binary Sequence

Latin symbols

A, B, C, D	Nominal system state space matrices
A, B, C, D, B_θ, C_θ	Changed system state space matrices
A, B, C, D, B_Δ, C_Δ	Perturbed state space matrices
F	Force (N)
G	General plant representation

L	Inductance (H)
K_i	Force/current coefficient (N/i)
K_s	Force/displacement coefficient (N/m)
H	Magnetic field intensity (T)
J	Cost function to be minimised
K	Controller
N	Number of coil turns (-)
S	Closed loop sensitivity transfer function
T	Closed loop complementary sensitivity transfer function
T_L	Left real modal transformation
T_R	Right real modal transformation
f	Force (N)
i_e	Excitation current (A)
s_0	Nominal air gap (m)
x	State vector of state space system
y	Output vector of state space system

Greek symbols

τ_e	Time constant of actuator dynamics (s)
θ	Identification Parameter
Δ	Uncertainty

Sub- and superscripts

f	Full finite element form
x, y	vertical and horizontal coordinate system
ζ, η	AMB coordinates (tilted 45 deg compared to vertical and horizontal coordinate system)
0	initial
$meas$	measured
i	input
o	output

Chapter 1

Introduction

1.1 Motivation

Active Magnetic Bearings

The use of Active Magnetic Bearings (AMBs) in industrial applications has increased over recent decades as the technology has grown more mature, further aided by advancements and decreasing prices of the electronic components. AMBs are well suited for highly demanding applications including turbo-machinery, blood pumps, centrifuges, machine drilling tools, energy storage flywheel etc.

Some advantages compared to conventional bearings include:

1. No mechanical contact and no lubrication allow for low maintenance and long operational life.

2. Can work in challenging environments such as in high or very low temperatures or in a vacuum.

3. Allows for very high rotational speed mainly limited to the strength of the rotor material. In practice other factors can be limiting such as saturation in amplitude and bandwidth of the actuators, and uncontrolled flexible modes.

4. The feedback control is usually implemented in software. This allows the bearing characteristics such as stiffness and damping to be tuned online and changed over time e.g. as function of online measured parameters using gain-scheduled control.

5. It is possible to make a rotor rotate about its inertial axis, and thus reduce vibrations transmitted to the base of the machine. This makes the AMBs equipped systems less sensitive to mass unbalance of the rotor.

6. The rotor position can be controlled very precisely within the bearing clearance. This position can be controlled independently of the bearing stiffness.

7. Control of the flexible shaft modes can be archived by proper design of the feedback controller, typically by use of modern control techniques. This can allow the system to safely pass rotor critical speeds.

8. The displacement sensors and AMBs are very suitable for general vibration monitoring, system identification and measurement of external forces without any additional equipment.

In respect of these points, it can be seen that utilising AMBs in a rotor system leads to a highly capable mechatronic system with advantages substantially beyond simply providing adjustable stiffness and damping values. Some of the drawbacks associated with AMBs are the increased cost, weight and complexity over other bearing types, as well as problems associated with touchdown behaviour - for instance in the event of power failure - necessitating backup bearings and possibly other safety features.

The basic principle of the AMB can be explained as follows: a displacement sensor measures the position of the rotor compared to a reference position, a feedback controller implemented in a microcontroller calculates an appropriate actuation signal based on the measurement, a power amplifier transforms this signal into a control current, and this current drives an electromagnet which generates magnetic field forces affecting the position of the rotor such that it stays in its levitated position. A schematic of an AMB is illustrated in Figure 1.1.

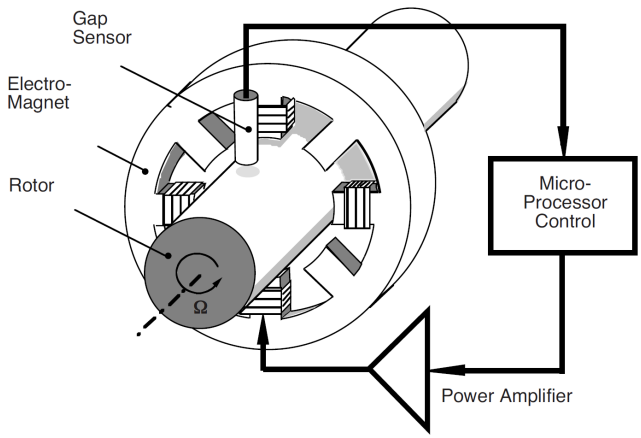

Figure 1.1: Operational principle of Active Magnetic Bearings (Schweitzer et al. 2009).

Proper design of the feedback controllers are crucial for ensuring good performance of AMB supported rotor systems to deal with the AMB's inherently unstable behaviour, mass unbalance forces, gyroscopic effects, rotor flexibility, aerodynamic interaction and disturbance, model uncertainties and changing operating conditions among other things.

Annular seals

Annular seals are a key component in turbomachinery. They prevent internal flow leakage from high pressure to low pressure regions and improve the overall machine efficiency. An schematic illustration of a smooth annular seal is shown in Fig. 1.2.

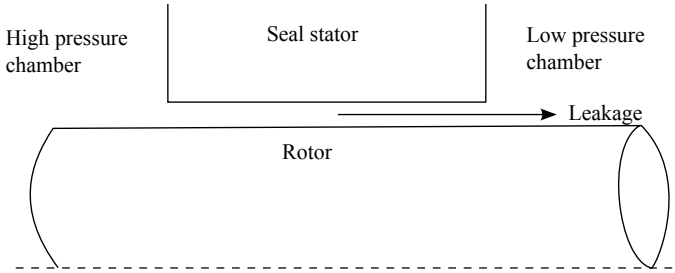

Figure 1.2: Illustration of a smooth annular seal.

A pressure difference across the seal, results in a pressure driven leakage flow. Small clearance is usually preferred for effective operation. However, in many applications the fluid interaction between the seal stator and the rotor affects the rotor-dynamic properties significantly. Hence they must be included in the rotor-dynamic stability analysis. Unfortunately, in many cases the seal forces are hard to model in advance due to complex geometries of the seal and characteristic of fluid in multiphase conditions (mixture of gas and liquid). At the moment there is no generally accepted method for determination of dynamic seal forces. Therefore, large uncertainties must be expected when modelling dynamic seal forces and consequently rotor-dynamic stability analysis.

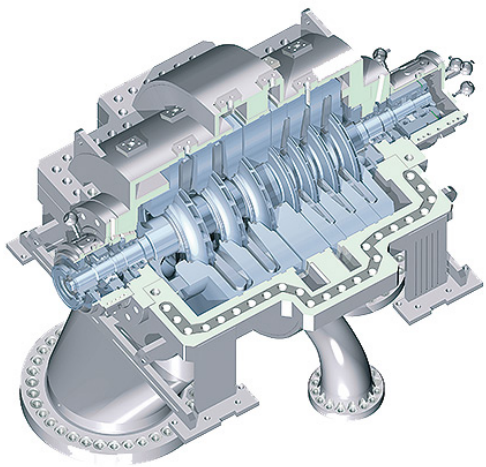

Figure 1.3: A single-shaft centrifugal multistage compressor (STC-SH, Siemens Turbocompressor, energy.siemens.com)

Annular seals are widely use in turobmachinary and a typical application is a multistage compressor with centrifugal impellers as shown in Fig. 1.3.

The large uncertainties in modelling of seals leads to a number of issues such as i) conservative design of the components, e.g. oversized bearings, larger clearance

than necessary, larger shaft diameter, ii) costly redesigns such as a replacement of the seals, iii) limiting the operational speed and thus the productivity and efficiency of the machine.

In AMB supported rotordynamic systems, the effect of gas seal destabilising forces can be significantly mitigated by employing feedback controllers, provided these controllers are properly designed and tuned. Designing and implementing feedback controllers for AMB supported rotordynamic systems taking into account the destabilising aerodynamic seal forces can be very challenging. The reasons are due to: i) the dependence of seal forces on the varying operating conditions such as rotational speed and pressure difference across the seal; ii) the changes in fluid (gas) properties; iii) changes in the process flow characteristics; and iv) model uncertainties. In this framework the necessity of designing robust controllers able to deal with uncertainties and parameter changes is clear.

1.2 State of the art

The work of this PhD thesis spans multiple scientific fields and the following sections will provide a literature review for the most relevant of those.

Control of AMB systems

The mechanical design of a standard radial bearing is rather simple and offers limited scope for improvement. Thus, most research effort related to AMBs focuses on smart sensing, specific applications, and control algorithms and software, rather than on the bearing hardware. With intelligent control, the bearing performance and characteristics can be optimised for the particular application. Some applications like grinding spindles requires precise position control and the bearings need to attenuate disturbances well from external loads. Controllers for turbo machinery should be able to handle disturbances from fluid film forces coming from e.g. seals, aerodynamic forces coming from impellers besides handling unbalance forces. Also the first critical speed often needs to be crossed. Controlling aerodynamic instabilities such as surge and rotation stall in turbo machinery using axial AMBs is also a possibility. The energy usage in some applications is of significant concern and must be minimised. This is typical the case for fly-wheel energy storage systems where efficiency is a key consideration. For some applications the motion of the machine base/foundation must be considered, such as applications where the base/foundation is in motion as on satellites and boats.

Robustness and performance measures of AMB systems

Two important measures when it comes to performance measurement of AMB supported system are the closed loop sensitivity transfer function $S = (I + GK)^{-1}$ and the compliance transfer function $G_f = G(I + GK)^{-1}$. The sensitivity function is discussed in the section below. The compliance transfer function describes the relationship between rotor displacements and external force inputs and can be used as a performance measure. This function is most typically required to be as low as possible at all frequencies to ensure good force disturbance rejections and small orbits. An upper bound of the amplitude of the compliance function can be found by calculating the maximum singular values of the compliance function. This function reveals the systems

ability to attenuate external disturbances in resonances frequencies from e.g. rigid and flexible modes.

Robust controller design for AMB systems

Several articles have focused on designing robust control for AMB systems. A popular choice for designing robust linear time-invariant (LTI) controllers for AMB systems is by using the $\mathscr{H}_\infty$ framework and an LFT formulation to represent the nominal system and uncertainty. Using $\mathscr{H}_\infty$ with an uncertainty representation of the plant allows for the direct synthesisation of the controller, ensuring the worst case performance. In many cases the conservativeness of the synthesised $\mathscr{H}_\infty$ controller can be reduced using DK-iteration, as done using the μ synthesis framework (Zhou et al. 1996). The robustness criteria for AMB systems are specified in ISO 14839-3 stating that the closed loop output sensitivity should be less than 3 for the system to be classified as Class A (ISO 2004). In the $\mathscr{H}_\infty$ framework such a requirement can be fulfilled by weighting the sensitivity function. Some articles report research efforts on fault-tolerant control methods. Cole et al. 2004 shows that improved tolerance to specific external faults is achieved through $\mathscr{H}_\infty$ optimised disturbance rejection. Specifically, increased robustness is shown in the case of mass loss of rotor in a testrig with a flexible shaft and moveable base. Improvement in performance of $\mathscr{H}_\infty$ controller based on nonlinear plant compared to $\mathscr{H}_\infty$ controller based on linear plant has been reported by Cole et al. 2016. Balas and Young 1995 show that robust controllers for uncertain rotational speed can be addressed using an LFT consisting of the nominal system and a representation of how the system changes due to gyroscopic effects using gyroscopic matrix scaled by a repeated uncertainty. The natural frequencies of the flexible shaft's bending modes are the main uncertainties treated by Schonhoff et al. 2000 and a robust controller is designed using μ synthesis. Robust stability to additive and multiplicative uncertainties can directly be ensured by applying complex weighting functions to the transfer functions $KS = K(I + GK)^{-1}$ (controller sensitivity) and $T = GK(I + GK)^{-1}$ (complementary sensitivity). The conservativeness of the robust controller design can be reduced in the case of a Linear Parameter Varying (LPV) controller design, where one or more parameters are measured in real time, and can represent changing dynamics, which otherwise would be considered uncertain. A measured parameter could be the rotation speed, which can be utilised to reduce synchronous vibrations as shown by Balini et al. 2012. A flexible rotor subjected to uncertain cross coupled stiffness (CCS) was considered by Mushi et al. 2008 and the CCS was generated by using an extra set of active magnetic bearings. It was found based on the experimental analysis that it is very hard to design robust controllers using μ synthesis able to compensate for uncertain cross coupled stiffness in flexible rotating systems. Adaptive controllers to detect and compensate for cross coupling forces have been reported by Wurmsdobler 1997 where the authors numerically simulated a rotordynamic system supported by AMB and subjected to a time variant CCS. An observer was built and theoretically demonstrated the ability to track the changes of CSS parameter in time. Using pole placement technique a controller was designed to work along with the observer. Lang et al. 1996 estimated on-line the unknown CSS parameter of a rotor by a recursive least square estimator. Simulation results of adaptive control in parallel with a baseline PID controller were considered by Hirschmanner and Springer 2002, where the controller was designed to compensate changes of CCS in time and periodic disturbance forces.

The work shows that the adaptive controller could handle much larger amplitudes of CCS forces than a fixed LTI LQR compensator. However, only numerical studies have been carried out so far dealing with the adaptive controller problem. In general stability and robustness are hard to guarantee in adaptive control systems which is crucial for implementation in industrial applications.

Modelling of seals forces

Uncompressible and compressible fluid flowing through very narrow gaps in annular seals can generate large forces. The influence of such liquid and gas seal forces on the lateral dynamics of rotating machines has been intensively investigated over several decades, by Fritz 1970, Black 1969; Black and Jenssen 1970, Childs and Dressman 1982 and Nordmann and Massmann 1984 among others. Under high pressure and high pre-swirl flow conditions such aerodynamic forces can destabilise the rotating shaft, leading to high levels of lateral vibration. In extreme cases of contact and rubbing between rotating shaft and seal stator catastrophic failures may occur.

In the last five decades the prediction of the dynamic behaviour of seals forces by means of mathematical models has been well documented in the literature, but it does not mean that an accurate prediction of seal forces is a solved problem. The publications have been focused on describing seal dynamics using either CFD (Baskharone and Hensel 1993; Hensel and Guidry 1992; Ishii et al. 1997; Schettel and Nordmann 2004) or Bulk-flow models (Childs 1989; Hirs 1973), and they have shown that for seals under well-defined single phase flow conditions and simple geometries a reasonable match between theoretical and experimental results can be achieved (Nielsen et al. 2012), especially in the case of incompressible fluids (Childs and San Andres 1997). Once a Bulk-flow model is built based upon several simplifying assumptions which do not necessarily hold (Hsu and Brennen 2002) in practical industrial applications, several ways of "tuning" uncertain model parameters based on experimental as well as theoretical approaches can be explored (Kirk and Guo 2004).

To illustrate the challenges associated with the modeling of dynamic seal forces and the accurate prediction of seal force coefficients a survey was conducted in 2007. Here 20 survey participants from both industry and academia were asked to predict the dynamics of a gas labyrinth seal and consequently the rotordynamic behaviour (Kocur et al. 2007). The seals dynamics was predicted using Bulkflow and CFD methods. The survey showed large variations in results and emphasises the need for continuous efforts towards modelling and uncertainty handling of seal forces, even for the single phase flow condition, as presented in this PhD thesis.

Seal forces under multiphase flow conditions, i.e. where the fluid is an inhomogeneous mixture of gas and liquid, are still an open and difficult modeling task (San Andrés 2012). In this framework, larger model uncertainties should be expected for seals under multiphase flow conditions due to a limited knowledge about the dynamic behaviour of fluid forces under such a condition, especially when combined with complex seal geometries, such as hole-pattern and labyrinth. Model uncertainties are thus unavoidable due to the complexity of the fluid-structure interaction and the limitations of mathematical modelling associated with simplifying assumptions.

Identification of parameters in AMB systems

It is almost impossible to avoid having a mismatch between the theoretical model of the AMB and the rotor system with experimental results, due to factors such as fabrication tolerances, alignment of shaft, simplified model assumptions and potentially unspecified dynamics. These are in addition to the uncertain/unknown seal dynamics, which is discussed in the next section. Hence, the mathematical model must typically be improved or corrected for precise prediction capabilities. For this reason, system identification techniques can be applied to obtain an accurate model.

Several methods have been described in the literature for system identification of dynamic systems in both the time and frequency domains. Some of the commonly used methods are: Prediction Error Method (PEM), Instrument Variables (IV) and H1/H2 frequency domain methods (Ljung 1999; Söderström and Stoica 1988). Some of the challenges associated with identification of systems supported by AMBs can be listed as:

1. The system is inherently unstable in open loop operation.
2. The system is a coupled MIMO (Multiple Input Multiple Output) system.
3. Potentially flexible behaviour of rotor.

Since the system is unstable in open loop operation, it means that the input-output data can only be obtained in a closed loop scheme including a stabilising controller. Standard open loop identification methods are generally ill suited to such situations, since they typically assume that the measurement noise is uncorrelated with the system inputs and outputs, which does not hold once the controller action links input and output signals.

Examples of several identification methods on different types of AMB systems are described in literature (Balini et al. 2010; Gahler et al. 1997; Li et al. 2006; Vázquez et al. 2001). Some methods focuses on establishing a model experimentally without the need for using mathematical models based on physical laws, but where the model structure and order is given in advance. A low-order precise model representation of a system consisting of two radial AMBs and a flexible rotor has been obtained using a subspace method by Balini et al. 2010. However, the control synthesis based on the system with flexible modes resulted in unstable controllers and could not be implemented in practise. Instead it was shown that a controller could be synthesised based on a lower order plant model, which in turn were designed to be robust against the neglected flexible behavior of the shaft. An obviously disadvantage of this kind of method, which is solely based on experimental data, is of course the limited prediction capabilities of the resulting controller - for instance such a model is generally unable to predict what happens if a physical parameters changes, such as a change in rotational speed. In that case, a new model must be identified for e.g. a new speed, and these models must be linked together in e.g. an LPV-model. For the same reason, a perturbed plant representation using a parametric uncertainty cannot directly be obtained, whereas it could be if the model had been established with parameters with physical meanings.

Another method is shown by Gahler et al. 1997 where the modal parameters are identified, i.e. the natural frequencies and damping, using a predefined model structure. Here the system matrices are represented using a two-stage optimisation. Li et al. 2006 presents a comprehensive modelling and identification method with individual

mathematical modelling and identification of the subcomponents, followed by an overall identification of a closed loop transfer function. The global system includes the dynamics of a flexible rotor, a flexible substructure base, two radial AMBs and the electronic components. The goal is to obtain a model for synthesising robust controllers. The obtained nominal model of 48th order fits well with experimental data.

Identification of seal forces

Experimental work has been carried out often with the goal of validating mathematical seal models, typically obtained with bulkflow and CFD techniques, as well as to understand the physics of the fluid structure interaction under different conditions.

There are two usual ways of experimentally identifying dynamic force coefficients of seals: i) by keeping the lateral movements of the rotor constrained while shaking the seal housing or ii) by shaking the rotor laterally while keeping the seal housing constrained. Examples of procedure i) are more common and thoroughly documented in the literature with testing performed at university laboratories (Brown and Childs 2012; Elrod et al. 1985; Ertas et al. 2012). Examples of procedure ii) where AMBs are used to identify and characterise fluid film forces are reported (Aenis and Nordmann 2002; Knopf and Nordmann 1998; Matros and Nordmann 1997; Nordmann and Aenis 2004; Wagner et al. 2009; Wagner and Steff 1997; Zutavern and Childs 2008). The design of a full scale magnetic bearing test-facility to levitate and excite the rotor with an annular test-seal mounted in the center of the rotor is presented by Wagner and Steff 1997. This work also presents the identification results of dynamic force coefficients of a labyrinth seal for high pressure turbomachinery. The labyrinth seal forces are compared with CFD results by Wagner et al. 2009. Identification of seal forces in a flexible rotor system using AMBs is also shown by Zutavern and Childs 2008. The AMB forces are measured using fiber-optic strain gauges which are bonded to the stator poles of the AMBs. Stiffness and damping coefficients are determined using a frequency domain identification method, utilising an FE rotor model which is adjusted to match the characteristics of the test rotor in free-free conditions. The use of AMB for identification of fluid film forces of a journal bearing are investigated among others by Aenis and Nordmann 2002; Knopf and Nordmann 1998; Matros and Nordmann 1997; Nordmann and Aenis 2004. Here the forces are measured by use of hall sensors and the dynamics of the journal bearing is represented by mass, stiffness and damping matrices which are a function of the rotational speed and pocket pressure ratio.

1.3 Shortcomings of the existing literature

Although there exist quite a lot of literature about modelling and identification seal forces, not much literature can be found on the controller design and performance of controllers with experimental validation, where seals have been experimentally tested. Most of literature on control of AMB systems addressing seal forces focuses on numerical simulation scenarios. Additionally, not much literature deals with AMB control design where the seal forces are considered uncertain.

1.4 Originality of the thesis (paper based)

This thesis aims to investigate to what extent, is it possible to improve the performance and stability of AMB systems subjected to uncertain seal forces using model based control design. In order to design model based controllers which can guarantee stability and performance of the system, it is essential to obtain a good model description but also to know the uncertainties of the model and how the model changes due to changes in operating conditions.

The test facility, which has mainly been used for identification and control experiments in this PhD project, is described in detail by Voigt 2016. The most important information of the test facility, which relate to the work presented in this thesis, are described in the papers [P2, P4-P5].

Basic information about AMBs have been omitted, to keep the thesis concise. This can be be found in Schweitzer et al. 2009.

The thesis consists of the five papers denoted P1 - P5. An overview of the papers and their original contribution are given in Sec. 1.4. The papers are listed in chronological order. An overview over the developed identification scheme is given below.

The developed identification scheme

For the work of this PhD project it is essential to have an accurate model representation of the complete rotordynamic test facility. The model should describe the dynamic behavior of the rotor, the flexible coupling linking the rotor with the motor, the characteristics of the electronics and the dynamic seal forces. The model needs to represent the system under nominal conditions as well as the dynamic behaviour due to parametric changes/uncertainties of dynamic seal coefficients and AMB parameters.

Black-box/grey-box modelling approaches are thus not suitable for this work since such techniques do not give a model with parameters that have physical meanings. Instead a method which can update the uncertain/unknown parameters in the model is desirable. It is chosen to develop an identification scheme which fits these needs.

The method seeks to

1. Tune the physically meaningful parameters of the mathematical model. Hence, use a known fixed model structure where some parameters are uncertain or unknowns and need to be identified.

2. Identify both the uncertain AMB parameters as well as the unknown seal coefficients.

3. Get an indication of the uniqueness of the identified parameters, i.e. the size of the correlation between the parameters.

4. The method should be simple and require a minimum of tuning parameters.

5. Obtain a low order model of LFT form with the purpose of synthesising model based controllers such as $\mathscr{H}_\infty$, μ and LPV controllers.

The model is found using optimisation techniques in time domain and does not require any frequency response function to be calculated. This has the advantage of no need for Fast Fourier Transformation (FFT) and windowing techniques, and selection

of parameters such as length of sample window and frequency range for optimisation that might affect the results. Only a few seconds of experimental and simulated data are needed for the optimisation process in order to obtain optimal parameters.

The scheme has been developed primarily in [P1-P2] by identifying AMB parameters. The scheme has been shown to perform well for identification of dynamic seal coefficients in this PhD project. It is worth to mention that other authors (Lusty 2016) have independently used the identification scheme developed in this thesis, showing the ability to identify parameters in a flexibly-mounted internal-stator magnetic bearings system.

Publication P1

Theoretical results of a developed identification scheme is presented by Lauridsen et al. 2015 (Publication P1, Chap. 2 at page 13). The focus of the work is on the development of a closed loop identification scheme to identify uncertain parameters in AMB systems. The challenge is to identify uncertain parameters in inherently unstable magnetic bearing systems where feedback control is required for stable operation. Youla parametrisation is used to construct a stable system which is used to construct a residual time response. By minimising the response using standard optimisation, optimal parameters are found. A simulation example shows that the method is able to identify a single uncertain negative stiffness of the AMBs.

The main original contribution of [P1], besides introducing the identification scheme, is the method presented to create a perturbed plant representation on LFT form using FE rotor dynamic system representation and modal reduction techniques. This representation has later been used to identify AMB and seal parameters in [P2] and [P4], and used for robust and LMI based control design in [P3] and [P5].

Publication P2

The identification method presented in [P1] has been extended to identify multiple parameters simultaneously and used to identify AMB parameters at the AMB-rotor-seal test facility, shown in Voigt et al. 2016 (Publication P2, Chap. 3 at page 21). Here the initial nominal model of the closed loop system (including AMBs, amplifiers, rotor and controller) poorly fits the experimental results. Updating the nominal model with the identified parameters results in precise models which fits experimental data well. The identified current/force factors are validated by using calibrated force transducers. Good agreement between the results from the two methods are seen, with discrepancies below 10 %. Hence, this verifies the uniqueness of the current/force parameters found by the method for the given system.

Publication P3

Lauridsen and Santos 2017b (Publication P3, Chap. 4 at page 31) demonstrates the advantages of using robust and linear parameter varying controllers for handling uncertain and varying seal forces in AMB supported systems.

The perturbation plant model used for robust control synthesis consists of parametric uncertainties on seal forces, using the method presented in P1. The robust controller

shows substantial performance improvement over the $\mathscr{H}_\infty$ controller based on nominal plant for handling uncertain seal forces.

The model of the hole pattern seal used in this work shows significant frequency dependence. For large variations in operational speed, it is more challenging to design a single robust LTI controller that provides satisfactory performance over the complete operational range. This paper demonstrates the performance improvement which an LPV controller can deliver, compared to a single robust LTI controller, using the nominal plant model.

Publication P4

Previously work on identification of seal forces has typically been with the focus of validating or tuning of mathematical models to fit experimental data. This has been carried out on test-rigs with accurate force measurement sensors or using calibrated force transducers.

In Lauridsen and Santos 2017c (Publication P4, Chap. 5 at page 45) the focus is on identification of seal forces in AMB supported systems, on-site, without the use of extra calibrated equipment, such as hall sensors, which is usually not present in industrial systems. The goal of this model is to predict stability and performance and have a model which can be used for model based control design (as shown in P5).

The seal dynamics are identified as the residual dynamics between the well known system dynamics from AMB-rotor (obtained in [P2]) and the experimental response including the seal forces.

It has been shown that a precise model including seal forces can be obtained using the suggested approach, which is suitable for model based control design. Using stepped sinusoidal excitations signals the frequency dependence of the seal are determined. The identified seal coefficients of the tested seal with gas fluid show practically no excitation frequency dependence. The most significant seal parameter is the cross-coupled stiffness which is highly dependent on the pressure across the seal.

Publication P5

Lauridsen and Santos 2017a (Publication P5, Chap. 6 at page 57) demonstrates theoretically as well as experimentally the capabilities of three types of controllers to handle and compensate for rotor lateral vibrations induced by destabilising aerodynamic seal forces. Numerical simulations of rotor lateral dynamics are carried out using the rotor dynamic model with identified seal coefficients, presented in Lauridsen and Santos 2017c. Comparison between theoretical and experimental results shows strong agreement, indicating that the identified models are suitable for model based control design. The objective of the controller design is to enhance the performance of the global system without increasing the direct stiffness or damping of the system.

A PID reference controller is compared with the performance of an $\mathscr{H}_\infty$ and a μ controller. The designed $\mathscr{H}_\infty$ controller shows significant performance improvements when the rotor-bearing-seal system operates close to design pressure conditions. The synthesised μ controller is able to handle pressure variations better than the $\mathscr{H}_\infty$ controller.

Chapter 2

Identifying parameters in active magnetic bearing system using LFT formulation and Youla factorization

Publication P1

The following conference paper was presented by the first author J. Lauridsen at the IEEE Multi-Conference on Systems and Control (MSC2015), Sydney, Australia in September 2015.

Identifying parameters in active magnetic bearing system using LFT formulation and Youla factorization

Jonas S. Lauridsen[1], André K. Sekunda[2], Ilmar F. Santos[3] and Henrik Niemann[4]

Abstract— **In this paper, a method for identifying uncertain parameters in a rotordynamic system composed of a flexible rotating shaft, rigid discs and two radial active magnetic bearings is presented. Shaft and disc dynamics are mathematically described using a Finite Element (FE) model while magnetic bearing forces are represented by linear springs with negative stiffness. Bearing negative stiffness produces an unstable rotordynamic system, demanding implementation of feedback control to stabilize the rotordynamic system. Thus, to identify the system parameters, closed-loop system identification techniques are required.**

The main focus of the paper relies on how to effectively identify uncertain parameters, such as stiffness and damping force coefficients of bearings and seals in rotordynamic systems. Dynamic condensation method, i.e. pseudo-modal reduction, is used to obtain a reduced order model for model-based control design and fast identification.

The paper elucidates how nodal parametric uncertainties, which are easily represented in the full FE coordinate system, can be represented in the new coordinate system of the reduced model. The uncertainty is described as a single column vector of the system matrix A of the full FE model while it is represented as several elements spread over multiple rows and columns of the system matrix of the reduced model. The parametric uncertainty, for both the full and reduced FE model, is represented using Linear Fractional Transformation (LFT). In this way the LFT matrices represent the mapping of the uncertainties in and out of the full and reduced FE system matrices. Scaling the LFT matrices easily leads to the amplitudes of the uncertainty parameters.

Youla Parametrization method is applied to transform the identification problem into an open-loop stable problem, which can be solved using standard optimization methods.

An example shows how to decouple and identify an uncertainty in the linear bearing stiffness of a reduced FE rotordynamic system.

I. INTRODUCTION

The Active Magnetic Bearing (AMB) has many advantages compared to conventional fluid film bearings and ball bearings, such as no mechanical contact, no lubrication, low maintenance, practically no friction, low vibration level and high rotational speed, which makes it extremely useful in special environments such as cleantech, subsea among others. Today the AMB is widely used on several types of industrial applications such as centrifugal compressors, turbo expanders, blood pumps, centrifuges, machine drilling tools, energy storage flywheel etc. The AMBs have been applied in turbomachinery equipment with capacities that range from a few kilowatts up to 29,000 kW and with operation speed up to 60,000 RPM.

Rotors levitated by AMB's are essentially unstable systems whose properties cause several challenges to the design of active control system due to: gyroscopic effects, mass unbalance, rotor flexibility, aerodynamic excitations among others. It is essential to have a global mathematical model which precisely predicts the real plant dynamics, in order to design a high performance control system and to predict its stability and performance.

Due to assembly tolerances and simplified model assumptions, discrepancies between the model and real plant typically exist and adjustment of some of the model parameters are often needed. System identification techniques should therefore be applied to find the deviation between model and the real plant, toward more accurate global mathematical models, which in turn makes improved controller design possible.

Due to the fact that AMB systems are open-loop unstable, input-output data is only possible to gather in a closed-loop scheme with a stabilizing controller. Standard open-loop identification methods are therefore ill suited [3] since they typically assume that the measurement noise is uncorrelated with the system inputs and outputs, which does not holds, once the controller action links input and output signals.

There are several methods which take into account that the plant is part of a closed loop scheme [3], [7], [14]. Each method has advantages and the method used in this paper is chosen for the easy translation to fault diagnosis of parameters. In this paper a method for closed-loop identification of the rotordynamic system (turboexpander) using a coprime factorization is proposed. The method is based on the well known Hansen scheme [17]. However classical identification using the Hansen scheme makes it difficult to take advantage of physical knowledge of the plant. The method proposed in this paper is therefore an extension which makes it possible to identify specific plant parameters through the identification of the open loop error dynamics. The method proposed in this paper has also been applied to estimate parametric faults in systems[1], [2].

The main originality of the work relies on parametrization and identification of uncertainties in FE rotordynamic systems. Focus is put on how LFT representation of a reduced

[1]Jonas S. Lauridsen is with Department of Mechanical Engineering, Danish University of Technology, 2800 Kgs. Lyngby, Denmark jonlau@mek.dtu.dk

[2]André K. Sekunda is with Department of Electrical Engineering, Control and Automation, Danish University of Technology, 2800 Kgs. Lyngby, Denmark aksek@elektro.dtu.dk

[3]Ilmar F. Santos is with Department of Mechanical Engineering, Danish University of Technology, 2800 Kgs. Lyngby, Denmark ifs@mek.dtu.dk

[4]Henrik Niemann is with Department of Electrical Engineering, Control and Automation, Danish University of Technology, 2800 Kgs. Lyngby, Denmark hhn@elektro.dtu.dk

a rotordynamic system.

This paper deals with a 700 kW turboexpander supported by AMB designed for air separation units. The turboexpander can essentially be considered as a flexible rotor spinning at angular velocities up to 31500 RPM, levitated by AMB forces. In this paper the modelling of the shaft is carried out using FE method including gyroscopic effects [11], [12], and the forces of the AMB have been characterized using the basic laws of electromagnetism [10].

The paper is structured as follows: Section II introduces the identification method of unstable systems based on Youla parmetrization; Section III contains a description of the system to be identified, modelling and reduction of the system, followed by representation of the uncertainty; Section IV discuss results obtained from a simulation example of applying the identification method to a plant with parameter uncertainties; Section V contains a conclusion on the results presented in the paper.

II. METHOD

Identification of system using Coprime factorization

In this section a method for identification of closed-loop systems using coprime factorization is given. The method uses the coprime factorisation of plant and controller and is based on the theory outlined in [4]. The closed-loop scheme is given as shown in Fig. 1. Let $G = G(0)$ be the nominal

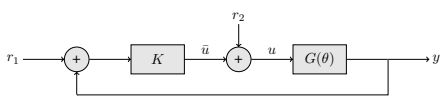

Fig. 1. Closed-loop system representation.

plant i.e. initial model guess and K be a stabilising controller to both the real plant $G(\theta)$ and the nominal plant G, where θ is the parameter uncertainty. Then G and K are given as:

$$G = NM^{-1} = \tilde{M}^{-1}\tilde{N} \tag{1}$$

$$K = UV^{-1} = \tilde{V}^{-1}\tilde{U} \tag{2}$$

For the 8 matrices given in Eq. (1) and Eq. (2) to be coprime factors, the double Bezout identity shown in Eq. (3) have to be satisfied.

$$\begin{bmatrix} I & 0 \\ 0 & I \end{bmatrix} = \begin{bmatrix} \tilde{V} & -\tilde{U} \\ -\tilde{N} & \tilde{M} \end{bmatrix} \begin{bmatrix} M & U \\ N & V \end{bmatrix} = \begin{bmatrix} M & U \\ N & V \end{bmatrix} \begin{bmatrix} \tilde{V} & -\tilde{U} \\ -\tilde{N} & \tilde{M} \end{bmatrix} \tag{3}$$

With a coprime factorization of the nominal plant G and of the controller K stabilizing both the real plant $G(\theta)$ and the nominal plant $G(0)$, Eq. (4) gives a parametrization of all stabilizing controllers, for the nominal plant, using the stable transfer matrix Q, from ϵ to η shown in Fig. 2 [4].

$$K(Q) = (\tilde{V} + Q\tilde{N})^{-1}(\tilde{U} + Q\tilde{M}) \tag{4}$$

$$K(Q) = \mathcal{F}_l\left(\begin{bmatrix} UV^{-1} & \tilde{V}^{-1} \\ V^{-1} & -V^{-1}N \end{bmatrix}, Q\right) \tag{5}$$

$$= \mathcal{F}_l(J_k, Q) \tag{6}$$

Equivalent, all plants stabilized by K can be parameterized

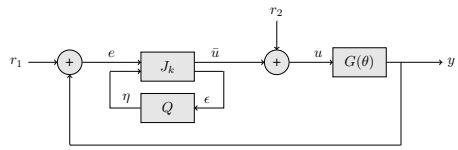

Fig. 2. Closed-loop system representation with all stabilizing controllers parametrised using a stable transfer matrix Q.

as Eq. (9). Taking advantage of the relationship given in Eq. (7) between the parametrized controller $K(Q)$ and the parametrized plant $G(S)$ [4], it is possible to show that Eq. (9) is a parametrization of all plants stabilized by the controller K using the stable system $S(\theta)$ being the transfer matrix from η to ϵ shown in Fig. 2.

$$S = \mathcal{F}_l(J_k, G(S)) \tag{7}$$

$$\epsilon = S(\theta)\eta \tag{8}$$

$$G(S) = (\tilde{M} + S\tilde{U})^{-1}(\tilde{N} + S\tilde{V})^{-1} \tag{9}$$

If the nominal plant is equal to the real plant, $S(\theta)$ is zero. As the nominal plant differs from the real plant, $S(\theta)$ increases and can thus be considered as a expression of the deviation between the nominal and the real plant.

A standard Luenberger observer is used for implementation of $S(\theta)$ for simulation examples. However any controller with its associated coprime factorization can be used. For a system such as shown in Fig. 2, the closed-loop transfer function can be written as [1].

$$\begin{bmatrix} y \\ u \\ \epsilon \end{bmatrix} = T_{cl}(S) \begin{bmatrix} r_1 \\ r_2 \\ \eta \end{bmatrix} \tag{10}$$

$$T_{cl}(S) = \begin{bmatrix} (N+VS)\tilde{U} & (N+VS)\tilde{V} & N+VS \\ (M+US)\tilde{U} & (M+US)\tilde{V} & M+US \\ \tilde{M}+S\tilde{V} & \tilde{N}+S\tilde{U} & S \end{bmatrix} \tag{11}$$

With input and output of the system defined, the uncertainties need to be given in regards to $S(\theta)$. Parameter uncertainties are given using a LFT description. Plant uncertainties are therefore given as in Eq. (12).

$$G(\theta) = \mathcal{F}_l\left(\begin{bmatrix} G_{yu} & G_{yw} \\ G_{zu} & G_{zw} \end{bmatrix}, \theta\right) \tag{12}$$

Here θ is a diagonal matrix with a parameter uncertainty in each diagonal element. It is worth noticing that $G(0)$ is equivalent to the nominal plant. A description of how to represent the parameter uncertainties as an LFT is shown in

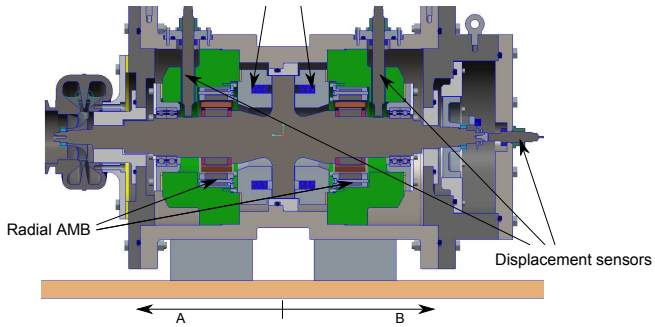

Fig. 3. Cross-section of the turboexpander testrig.

Section III-.7. With the uncertainties defined as in Eq. (12), $S(\theta)$ is found in [1] to be

$$S(\theta) = \mathcal{F}_l\left(\begin{bmatrix} 0 & \tilde{M}G_{yw} \\ G_{zu}M & G_{zw} + G_{zu}U\tilde{M}G_{yw} \end{bmatrix}, \theta\right) \quad (13)$$

Due to η not being correlated with the disturbances r_1 and r_2, Eq. (10) can be used for identification of the open loop error S. Estimation of the open loop error S from η to ϵ simplifies to Eq. (14), which can be considered as an open-loop identification problem of the stable system $S(\theta)$ with uncorrolated noise in the prediction [4].

$$\epsilon = S(\theta)\eta + D_1 r_1 + D_2 r_2 \quad (14)$$

Identification of parameter uncertainties using a LFT scheme is a well studied subject in open-loop identification of Linear Parameter Varying (LPV) systems [7], [8], [9]. The approach is to define a cost function and minimize the error between the measured and calculated output of the system. The cost function is given in Eq. (15) in its approximate quadratic form.

$$J(\theta) = \int_0^t \frac{1}{2}(\epsilon - S(\theta)\eta)^2 dt \quad (15)$$

The goal is to find the global minima of (15) which can be done using several different methods. In this paper the MATLAB function `fminsearch` is used, which is an general unconstrained nonlinear optimization method. Other methods, like gradient methods, has shown to yield faster convergence for specific types of plants, however this has not been the main focus.

III. SYSTEM AND UNCERTAINTY REPRESENTATION

In this section, the rotordynamic system is described and it is shown how dynamic uncertainties from such a system can be extracted and represented in Linear Fractional Transformation (LFT) form.

1) The real system: A cross-section schematic of the turboexpander investigated is shown in Fig. 3. The turboexpander essentially consists of a shaft levitated using axial and radial AMBs. It is assumed that the only forces acting on the rotor are the left and right radial AMB. The displacement sensors are placed close to the AMBs. The placement of the sensors and actuators will be denoted by A_x, A_y and B_x, B_y.

The analysis will be focused on rotor lateral movements and for simplicity the rotor axial movements will not be investigated. The term AMB will therefore refer to the radial AMBs in the following.

2) Model of AMBs: The model of the magnetic bearing is simplified to describe the forces acting on the rotor as function of the rotor lateral displacements s and the control current i_x. The linearized expression of the forces are given as [10]

$$f_b(i_x, s) = K_i i_x + K_s s \quad (16)$$

where K_i are K_s are constants. K_s can be considered as the stiffness of the bearing forces which is negative and thus makes the system open-loop unstable. The dynamics of the electromechanical system including the inductance of the coil and the amplifiers have been neglected.

3) Model of shaft: The rotating shaft has been modelled using the FE method and Bernoulli-Euler beam theory taking into account the gyroscopic effects of the shaft and discs

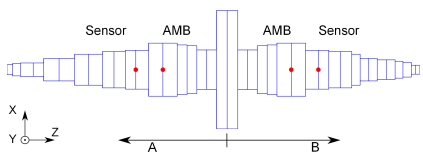

Fig. 4. Discretization of the shaft. Placement of sensors and AMBs are shown.

with 4 degrees of freedom each, which is x and y direction, and the rotation around the x and y axes, which yields 320 states in total. The discretization of node points of the shaft and the placement of sensors and AMBs is shown in Fig. 4. The goal is to control the rigid body motion of the rotating shaft and it is possible to obtain a reduced model of the rotor-bearing system with 8 states by using pseudo-modal reduction [15], [16] and removing all flexible modes, described in the following section. The reduction method are later used for LFT representation of uncertainties in the reduced FE plant model G.

Hence a MIMO system with 4 inputs (control current) and 4 outputs (rotor displacement) and 8 states have been obtained.

4) Model Reduction: The full order rotordynamic system G_f consisting of the finite element model of the shaft and negativ stiffness forces from the AMB can be written in state space form

$$\dot{x}_f = A_f x_f + B_f u, \quad y = C_f x_f \tag{17}$$

The system left and right eigenvectors (U_l and U_r) are found by solving the eigenvalue problem

$$A_f U_r = \lambda U_r \tag{18}$$
$$A_f^T U_l = \lambda U_l \tag{19}$$

The system can be sorted by the undamped natural frequencies, $|\mathcal{I}(\lambda)|$, since only the low frequency dynamics are of interest. The eigenvectors for the corresponding eigenvalues are used to create right and left transformation matrices

$$T_r = \begin{bmatrix} U_{r_1} & U_{r_2} & \dots & U_{r_n} \end{bmatrix} \tag{20}$$
$$T_l = \begin{bmatrix} U_{l_1} & U_{l_2} & \dots & U_{l_n} \end{bmatrix} \tag{21}$$

The reduced system is then given as

$$\dot{x}_c = A_c x_c + B_c u_c, \quad y_c = C_c x_c \tag{22}$$

where

$$x_c = T_l^T x_f \tag{23}$$
$$A_c = T_l^T A_f T_r \tag{24}$$
$$B_c = T_l^T B_f \tag{25}$$
$$C_c = C_f T_r \tag{26}$$

In this way the system is decomposed into a reduced system A_c which contains the dominant dynamics and the residual system A_{res} containing the residual dynamics, as shown below

$$\begin{bmatrix} \dot{x}_c \\ \dot{x}_{res} \end{bmatrix} = \begin{bmatrix} A_c & 0 \\ 0 & A_{res} \end{bmatrix} \begin{bmatrix} x_c \\ x_{res} \end{bmatrix} + \begin{bmatrix} B_c \\ B_{res} \end{bmatrix} u \tag{27}$$

Fig. 5 shows the singular values of the full and the reduced system. It is seen that the reduced 8 states system fits the dynamics very well up to approx. 20×10^3 rad/s which is above the frequency range of interest. The singular values are shown for the rotordynamic system when angular velocity is 31500 RPM since the system identification is assumed to take place at nominal operational conditions.

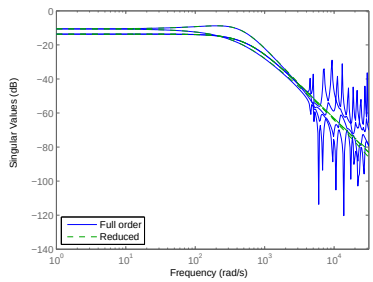

Fig. 5. Singular values of the full and the reduced rotor dynamic system shown at nominal angular velocity of 31500 RPM

5) Complex separation: The reduced state space model obtained by modal reduction consist of complex coefficients. This model can be rewritten to real form with $2n$ states, one state to represent the real part and one for the imaginary part [13]. This can be done by transforming the T_l^T and T_r to

$$T_{r_{sep}} = \begin{bmatrix} \mathcal{R}(T_{r_1}) & -\mathcal{I}(T_{r_1}) & \dots & \mathcal{R}(T_{r_n}) & -\mathcal{I}(T_{r_n}) \end{bmatrix} \tag{28}$$

$$T_{l_{sep}} = \begin{bmatrix} \mathcal{R}(T_{l_1}) & \mathcal{I}(T_{l_1}) & \dots & \mathcal{R}(T_{l_n}) & \mathcal{I}(T_{l_n}) \end{bmatrix} \tag{29}$$

Such that the new system G_s with new state vector x_s and the matrices A_s, B_s and C_s are given as

$$\dot{x}_s = A_s x_s + B_s u, \quad y = C_s x_s \tag{30}$$

$$x_s = \begin{bmatrix} \mathcal{R}(x_{c_1}) & \mathcal{I}(x_{c_1}) & \dots & \mathcal{R}(x_{c_n}) & \mathcal{I}(x_{c_n}) \end{bmatrix}^T, \tag{31}$$

$$A_s = \begin{bmatrix} \ddots & & 0 \\ & A_{c_{ii}} & \\ 0 & & \ddots \end{bmatrix}, \quad A_{c_{ii}} = \begin{bmatrix} \mathcal{R}(\lambda_i) & -\mathcal{I}(\lambda_i) \\ \mathcal{I}(\lambda_i) & \mathcal{R}(\lambda_i) \end{bmatrix}, \tag{32}$$

$$B_s = [\mathcal{R}(B_{c_1}), \mathcal{I}(B_{c_1}) ... \mathcal{R}(B_{c_n}), \mathcal{I}(B_{c_n})]^T, \tag{33}$$

$$C_s = [\mathcal{R}(C_{c_1}), -\mathcal{I}(C_{c_1}) ... \mathcal{R}(C_{c_n}), -\mathcal{I}(C_{c_n})], \tag{34}$$

6) Reduction of uncontrollable and unobservable modes: After complex separation the system consist of $2n$ states. By considering which states that is controllable and which are observable it becomes clear that some states are uncontrollable and can be removed. A similarity transform T_{sim} exists which transforms the complex separated system G_s into a controllable part and an uncontrollable part which can be removed

$$\bar{A} = T_{sim} A_s T_{sim}^T \tag{35}$$
$$\bar{B} = T_{sim} B_s \tag{36}$$
$$\bar{C} = C_s T_{sim}^T \tag{37}$$

and the transformed system has the form

$$\bar{A} = \begin{bmatrix} A_{ncon} & 0 \\ A_{21} & A_{con} \end{bmatrix}, \ \bar{B} = \begin{bmatrix} 0 \\ B_{con} \end{bmatrix}, \ \bar{C} = \begin{bmatrix} 0 \\ B_{con} \end{bmatrix} \tag{38}$$

The final transformation matrices denoted T_R and T_L can thus be found as the lower part of the products $T_{r_{sep}}T_{sim}^T$ and $T_{l_{sep}}^T T_{sim}$

$$T_{r_*} = T_{r_{sep}}T_{sim}^T \tag{39}$$
$$T_{l_*} = T_{sim}T_{l_{sep}}^T \tag{40}$$
$$T_R = T_{r_*}(:\,,\ n{+}1{:}2n) \tag{41}$$
$$T_L = T_{l_*}(n{+}1{:}2n\ ,\ :) \tag{42}$$

Thus the final reduced system matrices can be written as

$$A = T_L A_f T_R \tag{43}$$
$$B = T_L B_f \tag{44}$$
$$C = C_f T_R \tag{45}$$

The transformation matrices T_R and T_L will later be used to map the uncertainty from the full system to the reduced system.

7) Identification of parameter uncertainty using LFT of full system: LFT can be used for representing a nominal system with a parameter uncertainty. A lower LFT can be written as [6]

$$\mathcal{F}_l(G,\theta) = G_{yu} + G_{yw}\theta(I - G_{zw}\theta)^{-1}G_{zu} \tag{46}$$

If G_{zw} is zero, the LFT representation can be simplified to

$$\mathcal{F}_l(G,\theta) = G_{yu} + G_{yw}\theta G_{zu} \tag{47}$$

G_{yw} and G_{zu} can be considered as the mapping of the uncertainty in and out of the the states of the system, where G_{yu} can be considered as the nominal system as if the uncertainty is zero ($G(0)$).

It is chosen to investigate the possibility of identifying the uncertainty of a parameter in the system. A change in the negative bearing stiffness in a single direction, in a single position, is considered, which happens at e.g. B_y, see Fig. 4.

It is therefore investigated if the change in negative stiffness can be described by an LFT using G_{yw_f} and G_{zu_f} scaled by θ, on the form shown in Eq. (47). The subscript f denotes the full system i.e. the full finite element system with 40 nodes and 320 states (before model reduction). It can be proved that a change in stiffness (or damping) at a single direction at e.g. B_y corresponds to a change in a single column of system matrix A, which corresponds to the node j where the stiffness has changed.

$$A_{\Delta_f} = \begin{bmatrix} 0 & \dots & 0 & a_{1,j} & 0 & \dots & 0 \\ 0 & \dots & 0 & a_{2,j} & 0 & \dots & 0 \\ \vdots & \ddots & \vdots & \vdots & \vdots & \ddots & \vdots \\ 0 & \dots & 0 & a_{i,j} & 0 & \dots & 0 \end{bmatrix} \tag{48}$$

G_{yw_f} and G_{zu_f} can then easily be obtained by selecting G_{yw_f} to be the column of system matrix A which has

$$G_{yw_f} = \begin{bmatrix} a_{1,j} \\ a_{2,j} \\ \vdots \\ a_{i,j} \end{bmatrix} \tag{49}$$

and select G_{zu} to be

$$G_{zu_f} = \begin{bmatrix} 0 & 0 & \dots & 1 & \dots & 0 & 0 \end{bmatrix} \tag{50}$$

where 1 should be placed at the position of column which has changed in A (node position). θ is simply selected to 1 which would correspond to a 100% change in the system parameter.

8) LFT of reduced system: The LFT of the reduced system can now simply be described using the transformation matrices given in Eq. (41) and Eq. (42) to transform the uncertainty mapping G_{yw_f} and G_{zu_f} from the full finite element system to the reduced system on modal form given by Eq. (43).

$$G_{yw} = T_L G_{yw_f} \tag{51}$$
$$G_{zu} = G_{zu_f} T_R \tag{52}$$

IV. RESULTS

This section demonstrates that it is possible to identify an uncertainty using the method introduced in Section II on a rotordynamic system and uncertainty representation as presented in Section III.

Before identification of the plant is conducted, it is shown why open-loop identification of the plant is not possible. On Fig. 6 the poles and zeros of real plant $G(\theta)$ is shown, hence the real plant to be identified. It is easy to see that any input given to the plant would make the output increase to infinity, due to poles in the right half plane. Such right half plane poles are not present in $S(\theta)$, as can be seen in Fig. 7, why open-loop identification of $S(\theta)$ is possible.

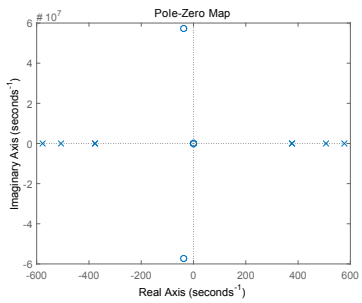

Fig. 6. Pole-Zero plot of $G(\theta)$. Poles are marked using $\times$'s and zeros are marked using $\circ$'s.

A simulation is conducted with a controller stabilizing both nominal model plant and the real plant. A stiffness reduction

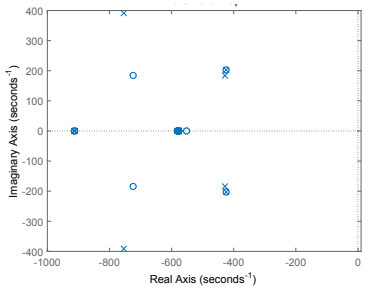

Fig. 7. Pole-Zero plot of $S(\theta)$. Poles are marked using $\times$'s and zeros are marked using $\circ$'s.

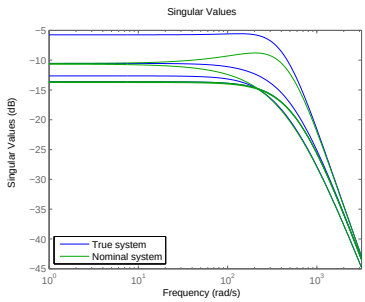

Fig. 8. Comparison of the singular values of the real system to be identified and the nominal system

of 50 % ($\theta = 0.5$) is introduced to the real plant compared to the nominal plant model.

The frequency response of the nominal and real plants are shown in Fig. 8. The plot shows that the uncertainty injected through the LFT change the dynamics of the system.

For the identification, a random binary signal is chosen for η and both r_1 and r_2 are set to 0. The variables η, r_1 and r_2 are shown in Fig. 2. A time period of $0.5\,\mathrm{s}$ and a time step of $0.001\,\mathrm{s}$ are chosen. The uncertainty, θ, is identified to be 0.502 which is practically the same as the theoretical result ($\theta = 0.5$).

V. CONCLUSION

The problem of estimating uncertain dynamics in a rotordynamic system supported by AMB is considered. Finite element and modal reduction methods are applied to establish a reduced model of the system and to parametrize uncertain dynamics in the system into uncertain parameters, which then can be identified. Youla parametrization theory is applied to show how the unstable system in connection with a standard observer based feedback structure can be used to transform tion describing the change of dynamics between the modelled system and the real system. This method is proposed for rotordynamic systems, in which the finite element model of shaft is known in advance, but where e.g. bearing or seal dynamics is uncertain.

From the example it can be concluded that the method works when considering an ideal case where the bearing stiffness in one direction is uncertain. The ideal case is used to give a clear overview of the methodology proposed. The example shows that the bearing stiffness is efficiently identified, while the shaft is spinning at nominal angular speed.

There are various possibilities to be investigated with this method such as to extend the shaft model to include flexible modes, identify multiples parameters simultaneously, investigate the effect of disturbances, investigate the effect of uncertain shaft dynamics and carry out experimental tests.

REFERENCES

[1] Niemann H. and Poulsen N. K, Estimation of parametric fault in closed-loop systems, 2015 American Control Conference(ACC) June 1-3, Chicago, Illinois, USA.

[2] Niemann H., Stoustrup J., and Poulsen N. K, "Controller modification applied for active fault detection." American Control Conference (ACC), 2014.

[3] Anderson B. D. O., "From Youla Kucera to identification, adaptive and nonlinear control." Automatica 34.12 1998: 1485-1506.

[4] Tay, T. T., Mareels I., and Moore J. B., "High performance control" Springer Science & Business Media, 1998.

[5] Niemann H., "Architecture for fault diagnosis and fault-tolerant control", Department of Electrical Engineering DTU, 2015.

[6] Zhou K., and Doyle J. C. "Essentials of robust control", Vol. 180. Upper Saddle River, NJ: Prentice hall, 1998.

[7] Wolodkin G., Rangan S. and Poolla K. "An LFT approach to parameter estimation." American Control Conference, 1997. Proceedings of the 1997. Vol. 3. IEEE, 1997.

[8] Hsu K, et al. "An LFT approach to parameter estimation." Automatica 44.12 (2008): 3087-3092.

[9] Casella F. and Marco L., "LPV/LFT modelling and identification: overview, synergies and a case study." Computer-Aided Control Systems, 2008. CACSD 2008. IEEE International Conference on. IEEE, 2008.

[10] H Bleuler, et al. "Magnetic bearings: theory, design, and application to rotating machinery", Eds. Gerhard Schweitzer, and Maslen E. H., Springer Science & Business Media, 2009.

[11] Nelson, H. D., and McVaugh, J. M., "The dynamics of rotor-bearing systems using finite elements." Journal of Manufacturing Science and Engineering 98.2 (1976): 593-600.

[12] Nelson, H. D., "A finite rotating shaft element using Timoshenko beam theory." Journal of mechanical design 102.4 (1980): 793-803.

[13] Christensen, R. H., and Santos I. F., "Design of active controlled rotor-blade systems based on time-variant modal analysis." Journal of sound and vibration 280.3 (2005): 863-882.

[14] Söderström T., and Stoica P. "System Identification", London, UK: Prentice hall, 1989.

[15] Roehrle, H. (1980) "Reduktion von Freiheitsgraden bei Strukturdynamikaufgaben", VDI Reihe 1, Nr. 72.

[16] Bucher, C. (1985) "Contributions to the Modeling of Flexible Structures for Vibration Control", PhD Thesis, Swiss Federal Institute of Technology Zrich, Switzerland.

[17] Hansen F., Franklin G. and Kosut Robert(1989), Closed-Loop Identification via the Fractional Representation: Experiment Design, In Proc. Amer. Control Conf., pp. 386-391

Chapter 3

Identification of Parameters in Active Magnetic Bearing Systems

Publication P2

The following conference paper was presented by the first author A. Voigt at the 15th International Symposium on Magnetic Bearings (ISMB15), Kitakyushu, Japan in August 2016. The paper is reformatted for the thesis.

Identification of Parameters in Active Magnetic Bearing Systems

Andreas J. Voigt
PhD student
Lloyd's Register Consulting
Copenhagen, Denmark

Jonas S. Lauridsen
PhD student
Department of Mechanical Engineering
Technical University of Denmark

Christian Mandrup-Poulsen
MSc student
Department of Mechanical Engineering
Technical University of Denmark

Kenny K. Nielsen
PhD
Lloyd's Register Consulting
Copenhagen, Denmark

Ilmar F. Santos
Professor
Department of Mechanical Engineering
Technical University of Denmark
Email: ifs@mek.dtu.dk

1 Introduction

Active Magnetic Bearings (AMBs) are commonly employed in turbomachinery applications, due to their many advantages over conventional bearing elements (Schweitzer, 2002). The operability of AMB based rotordynamic systems are dependent on a well performing feedback control scheme. This highlights the need for a precise mathematical model of the AMB-rotor system as this lays the foundation for both controller design and performance evaluation of the overall rotordynamic system. Uncertainties in AMB parameters and unmodelled AMB dynamics are sources of inconsistencies between the physical AMB system and its mathematical representation. The uncertain parameters are commonly electromechanical in nature and the uncertainties originate from production tolerances, misalignment issues and variations in material specifications, among others. Conventionally unmodelled AMB dynamics include the formation of Eddy currents which can influence the electrodynamic behaviour of the AMB actuators. To achieve the necessary level of model certainty for ensuring satisfactory performance of the AMB system, it is often necessary to identify the uncertain parameters and relevant dynamical effects experimentally, preferably in-situ, and update the mathematical model accordingly. However, as AMB based rotordynamic systems are inherently open loop unstable and requires feedback control to operate, measurement noise embedded in the system outputs, e.g. in the rotor displacement signals, can not be assumed uncorrelated with system inputs. This entails that applying conventional open loop identification techniques is not suitable (Anderson, 1998). Closed loop identification methods have previously been employed with success (Sun et al., 2014, Sun et al., 2014, Tiwari and Chougale, 2014) and are commonly based on frequency domain techniques to capture rotordynamic system performance. This paper describes a newly developed fast and transparent time domain closed loop identification (CLI) method (Lauridsen et al., 2015) and its application to an industrial scale AMB based rotordynamic testing facility. The testing facility is designed to be used for identifying rotordynamic properties of turbomachinery seals subjected to multiphase flow conditions (Voigt et al., 2016). The CLI method is capable of identifying specific AMB parameters, thus enabling utilization of a-priori knowledge of the AMB-rotor model structure. To illustrate the applicability of the CLI method to AMB-rotor systems the focus of this paper is oriented at identifying AMB force/current factors $\mathbf{K}_i$ and force/displacement factors $\mathbf{K}_s$ experimentally. Additionally, a time constant τ_e for a first order transfer function describing the conventionally unmodelled correlation between imposed coil current and actuator flux formation is identified experimentally. Furthermore, as the CLI method has not previously been applied experimentally to AMB systems, a subset of the CLI method results are compared to results obtained using a static

load (SL) method, in order to assess the capabilities of the CLI method. Specifically, $\mathbf{K}_i$ parameters identified using both methods are reported for comparison.

2 Experimental Facilities

The experimental facilities employed in the underlying work of this paper consists of a AMB-based rotordynamic test bench and a calibration facility presented in Fig. 1(a). The AMBs radially support a symmetric rigid rotor which is driven by an asynchronous motor through an intermediate shaft and a flexible coupling. Angular contact ball bearings, supporting the intermediate shaft housed in the intermediate shaft pedestal, compensate for axial forces acting on the rotor. The radial AMBs are of the eight pole heteropolar type featuring an embedded Hall sensor system which can be utilised to quantify forces exerted on the rotor by the AMBs, see Fig. 1(b). In Fig. 1(b) both the global reference frame denoted by x, y and the actuator reference frame denoted by ζ, η is introduced. The actuators are tilted 45° with respects to the global reference frame. Throughout the paper subscripts ζ, η are used to denote quantities belonging to the actuators aligned with the respective axes of the stator reference frame. The two AMB stators have been manufactured using two different production methods yielding different geometric tolerances for the AMBs. The AMBs are supplied by four commercially available 3 kW switch-mode laboratory amplifiers, not specifically designed for AMB use. The AMBs are controlled using a standard decentralized PID scheme. The calibration facility depicted in Fig. 1(c), includes four controllable pneumatic pistons that can be applied to exert static forces of varying direction and magnitude onto the rotor. Forces are transferred from the pistons to the rotor via a force transducer mounted on the calibration clamp which in turn is mounted on the rotor as seen exemplified for a single piston set-up in Fig. 1(d). A full description of the test facility can be found in (Voigt et al., 2016), which also presents the calibration of the Hall sensor system. Design parameters for the rotordynamic test bench can be found in Table 1.

3 Mathematical Representation of the AMB-Rotor System

The global AMB-rotor system is described mathematically by a rotor model and a model of the two radial AMBs. The rotor is considered rigid in the operating range of the test facility and it is assumed in the modelling that the only significant external forces acting on the rotor originates from the radial AMBs.

3.1 Model of AMB Forces

The forces generated by an AMB acting on the rotor can be described as function of the lateral AMB rotor displacements $\mathbf{s}$ and the imposed control currents $\mathbf{i}_c$. The linearised AMB forces can be represented as (Bleuler et al., 2009)

$$\mathbf{f}_b(\mathbf{i}_c, \mathbf{s}) = \mathbf{K}_i \mathbf{i}_c + \mathbf{K}_s \mathbf{s} \tag{1}$$

Table 1: Design parameters for the rotordynamic test bench

Rotor length	860	mm
Rotor assembly mass	69	kg
1st rotor bending mode @	550	Hz
Stator inner diameter	151	mm
Nominal radial air gap	0.5	mm
Winding configuration	N-S-S-N-N-S-S-N	[-]
Lamination thickness	0.35	mm
Laminate material	SURA M270-35A	
Max. static load capacity (per AMB)	7500	N
Bias current range	4 to 10	A
Number of Hall sensors per AMB	8	
Hall sensor type	F.W. Bell - FH-301	

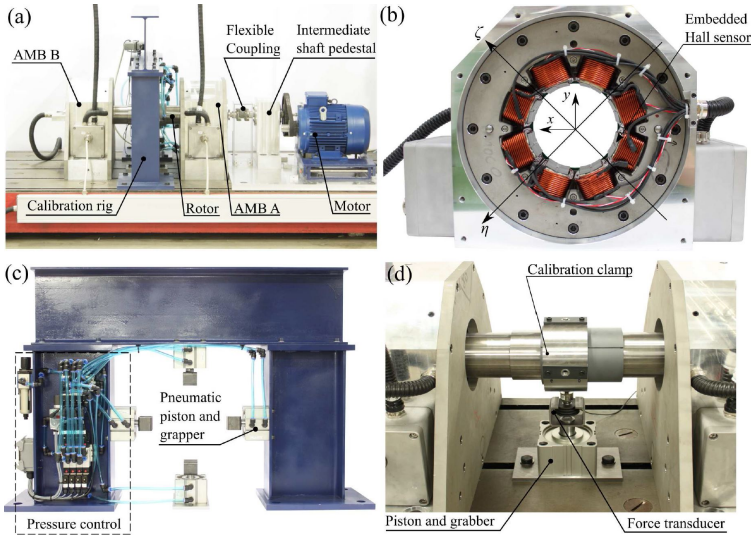

Fig. 1: Experimental facilities used throughout the study. (a) Rotordynamic test bench, showing main components. (b) Test bench AMB showing the placement of the embedded Hall sensors as well as AMB actuator and global reference frame definitions. (c) Calibration facility showing the pneumatic pistons and pressure control unit. (d) Interface between calibration facility and rotor showing a single piston with grabber as well as the calibration clamp mounted on the rotor.

in which $\mathbf{K}_i$ are $\mathbf{K}_s$ are matrices containing parameters defined as

$$\mathbf{K}_i = \begin{bmatrix} K_{i,A_\zeta} & 0 & 0 & 0 \\ 0 & K_{i,A_\eta} & 0 & 0 \\ 0 & 0 & K_{i,B_\zeta} & 0 \\ 0 & 0 & 0 & K_{i,B_\eta} \end{bmatrix}, \quad \mathbf{K}_s = \begin{bmatrix} K_{s,A_\zeta} & 0 & 0 & 0 \\ 0 & K_{s,A_\eta} & 0 & 0 \\ 0 & 0 & K_{s,B_\zeta} & 0 \\ 0 & 0 & 0 & K_{s,B_\eta} \end{bmatrix} \tag{2}$$

which defines a dedicated force/current and force/displacement factor for each actuator of the two AMBs. The subscripts A_ζ, A_η, B_ζ, and B_η designates to which AMB and which actuator the factor belongs, respectively, see Fig. 1(b).

3.2 Rotor Model

The rotor is modelled using a conventional Finite Element (FE) method since the CLI method utilizes the structure of the FE based rotor model for uncertainty representation (Lauridsen et al., 2015). Furthermore, using the FE approach retains generality of the methodology, and by applying modal truncation techniques, real left and right transformation matrices can be determined which allows transforming the full order FE model to reduced form. Here the global rotor model has been truncated to only include rigid modes. It is noted that the shaft is non-rotating through the entirety of the study. The resulting rotor model can be written in state space form as

$$\dot{\mathbf{x}}_f = \mathbf{A}_f\mathbf{x}_f + \mathbf{B}_f\mathbf{u}, \quad \mathbf{y} = \mathbf{C}_f\mathbf{x}_f \tag{3}$$

4 Closed Loop Model and Identification Scheme

The CLI method is based on theory presented in (Lauridsen et al., 2015) and is in this paper adapted for experimental application. The schematic block diagram shown in Fig. 2 acts as the basis for the CLI method, and shows the elements

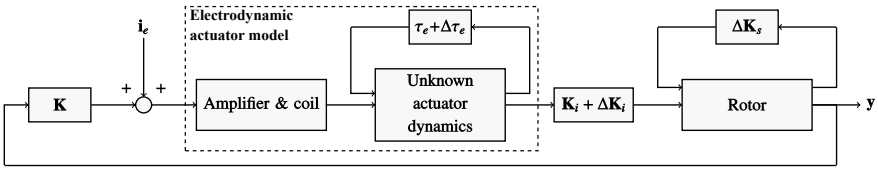

Fig. 2: Closed loop schematic of the AMB-rotor system.

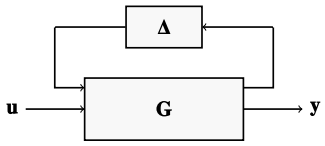

Fig. 3: Uncertain plant representation using upper LFT, $\mathbf{G}_{unc} = \mathcal{F}_u(\mathbf{G}, \Delta)$

of the global closed loop system in a vectorised formulation where $\mathbf{K}$ represents the known controller. The electrodynamic model of the AMB actuator contains two first order transfer functions as indicated on Fig. 2. The block denoted "Amplifier and coil" represents a known first order transfer function from the current reference signals to the actual current flowing in the coils, consequently approximating the dynamics originating from the coil inductance and the power amplifier. Similarly, the block "Unknown actuator dynamics" is an assumed first order transfer function with unknown time constant τ_e, which aims at describing the dynamics originating from eddy current formation and unknown amplifier dynamics. The unknown time constant appended to the block "Unknown actuator dynamics" is represented by a nominal value τ_e, serving as an initial guess, plus the variation $\Delta\tau_e$. All four actuators share one common time constant τ_e. The current/force factor is here composed of a nominal initial guess $\mathbf{K}_i$ and an appended uncertainty $\Delta\mathbf{K}_i$. The block "Rotor" contains the rotor model with the nominal displacement/force factor $\mathbf{K}_s$ and an actuator uncertainty mapping. The uncertainty mapping describes how a change $\Delta\mathbf{K}_s$ in the nominal displacement/force factor modifies the overall dynamic behaviour of the rotor. The rotordynamic model is represented on reduced modal form and the uncertain parameters of the rotor model, here $\mathbf{K}_s$, is extracted and described using a Linear Fractional Transformation (LFT) which is treated subsequently.

4.1 LFT Representation of Uncertain Rotordynamic Systems

The rotordynamic system with unknown $\Delta\mathbf{K}_s$ is formulated using a LFT as described in this section. To retain generality, the block termed "Rotor" and the block containing $\Delta\mathbf{K}_s$ in Fig. 2 are in the following denoted by $\mathbf{G}$ and Δ, respectively. The uncertain rotor model $\mathbf{G}_{unc}$ is constructed using the nominal model and the uncertainty representation, which combined is written on LFT form as illustrated in Fig. 3 for the global AMB-rotor model. In Fig. 3 Δ denotes a 4×4 diagonal matrix representing $\Delta\mathbf{K}_s$. The matrix $\mathbf{G}$ is constructed as outlined in the following and is described in detail in (Lauridsen et al., 2015). It can be proved that changing a component in $\mathbf{K}_s$, i.e. changing the displacement/force factor for a single actuator direction, imposes a change in a single column with index j of the full order system matrix $\mathbf{A}_f$. The column corresponds to a specific node with index j in the FE representation of the rotor where the AMB forces are imposed on the rotor model. This can be expressed as

$$\mathbf{A}_{\Delta_f} = \begin{bmatrix} 0 \dots 0 \; a_{1,j} \; 0 \dots 0 \\ 0 \dots 0 \; a_{2,j} \; 0 \dots 0 \\ \vdots \; \ddots \; \vdots \; \vdots \; \vdots \; \ddots \; \vdots \\ 0 \dots 0 \; a_{i,j} \; 0 \dots 0 \end{bmatrix} \tag{4}$$

It is assumed that the matrix $\mathbf{A}_\Delta$ expressing the change in the system matrix can be reduced by applying the same modal truncation matrices used to reduce the full order nominal system. This is presented in Eq. (5) and has shown to hold in practice. The matrix $\mathbf{A}_{f,\Delta}$ found in Eq. (4) can be written as the product of the column vector $\mathbf{B}_{f,\Delta}$, the scalar Δ and the row vector $\mathbf{C}_{f,\Delta}$ as shown in Eq. (6). Consequently the input mapping $\mathbf{B}_\Delta$ and output mapping $\mathbf{C}_\Delta$ of the uncertainties in the

reduced system is described by Eq. (7).

$$\mathbf{A}_\Delta = \mathbf{T}_L\, \mathbf{A}_{f,\Delta}\, \mathbf{T}_R \tag{5}$$
$$= \mathbf{T}_L \mathbf{B}_{f,\Delta}\, \Delta\, \mathbf{C}_{f,\Delta_f} \mathbf{T}_R \tag{6}$$
$$= \mathbf{B}_\Delta\, \Delta\, \mathbf{C}_\Delta \tag{7}$$

The process outlined above is repeated for each uncertain entry in the current/force matrix $\mathbf{K}_s$. Assembling the columns of $\mathbf{B}_\Delta$ and rows of $\mathbf{C}_\Delta$ and casting Δ as an 4×4 diagonal matrix, the complete uncertainty representation illustrated in Fig. 3 can be determined by (7). The matrix $\mathbf{G}$ can be written on state space form, as shown in Eq. (8), where $\mathbf{A}$, $\mathbf{B}$ and $\mathbf{C}$ are the nominal system matrices on reduced form. Here the input and output matrices are extended from the nominal model to include B_Δ and $\mathbf{C}_\Delta$. Note that no extra system dynamics is added since the LFT only changes the nominal system matrix $\mathbf{A}$.

$$\mathbf{G} = \left[\begin{array}{c|cc} \mathbf{A} & \mathbf{B}_\Delta & \mathbf{B} \\ \hline \mathbf{C}_\Delta & 0 & 0 \\ \mathbf{C} & 0 & 0 \end{array}\right] \tag{8}$$

4.2 Estimation of Optimal Parameters

As indicated in Fig. 2, a Pseudo-Random Binary Sequence (PRBS) current signal $\mathbf{i}_e$ can be imposed to perturb the system model and time domain simulation can be employed to yield the displacement response $\mathbf{y}$, which can be compared to a response quantified experimentally. To estimate the uncertain AMB parameters the CLI scheme is formulated as a minimization problem that iterates through the uncertain parameters to decrease the discrepancy between the simulated response and the experimentally acquired response. The goal is to find the parameters which provides the best fit between simulation data and experimental data. This can be done by finding the global minimum of the cost function shown in Eq. (9) which is defined as the sum of squares of the discrepancy between simulation data and experimental data as

$$J(\theta) = \left\| \mathbf{y}_{meas} - \mathbf{y} \right\|_2^2 \tag{9}$$

in which $\mathbf{y}_{meas}$ and $\mathbf{y}$ denotes matrices containing the measured and simulated rotor displacements, respectively. The simulated displacements $\mathbf{y}$ can be expressed as

$$\mathbf{y} = \mathbf{T}(\theta) i_e, \text{ where } \theta = \left\{ K_{i,A_\xi}, K_{i,A_\eta}, K_{i,B_\xi}, K_{i,B_\eta}, K_{s,A_\xi}, K_{s,A_\eta}, K_{s,B_\xi}, K_{s,B_\eta}, \tau_e \right\} \tag{10}$$

where $\mathbf{T}(\theta)$ is a transfer function for the closed loop response from the excitation current input $\mathbf{i}_e$ to the displacement $\mathbf{y}$ for a given θ vector. Minimization of the cost function seen in Eq. (9) has been implemented using MATLAB's `lsqnonlin` function. The CLI method has shown to converge fast towards optimal parameters, even for the specific case where nine parameters are simultaneously identified.

5 Experimental Methodology and Data Post Processing

Two different experimental procedures (CLI and SL) are employed in the study, and both are conduced for the same operation conditions and the same choices of bias currents namely 6 A, 8 A, and 10 A. The experiments are conducted five times for both methods to assess the repeatability of the results. Generating data for the CLI method is relatively straight forward and shortly outlined in the following. The rotor is levitated to the nominal position, and a PRBS disturbance signal is imposed on the control currents, resulting in purely lateral displacement of the rotor, while simultaneously capturing control currents and rotor position signals. The captured signals are used as input for the CLI method to experimentally determine the $\mathbf{K}_i$, $\mathbf{K}_s$ and τ_e parameters.

The secondary experimental SL procedure is introduced with the ultimate goal of obtaining the $\mathbf{K}_i$ parameters, consequently allowing for a comparison with results obtained using the CLI scheme. The basic principle of the alternative experimental procedure is to apply a known load to the centre of the shaft, see Fig. 1(d), using the pneumatic pistons of the calibration facility, see Fig. 1(c), and measure the force and amplifier current signals of all amplifiers. In this case no perturbation of the rotor is imposed, and the force applied to the rotor is quantified using calibrated strain-gauge based HBM U9C force transducers mounted between the pistons and the rotor (Voigt et al., 2016). The applied force is varied in both direction and

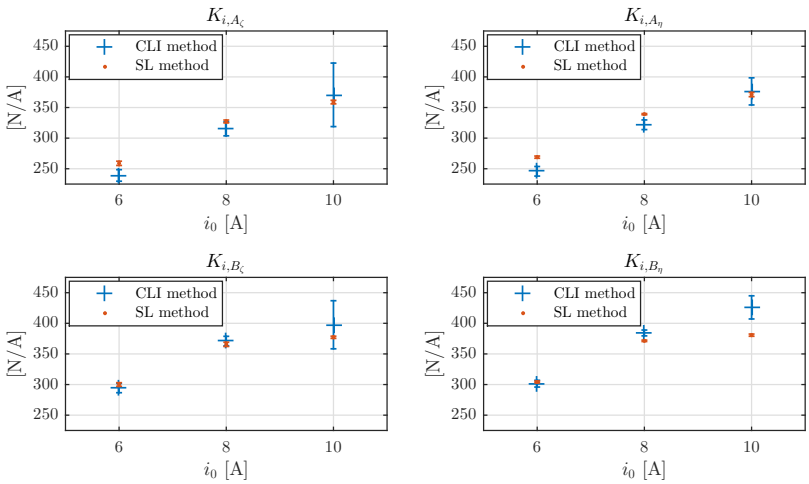

Fig. 4: K_i values for the different bias currents i_0. Top row, from left to right: $K_{i,A\zeta}$ for actuator ζ and $K_{i,A\eta}$ for actuator η in AMB A, respectively. Bottom row, from left to right: $K_{i,B\zeta}$ for actuator ζ and $K_{i,B\eta}$ for actuator η in AMB B, respectively. The error bars mark the 95 % confidence interval based on 5 repeated experiments.

magnitude, using the four pistons and the pressure control unit seen in Fig. 1(c). Summing forces and moments acting on the rotor allows a set of four equilibrium equations to be established. Furthermore, using Eq. (1) and realizing that the rotor is in static equilibrium, and consequently the variations in rotor displacement is zero leading to $\mathbf{f}_b(\mathbf{i}_c,\mathbf{s}) = \mathbf{K}_i\mathbf{i}_c + \cancelto{0}{\mathbf{K}_s\mathbf{s}}$, the applied force can be expressed solely as a function of the AMB coil currents. This enables casting the equilibrium equations in matrix form as $\mathbf{A}\mathbf{x} = \mathbf{b}$ where $\mathbf{A}$ is a $4n \times 4$ matrix of measured control currents containing n discrete load steps spanning both increasing and decreasing external loads in all four loading directions. The current/force factors to be determined are contained in $\mathbf{x} = \left\{K_{i,A_\zeta}, K_{i,A_\eta}, K_{i,B_\zeta}, K_{i,B_\eta}\right\}^T$, and $\mathbf{b}$ is a $4n \times 1$ vector containing the external forces applied using the calibration facility during the experimental procedure. The system of equations can be utilized to obtain the current/force factors by employing a Least Squares scheme.

6 Results

The main objective of this study is to determine the precision with which the parameters of a AMB-rotor can be estimated using the CLI methodology. To this end, the current/force factors, contained in $\mathbf{K}_i$, obtained experimentally using both the CLI and the SL approaches are used as a basis for a comparison of the two methods. Fig. 4 shows the $\mathbf{K}_i$ factors obtained for the three choices of bias currents. The plots includes errorbars indicating the 95 % confidence interval which is determined on the basis of five repeated tests conducted for both experimental methods. Good agreement between the results from the two methods are seen, with discrepancies below approximately 10 %. The $\mathbf{K}_i$ factors generally increase with the bias current and are similar for the two actuator directions ζ, η in each AMB, respectively. AMBs A and B are significantly different in terms of the magnitude of their respective current/force factors. The difference is mainly attributed to the different ways of manufacturing the AMB A and AMB B stators which ultimately leads to the nominal air gap of AMB A being $15-20$ % smaller than the nominal air gap of AMB B. Furthermore, the current/force factors identified for AMB B using the SL method are seen to saturate when the bias current is increased above 8 A. This effect is not as pronounced for AMB A, and could be attributed to the fact that as the nominal air gap is smaller in AMB B compared to AMB A, leading to premature saturation of the AMB B stator. Additionally, saturation is an inherently non-linear phenomenon and consequently not captured by the assumed linear model structure upon which the CLI method is based. This is suspected to be of significant influence for the decrease in the overall fitting quality for the 10 A case included in Table 2. The fitting quality is determined as a Goodness of fit parameter using a normalized root mean square error approach.

In addition to current/force factors the CLI method is used to quantify the uncertain displacement/force factors. The results

Table 2: Nominal K_s parameters identified with the CLI method. Additionally RSD values in percent calculated from the five repeated tests are included.

Bias current	6 A		8 A		10 A	
Actuator	k_s [N/m]	RSD [%]	k_s [N/m]	RSD [%]	k_s [N/m]	RSD [%]
A_ζ	$2.39 \cdot 10^6$	2.4	$4.09 \cdot 10^6$	1.9	$5.69 \cdot 10^6$	7.7
A_η	$2.49 \cdot 10^6$	2.1	$4.27 \cdot 10^6$	1.5	$5.94 \cdot 10^6$	3.0
B_ζ	$3.13 \cdot 10^6$	1.4	$5.16 \cdot 10^6$	1.1	$6.49 \cdot 10^6$	5.7
B_η	$3.19 \cdot 10^6$	1.1	$5.34 \cdot 10^6$	0.7	$7.00 \cdot 10^6$	2.3
Average fitting quality	95.2 %		93.4 %		84.5 %	

Table 3: Identified time constant τ_e for all bias current cases

Bias current	6 A		8 A		10 A	
Quantity	τ_e [s]	RSD [%]	τ_e [s]	RSD [%]	τ_e [s]	RSD [%]
Both AMBs	0.021	5.9	0.028	59	0.010	0.0

are summarised in Table 2. As expected the values of displacement/force factors are seen to increase for increasing bias currents and the two displacement/force factors values belonging to each AMB are approximately equal with higher values for AMB B again attributed to the geometrical differences between the AMB stators as discussed above. The Relative Standard Deviation (RSD) is calculated as the standard deviation in percent of the mean value of the displacement/force factors for all five tests and included in Table 2. The RSDs are generally low for the 6 A and 8 A cases, however larger for the 10 A case.

Finally the identified time constant τ_e is reported in Table 3. The values reported are the mean values and the RSD obtained from the five tests. For the 6 A and 8 A cases, τ_e is estimated within the same order of magnitude. For the 10 A case the CLI method returns a average value of τ_e which is significantly different than for the 6 A and 8 A cases. This is reflected in the very low average fitting quality values reported in Table 2 for the 10 A case, indicating that further variation of $\Delta\tau_e$ does not yield a better fit between simulated data and data obtained experimentally. This could indicate that the model fails to represent the electrodynamic behaviour of the AMB actuators for large bias currents due to the onset of non-linear operating regime under these conditions as discussed previously. The RSD values for the 6 A and 8 A are 5.9 % and 59 %, respectively and the growing RSD values could be a manifestation of the fact that the first order representation of the unknown actuator dynamics is insufficient, and the resulting τ_e should be used with care for high bias currents.

A representative visualisation of the performance of the CLI methodology is shown in Fig. 5, depicting both experimental and simulated time series responses for the imposed PRBS current perturbation. It is important to notice that the simulated results are obtained with the nine optimal parameters determined using Eq. (9). Good agreement between the experimental and simulated time series of lateral rotor displacements are seen in Fig. 5(a). The simulated versus measured AMB control currents for AMB B are seen in Fig. 5(b). Qualitatively good agreement is seen and the model captures the experimental trends, albeit significant noise levels are seen on the experimental data. High frequency oscillations are seen in the current signal obtained experimentally which the model fails to capture. This discrepancy could potentially be attributed to a too low model order for the commercial amplifiers. However, further research is required to establish if this is the case.

7 Conclusion and outlook

The CLI and SL methods produce similar results for $\mathbf{K}_i$, which indicates that the CLI method is able to perform closed loop identification of uncertain AMB parameters. The CLI method has proved very useful for providing quick, transparent and sufficiently accurate estimation of uncertain parameters during the controller tuning phase. The CLI method is orders of magnitudes faster than the SL method and does not require additional external hardware as the SL does. Additionally, the CLI method is general and allows for identification of multiple types of parameters such as $\mathbf{K}_i$, $\mathbf{K}_s$ and τ_e even for flexible rotor systems. However, the linear structure adopted in the presented formulation of the CLI method appears to

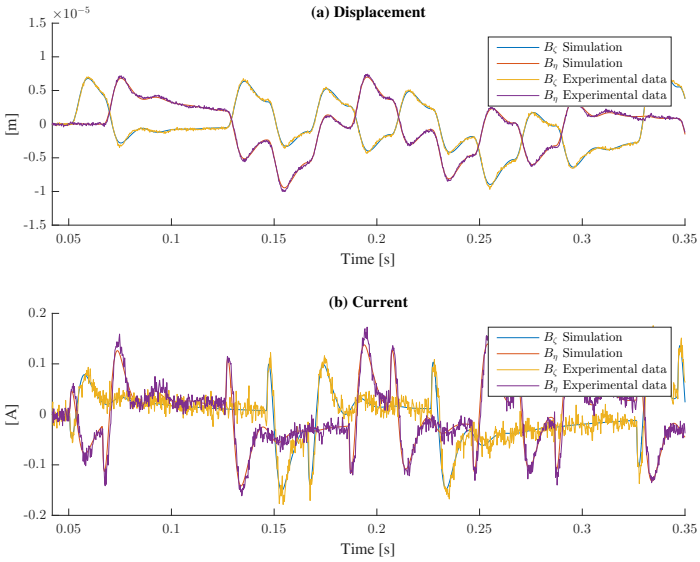

Fig. 5: Comparison of simulated and experimental data, here shown for AMB B. (a) Displacements and (b) control currents for a PRBS current input disturbance with an amplitude of 100 mA. Data obtained for a bias current of 6 A.

lead to challenges in the non-linear operational domain of the AMBs. The non-linearities originate from saturation of the AMB actuators operated at high bias currents, for which the CLI methods over-predicts $\mathbf{K}_i$ compared to the the SL method. Furthermore, discrepancies between the simulated and measured current time series are suspected to originate from a too low model order for the amplifiers which is a relevant subject for future work. It is evident from the studies presented here that the electrodynamic model of the actuator requires additional attention. The embedded Hall sensor system of the AMBs could prove a powerful tool in this regard, as it enables quantification of the flux density generated in the stator. Consequently dynamics caused by the generation of Eddy currents in the AMB stators could potentially be quantified experimentally.

References

[1] Schweitzer, G. "Active magnetic bearings - chances and limitations." IFToMM Sixth International Conference on Rotor Dynamics, Sydney, Australia. Vol. 1. 2002.

[2] Anderson., B. D. From Youla Kucera to identification, adaptive and nonlinear control, Automatica 34, pp. 1485-1506, 1998.

[3] Sun, Z., Zhao, J., Shi, Z. "Identification of magnetic bearing system using a novel subspace identification method" In Proceedings of ISMB14, pp. 87-90, 2014.

[4] Sun, Z., He, Y., Zhao, J., Shi, Z., Zhao, L., Yu, S. "Identification of active magnetic bearing system with a flexible rotor." Mechanical Systems and Signal Processing 49.1 (2014): 302-316.

[5] Tiwari, R., Chougale, A. "Identification of bearing dynamic parameters and unbalance states in a flexible rotor system fully levitated on active magnetic bearings." Mechatronics 24.3 (2014): 274-286.

[6] Lauridsen, J. S., Sekunda, A. K., Santos, I. F., Niemann, H. "Identifying parameters in active magnetic bearing system using LFT formulation and Youla factorization." Control Applications (CCA), 2015 IEEE Conference on. IEEE, 2015.

[7] Voigt, A. J., Mandrup-Poulsen, C., Nielsen, K. K., Santos, I. F. "Design and Calibration of a Full Scale Active Magnetic Bearing Based Testing Facility for Investigating Rotordynamic Properties of Turbomachinery Seals in Multiphase Flow". Proceedings of the ASME Turbo Expo 2016 (recommended for journal publication). Seoul, South Korea.

[8] Bleuler, H., Cole, M., Keogh,P., Larsonneur, R., Maslen, E., Okada,Y., Schweitzer, G., Traxler, A. ”Magnetic bearings: theory, design, and application to rotating machinery”. Eds. Gerhard Schweitzer and Eric H. Maslen. Springer Science & Business Media, 2009.

Chapter 4

Design of Robust AMB Controllers for Rotors Subjected to Varying and Uncertain Seal Forces

Publication P3

This paper is accepted for the special issue of the Mechanical Engineering Journal on the name of "Advances in Magnetic Bearing Technology", to be published by the JSME (Japan Society of Mechanical Engineers) in October 2017.

Bulletin of the JSME Vol.4, No.5, 2017
Mechanical Engineering Journal

Design of robust AMB controllers for rotors subjected to varying and uncertain seal forces

Jonas LAURIDSEN* and Ilmar SANTOS*
* Dept. of Mechanical Eng., Technical University of Denmark
Copenhagen, Denmark
E-mail: ifs@mek.dtu.dk

Received: 16 November 2016; Revised: 19 April 2017; Accepted: 8 May 2017

Abstract
This paper demonstrates the design and simulation results of model based controllers for AMB systems, subjected to uncertain and changing dynamic seal forces. Specifically, a turbocharger with a hole-pattern seal mounted across the balance piston is considered. The dynamic forces of the seal, which are dependent on the operational conditions, have a significant effect on the overall system dynamics. Furthermore, these forces are considered uncertain. The nominal and the uncertainty representation of the seal model are established using results from conventional modelling approaches, i.e. Computational Fluid Dynamics (CFD) and Bulkflow, and experimental results. Three controllers are synthesized: I) An $\mathcal{H}_\infty$ controller based on nominal plant representation, II) A μ controller, designed to be robust against uncertainties in the dynamic seal model and III) a Linear Parameter Varying (LPV) controller, designed to provide a unified performance over a large operational speed range using the operational speed as the scheduling parameter. Significant performance improvement is shown for robust control, incorporating model uncertainty, compared to nominal model based control.

Key words : Uncertain dynamic seal forces, Robust control, LPV control, AMB, Turboexpander, Hole-pattern seal, Fluid interaction

1. Introduction

Annular seals in rotordynamic systems can generate significant dynamic forces, and under certain conditions, destabilize the system leading a to machine failure. In rotordynamic systems supported by Active Magnetic Bearings (AMBs) these forces can, to a certain degree, be compensated for by employing appropriate feedback controllers. However, incorporating seal dynamics into the control design can be challenging due to, among other things, the frequency dependence of seal forces, varying operating conditions, process fluid characteristics and model uncertainties.

A number of publications have been presented focusing on the mathematical description of seal dynamics using either CFD or empirically-based Bulkflow models, and it has been shown that for seals under well defined single phase conditions a reasonable match between theoretical and experimental results can be achieved (Nielsen et al., 2012). However, seal dynamics under multiphase conditions, i.e. where the fluid is a mixture of gas and liquid, are still challenging. Larger model uncertainties should be expected for seals under multiphase conditions due to a limited knowledge of the dynamic behaviour of such fluids, especially when combined with complex seal geometries such as hole-pattern and labyrinth. Model uncertainties are thus inevitable due to these limitations of the mathematical models. Furthermore, seal model parameters change depending on operational conditions such as rotational speed and pressure difference across the seal.

A large quantity of research has focused on designing robust control for AMB systems. A popular choice for designing robust Linear Time Invariant (LTI) controllers for AMB systems is by using the $\mathcal{H}_\infty$ framework and an Linear Fractional Transformation (LFT) formulation to represent the nominal system and uncertainty.

Paper No.16-00618
J-STAGE Advance Publication date: 17 May, 2017
[DOI: 10.1299/mej.16-00618]

Using $\mathcal{H}_\infty$ with an uncertainty representation of the plant, the controller is directly synthesized to ensure a satisfactory worst case performance. The conservativeness of the synthesised $\mathcal{H}_\infty$ controller can in many cases be reduced using DK-iteration, as done using the μ-synthesis framework (Zhou et al., 1996).

A side benefit of using the $\mathcal{H}_\infty$ framework for synthesising controllers for AMB based systems is the ability to optimize the response due to worst case mass unbalance distribution. Singular Value Decomposition (SVD) can be used as a worst case measure, since the actual distribution of mass unbalance is unknown in terms of magnitude and phase. This can be applied for control synthesis shown in (Schweitzer et al., 2009) as well as for analysis shown in (Cloud et al., 2005) and with application to a subsea compressor with a flexible rotor (Maslen et al., 2012).

The robustness criteria for AMB systems are specified as the sensitivity (ISO 14839-3, 2006), stating that the closed loop sensitivity should be less than 3 for the system to be classified as Class A. Also this requirement can explicitly be dealt with using $\mathcal{H}_\infty$, by weighting the sensitivity function.

Balas & Young (1995) show that robust controllers for uncertain rotational speed can be addressed using a LFT consisting of the nominal system, a representation of how the system changes due to gyroscopic effects and a repeated uncertainty. In (Schonhoff et al., 2000) uncertainties of the natural frequencies of the flexible shaft's bending modes are considered and a robust controller is designed using μ synthesis. Robust stability to additive and multiplicative uncertainties can directly be ensured by applying complex weighting functions to the transfer functions KS (controller sensitivity) and T (complementary sensitivity). The conservativeness of the robust controller design can be reduced in the case of Linear Parameter Varying (LPV) controller design, where one or more parameters are measured in real time, and can represent changing dynamics, which otherwise would be considered uncertain. A measured parameter could be the rotation speed, which can be utilized to reduce synchronous vibrations as shown in (Balini et al., 2012).

In (Mushi et al., 2008) a system consisting of a flexible rotor subjected to cross coupled stiffness (CCS) is considered theoretically and experimentally. The CCS is generated using an extra set of AMBs. It is found that it is very hard to design robust controllers using μ-synthesis that can compensate for uncertain cross coupled stiffness specifically for the flexible rotor system considered in the work.

In (Pesch & Sawicki, 2015) a μ controller is designed to control the oil whip and oil whirl occurring from a journal bearing using AMBs. The idea is to use the journal bearing to provide high load capacity and the AMB to increase stability margin. The controller is based on the Bently-Muszynska fluid film bearing model to predict the unstable bearing behaviour and is designed to be robust due to angular velocity changes. Experimental results shows that the controller increases the stability margin significantly. It is, however, challenging in the case of such a hybrid bearing system to balance the load sharing between the journal and magnetic bearings such that they do not counteract each other. This can be explained by considering the equilibrium positions of each of the journal and magnetic bearings. In the case of the journal bearing, the equilibrium position changes with rotor angular velocity due to the interactions between the rotor and the fluid film, and may not be precisely known in advance. On the other hand, an AMB equilibrium position is traditionally controlled to a fixed reference point. However, it is desirable that the AMB equilibrium position is constantly adjusted to align with the (varying) equilibrium position of the journal bearing, such that the journal bearing is always supporting the static load, while the AMB acts purely as an active control actuator, providing zero static force. This issue is recently addressed in (Caple et al., 2016) in which a method is presented to enable the AMB to adapt its bias distribution to produce a zero static force, using a low frequency periodic bias carrier signal. The idea is conceptually sound, although simulation results show that several issues regarding this approach still needs to be addressed. One issue is that a residual coupling between the carrier signal and the control signal can result to unintended excitation of lightly damped flexible modes. Another example of hybrid bearing can be found in (Jeong et al., 2016). Here the AMB and controllers is designed to operate along with air foil bearings.

Adaptive controllers to detect and compensate for CCS forces have been reported. Wurmsdobler & Springer (1996) presents simulation results of a rotordynamic system supported by AMBs and subjected to a time invariant CCS magnitude. An observer is constructed and shows the ability to track the changing CSS magnitude over time. A controller designed using pole placement technique was designed to work along with the observer. Similar work is shown in (Lang et al., 1996) but here the unknown CSS parameter of a rotor are estimated on-line by a standard least-square estimator along with a time-varying forgetting factor. Simulation results of adaptive control in parallel with a baseline PID controller is considered in (Hirschmanner & Springer 2002) of

[DOI: 10.1299/mej.16-00618]

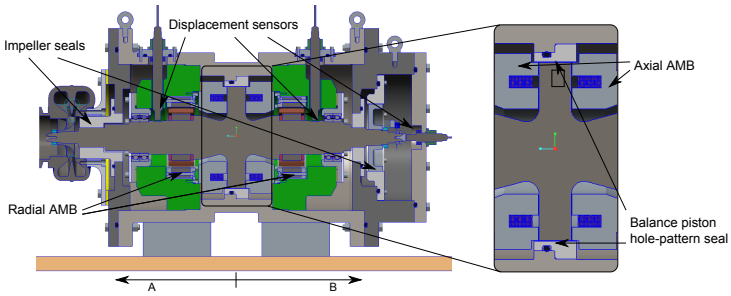

Fig. 1 Cross section of the turboexpander testrig. An enlargement of the center section section shows the balance piston on which the axial bearings acts and where the hole-pattern seal are placed

a non-linear simulation model. Here the controller is designed to compensate changing CCS magnitude over time as well as to compensate for periodic disturbance forces. The work shows that the adaptive controller can handle much larger amplitudes of CCS forces than a LTI LQR compensator. However, only numerical studies have been carried out so far on the adaptive controllers. Stability and robustness is in general hard to guarantee in adaptive control systems, which of course is crucial for implementation in industrial applications.

This paper presents a mathematical model of a high speed turboexpander unit used for cryogenic air separation and the design of model-based feedback controllers for the pair of radial AMBs responsible for magnetic levitation and stabilization. One hole-pattern seal is placed across a balance piston in the center of the turboexpander generating a thrust force to oppose the sum of the impeller thrust forces. The seal dynamics are considered uncertain and further changes due to operating conditions. A robust LTI controller is designed using μ synthesis to compensate for uncertain seal forces and is compared to an $\mathcal{H}_\infty$ controller based on the nominal model. For improved performance, an LPV controller is designed, which schedules controllers depending on the rotational speed. A performance comparison between the controllers based on the nominal model, the uncertain system representation and parameter varying model is presented.

2. Modelling of the Turboexpander

A cross-section schematic of the turboexpander investigated is shown in Fig. 1. The turboexpander essentially consists of a shaft levitated using axial and radial AMBs, and three annular seals. It is assumed that the only significant forces acting on the rigid rotor are the left and right side radial AMB and the seal in the center. The displacement sensors are placed close to the AMBs. The axial placement of the sensors and actuators are denoted by A and B, indicated in Fig. 1, with subscript x, y indicating the radial movement in the global horizontal and vertical coordinate system. The analysis will be focused on rotor lateral movements; for simplicity the rotor axial movements will not be investigated. The term AMB will therefore refer to the radial AMBs in the rest of this work.

2.1. AMB Model

The model of the magnetic bearing is simplified to describe the forces acting on the rotor as function of the rotor lateral displacements to AMB s_x and the control current i_x. The linearised expression of the forces are given as

$$f_b(i_x, s_x) = K_i i_x + K_s s_x \tag{1}$$

where K_i are K_s are constants. The dynamics of the electromechanical system, including the inductance of the coil and the amplifiers, is approximated as a first order system with a 3 dB cut-off frequency ω_c at 1.5 kHz, denoted G_{act}.

[DOI: 10.1299/mej.16-00618]

$$G_{act} = \frac{K_i}{1 + \frac{s}{\omega_c}} \tag{2}$$

2.2. Model of Shaft

The rotating shaft is modelled using the Finite Element (FE) method and Bernoulli-Euler beam theory taking into account the gyroscopic effects of the shaft and discs (Nelson, 1980). The shaft model is discretized into 40 node points with 4 degrees of freedom each, i.e. x and y direction, and the rotation around the x and y axes, which yields 320 states in total. The full order rotordynamic system G_f consisting of the finite element model of the shaft and negative stiffness forces from the AMB can be written in state space form

$$\dot{x}_f = A_f x_f + B_f u, \quad y = C_f x_f \tag{3}$$

Using modal truncation techniques, real left and right modal transformation matrices are obtained which transform the full order FE system to a reduced form, shown in Eq. (4). The first bending mode of the shaft lies at approx. 1 kHz. Since this is substantially above the frequency range of interest in this work, the shafts is assumed rigid and all bending modes have thus been removed in the reduced order model. The FE model is selected though for generality and for possibility of to extend the model to included some of the bending modes if needed.

$$x = T_L{}^T x_f, \quad A = T_L{}^T A_f T_R, \quad B = T_L{}^T B_f, \quad C = C_f T_R \tag{4}$$

2.3. Seal Model - CFD vs Bulkflow

CFD and Bulkflow methods are typically used to obtain the static and dynamic properties of seals. CFD has been shown to be able to find seal forces even with complex geometries but can be extremely time demanding and computational heavy, since full 3D flow and pressure fields have to be calculated. On the other hand Bulkflow models are much simpler since these are based on simplified 1D models heavily linked to empirical parameters. The results of both CFD and Bulkflow modelling are usually validated against experimental data. Industrial software like ISOTSEAL is based on Bulkflow models and is widely used in the industry. Independent of the modelling approach, the dynamic seal forces are usually represented by their linearised force coefficients: stiffness, damping and sometimes mass matrices:

$$\begin{bmatrix} f_x \\ f_y \end{bmatrix} = \begin{bmatrix} K & k \\ -k & K \end{bmatrix} \begin{bmatrix} x \\ y \end{bmatrix} + \begin{bmatrix} C & c \\ -c & C \end{bmatrix} \begin{bmatrix} \dot{x} \\ \dot{y} \end{bmatrix} + \begin{bmatrix} M & 0 \\ 0 & M \end{bmatrix} \begin{bmatrix} \ddot{x} \\ \ddot{y} \end{bmatrix} \tag{5}$$

This model has a symmetric structure since the shaft is assumed to be approximately in the center. The sign difference of the cross coupled stiffness and damping coefficients is commonly known to cause instability. The coefficients are a function of the rotational speed and the excitation frequency. The seal used in the turboexpander application is a hole-pattern seal with coefficients taken from (Nielsen et al., 2012). The coefficients are given for a constant rotational speed of 20,200 RPM and with excitation frequencies varying from 20-300 Hz, and the specifications are stated in Fig. 2. The stiffness and damping coefficients are shown in Fig. 3 & 4 and are found using CFD, ISOTSEAL and experimental work originating from Turbolab (Nielsen et al., 2012; Dawson et al., 2002). The estimated model uncertainty between the CFD and experimental results is marked as the grey area in the figures, and this information is utilized when synthesizing robust controllers. In the case of using ISOTSEAL as a nominal seal model, larger uncertainties must be expected and hence included in the uncertainty model.

3. Robust Control Design

In this section a robust controller is designed using μ synthesis to handle realistic uncertainties and changes in the seal dynamics. This controller is compared to a $\mathcal{H}_\infty$ controller based on a nominal system model.

3.1. Control Design Objectives and Challenges

- Due to model uncertainties and changes in operational conditions, the controller should deliver robust performance to plants with seal stiffness and damping coefficients within ±40 % of the nominal values. All

[DOI: 10.1299/mej.16-00618]

Parameter	Value
Seal Length [mm]	85.70
Rotor Diameter [mm]	114.74
Inlet Clearance [mm]	0.2115
Exit Clearance [mm]	0.2102
Hole Depth [mm]	3.30
Hole Diameter [mm]	3.18
Hole Area Ratio	0.684
Rotor Speed [rpm]	20200
Inlet Pressure [bar]	70.0
Outlet Pressure [bar]	31.5
Res. Temperature [C]	17.4
Preswirl	0

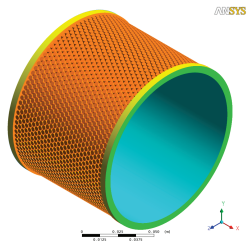

Fig. 2 Hole-pattern seal specification and parameters (left) & fluid structure (right). From (Nielsen et al., 2012)

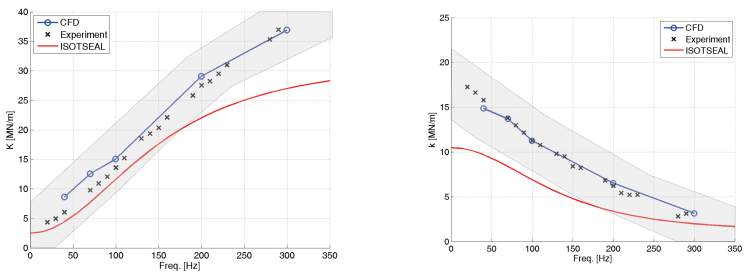

Fig. 3 Hole-pattern seal direct and cross coupled stiffness coefficients obtained using CFD, Experiment and ISOTSEAL. Figures adapted from (Nielsen et al., 2012)

8 coefficients are considered uncertain independent to each other, i.e. although, for example, the direct coupled stiffness K has the same nominal value in both vertical and horizontal directions they have independent uncertainties. Mass coefficients are neglected since the fluid is air (Nielsen et al., 2012).

- The system should be robust against other unmodelled dynamics and against system changes over time due to wear and ageing. These robustness criteria are specified in ISO 14839-3, which states that the closed loop sensitivity (disturbance to error) should be less than 3 for all frequencies in order to be classified as Zone A (ISO 14839-3, 2006).
- Unbalance response should be less than $10\,\mu$m for the complete operating range, assuming the shaft is balanced according to the G2.5 standard.
- The control currents should stay well within the actuation limits of ± 5 A.
- Settling time should be less than 20 ms for step disturbances on input (force) for good force disturbance rejection.

3.2. Uncertainty Representation

The nominal rotordynamic model consists of the reduced order shaft model, the negative stiffness from the AMBs and the nominal stiffness and damping from the seals. The perturbation model G_{fi} is constructed using the nominal model and the uncertainty representation, which are combined and written in LFT form, illustrated in Fig. 5. Here Δ is a 8×8 diagonal matrix representing the normalized uncertainties and satisfy $\|\Delta\|_\infty \leq 1$. G_{fi} can be written in state space form, as shown in Eq. (6), where A, B and C are the nominal system matrices. Here the input and output matrices are extended from the nominal model to include the input and output mapping B_Δ and C_Δ. Note that no extra system dynamics is added since the LFT only changes the

[DOI: 10.1299/mej.16-00618]

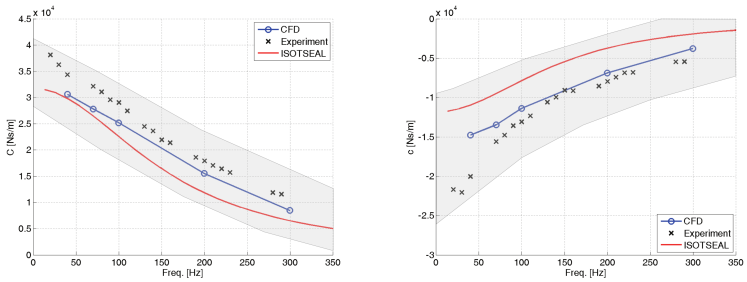

Fig. 4 Hole-pattern seal direct and cross coupled damping coefficients obtained using CFD, Experiment and ISOTSEAL. Figure adapted from (Nielsen et al., 2012)

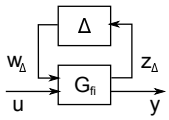

Fig. 5 Uncertain plant representation using upper LFT, $G_{unc} = \mathcal{F}_u\left(G_{fi}, \Delta\right)$

nominal system matrix A.

$$G_{fi} = \left[\begin{array}{c|cc} A & B_\Delta & B \\ \hline C_\Delta & 0 & 0 \\ C & 0 & 0 \end{array}\right] \tag{6}$$

B_Δ and C_Δ are constructed as follows and a thorough description of this process can be seen in (Lauridsen et al., 2015). It can be shown that changes in stiffness (or damping) in a single direction at e.g. A_x corresponds to a change in a single column of system matrix A, which corresponds to the node j where the stiffness (or damping) is altered.

$$A_{\Delta_f} = \begin{bmatrix} 0 & \dots & 0 & a_{1,j} & 0 & \dots & 0 \\ 0 & \dots & 0 & a_{2,j} & 0 & \dots & 0 \\ \vdots & \ddots & \vdots & \vdots & \vdots & \ddots & \vdots \\ 0 & \dots & 0 & a_{i,j} & 0 & \dots & 0 \end{bmatrix} \tag{7}$$

The change of the system matrix in reduced form A_Δ is found using the same modal truncation matrices as used to reduce the nominal system, as shown in Eq. (8). It is noted that the applicability of using the same modal truncation matrices to reduce the matrix representing the change in system dynamics – as were used for reducing the nominal system matrix – is based on assumption rather than proof, however, this assumption has been shown to hold well in practice. A_{Δ_f} in Eq. (7) can also be written as a column vector B_{Δ_f} and a row vector C_{Δ_f} and the change/uncertainty Δ. The input mapping B_Δ and output mapping C_Δ of the uncertainties are thus given as shown in Eq. (10). Repeating this process 8 times (one for each stiffness and damping parameter) and assembling the coloums of B_Δ and rows of C_Δ and making Δ an 8×8 diagonal matrix, yields the complete uncertainty representation.

$$A_\Delta = T_L\, A_{\Delta_f}\, T_R \tag{8}$$

$$= T_L B_{\Delta_f}\, \Delta\, C_{\Delta_f} T_R \tag{9}$$

$$= B_\Delta\, \Delta\, C_\Delta \tag{10}$$

[DOI: 10.1299/mej.16-00618]

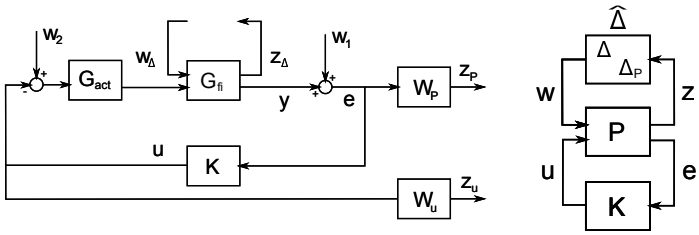

Fig. 6 Left figure: Interconnection of actuator model G_{act}, rotordynamic model with uncertainty representation G_{fi}, performance weight functions W_P and W_u, and controller K. Right figure: interconnection rearranged to the augmented system P, externally connected to the controller and $\hat{\Delta}$ containing Δ for uncertain plant representation and Δ_P as full complex perturbation for performance specification.

3.3. Robust Control Design Interconnection and Weight Functions

The interconnection in Fig. 6 is used for robust controller synthesis, This is similar to the structure suggested in (Balini et al., 2012). W_p shapes the sensitivity functions i.e. the relationship from input and output disturbances W_1 and W_2 to the displacement error e. W_p is formulated with the structure suggested in (Skogestad & Postlethwaite, 2007)

$$W_p = \frac{\frac{s}{M} + w_B}{s + w_B A} \tag{11}$$

The inverse of W_p is shown in Fig. 7 and the weighting function has multiple purposes: I) Set a low sensitivity at low frequencies to obtain an integral effect, which eliminates steady state error in position reference. A indicates the steady state error and is set to $\frac{1}{1000}$. II) M indicates the maximum peak of the sensitivity functions and is tuned to obtain an peak less than 3 (or 9.5 dB) for robustness. III) The crossover frequency w_B indicates the desired bandwidth of the closed loop system (Skogestad & Postlethwaite, 2007). This parameter is tuned to achieve a disturbance settling time of less than 20 ms. The weight W_u is a high-pass filter with a crossover frequency at 1.4 kHz which limits the bandwidth of the control action. The inverse of W_u is shown in Fig. 8.

3.4. Robust Control Synthesis

Fig. 6 (right) shows the interconnection rearranged for controller synthesis such that P is the fixed augmented plant. Note that Δ for uncertain plant representation and Δ_P (full perturbation matrix representing the $\mathcal{H}_\infty$ performance specification) are collected into the diagonal elements of $\hat{\Delta}$. Hence synthesising a controller can be done by finding a controller that minimises the ∞ norm of the transfer function from w to z, formulated as a lower LFT

$$\gamma = \|F_l(P, K)\|_\infty \tag{12}$$

The uncertainty is scaled to 1, meaning that robust performance is met when γ is below 1. γ larger than 1 means that either the uncertainty, the performance weights or both should be scaled by $\frac{1}{\gamma}$ for the solution to hold. Solving Eq. (12) using $\mathcal{H}_\infty$ synthesis resulted in a $\mathcal{H}_\infty$ controller with γ of 618. Since this is far above 1, this controller does not guarantee robust performance.

Reduce Conservatism by D-scaling Using $\mathcal{H}_\infty$ directly on the problem in Fig. 6 (right) is known to suffer from conservatism since the $\hat{\Delta}$ would be considered to be a full order complex perturbation. This is commonly solved using DK-iteration, where a scaling matrix D is found, scaling w and z by D and D^{-1} to reduce the conservatism. The D matrix is found using μ synthesis in Matlab which results in a performance index of 1.1, meaning that the system nearly guarantees robust performance.

3.5. Results

The input and output closed loop sensitivity functions, S_i and S_o, with parameter variations of ±40 % relative to the nominal plant are shown in Fig. 7 (left) using an $\mathcal{H}_\infty$ controller based on a nominal plant and

[DOI: 10.1299/mej.16-00618]

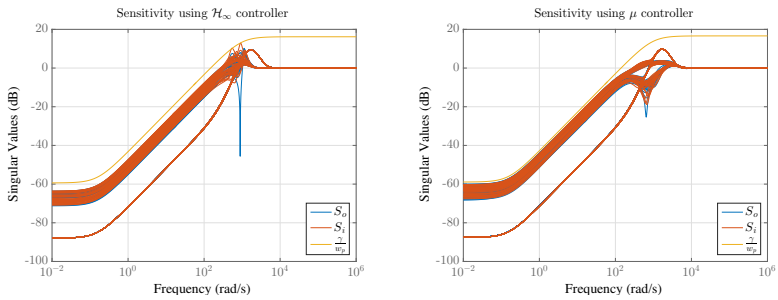

Fig. 7 Closed-loop sensitivity using $\mathcal{H}_\infty$ synthesized controller based on nominal plant (left) and using μ synthesized controller based on perturbation plant (right)

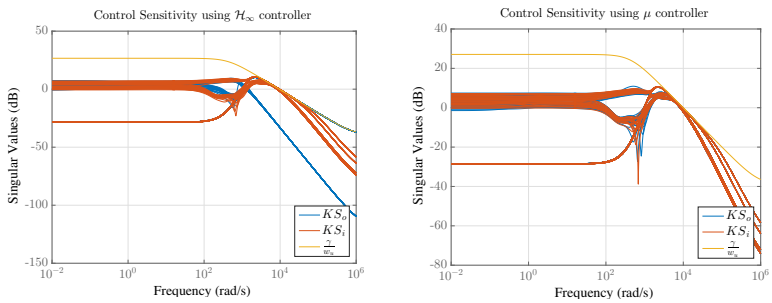

Fig. 8 Closed-loop control sensitivity using $\mathcal{H}_\infty$ synthesized controller based on nominal plant (left) and using μ synthesized controller based on perturbation plant (right)

is shown in Fig. 7 (right) using μ synthesized controller based on the uncertain plant representation. The sensitivity peak is above 10 dB using the $\mathcal{H}_\infty$ controller based on nominal plant, and thus does not meet the requirements. The closed loop control sensitivity functions, KS_i and KS_o, with parameter variations of ±40 % relative to nominal plant are shown in Fig. 8 (left) using an $\mathcal{H}_\infty$ controller based on a nominal plant and is shown in Fig. 8 (right) using μ synthesized controller based on the uncertain plant representation. Both controllers stays within the weight function limits and stays within the bandwidth requirements.

Fig. 9 and Fig. 10 shows the displacement and control currents of an impulse response of the closed loop system. Nodes A_x, A_y, B_x and B_y are the locations of AMB A and B. The impulse disturbance has an amplitude of 100 N and length of 2 ms and enters through node A_x. Multiple simulations are shown for different parameter variations within ±40 %. It is clearly seen that the μ controller delivers consistent robust performance, whereas the $\mathcal{H}_\infty$ controller does not, even turning unstable for some parameter variations. It is observed that although the system is disturbed in x-direction, there is also movement in y-direction due to cross-coupling from the seal and gyroscopic forces.

Worst Case Unbalance Response The compliance function, denoted $G_f(\Delta)$, maps the external force disturbance input to the rotor displacement

$$G_f(\Delta) = \mathcal{F}_u\left(G_{fi}, \Delta\right) S_i \tag{13}$$

A low compliance function indicates good force disturbance rejection. Finding the maximum singular values of the compliance function multiplied by the unbalance force $F_u(\Omega)$ yields a conservative indication of the worst

[DOI: 10.1299/mej.16-00618]

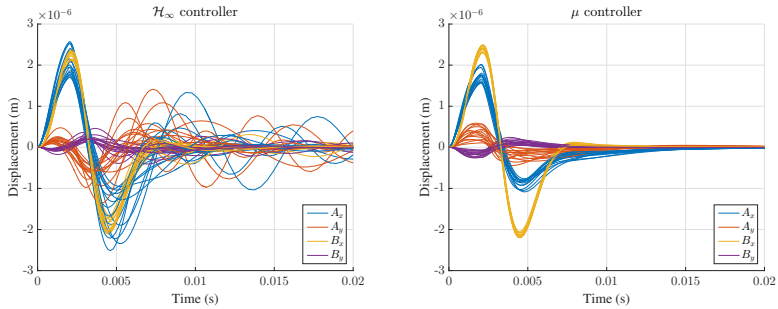

Fig. 9 Impulse response using $\mathcal{H}_\infty$ synthesized controller based on nominal plant (left) and using μ synthesized controller based on perturbation plant (right)

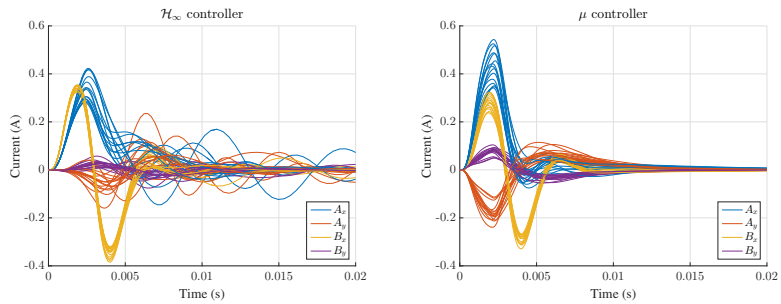

Fig. 10 Control action in response to an impulse disturbance using $\mathcal{H}_\infty$ synthesized controller based on nominal plant (left) and using μ synthesized controller based on perturbation plant (right)

case unbalance response y_{max} due to uncertain seal forces

$$y_{max} = \bar{\sigma}(G_f(\Delta))F_u(\Omega) \quad \forall\Omega \tag{14}$$

Where Ω is the rotational speed and $F_u(\Omega)$ is given by the $G2.5$ unbalance specification. Solving (14) numerically for Ω within the range 20-300 Hz, using the μ controller, shows that displacement stays within 4 μm for ±40 % parameter variations and thus meets the requirements.

4. LPV Control Design

A Linear Parameter Varying (LPV) controller is synthesized using the Linear Matrix Inequality (LMI) formulation from (Apkarian & Adams, 1998) and using the control interconnection and weighting functions shown in Fig. 6. However, instead of using the perturbed plant representation G_{fi}, a LPV plant is used for control synthesis and simulation. For this case study it is assumed that the coefficients for the hole pattern seal over the excitation frequency range of 20-300 Hz represents the synchronous coefficients for the rotational speed range of 20-300 Hz.

Results of Spin-up Test - LPV vs μ Controller A spin-up simulation response, demonstrating the performance of the LPV and μ controller over the operating range of 20-300 Hz with a duration of 1 s, is carried out. The μ controller is designed for an operational speed of 140 Hz and to deliver robust performance to plants with seal stiffness and damping coefficients within ±40 % of the nominal values. Step disturbances are applied every 50 ms,

[DOI: 10.1299/mej.16-00618]

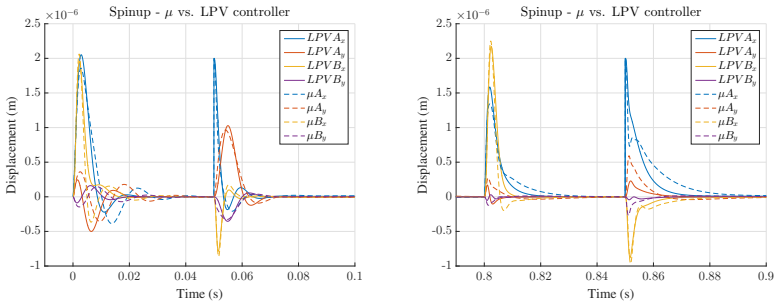

Fig. 11 Spin-up test time response comparison, using LPV and μ controllers. A force input disturbance of 100 N enters after 0 s and 0.8 s and a displacement output disturbance of 2 μm enters after 0.05 s and 0.85 s, both at A_x. The μ controller is designed for operation at 140 Hz rotational speed.

alternating between acting on the input and output signals. A force input disturbance of 100 N enters after 0 s and a displacement output disturbance of 2 μm enters after 50 ms, both at A_x. The μ controller performs, not surprisingly, best near its design operational point at 140 Hz and worse when operating away from it. Worst case performance of the μ controller is illustrated in Fig. 11 (left) for low operational speeds in the beginning of the spinup and in Fig. 11 (right) for high operational speeds. It is observed, that for these operational ranges, the LPV controller has a faster settling time, below 20 ms as required, where the μ controller takes longer time. Also, the response is more oscillatory in the case of the μ synthesized controller compared to the LPV controller.

Fig. 12 shows S_o using LPV and μ controllers for plant variations due to plant changes in the operational speed range of 20-300 Hz. The plot confirms worse performance of the μ synthesized controller, i.e: I) Oscillatory behaviour due to higher peak of S_o. II) Slower disturbance rejection due to lower crossover frequency.

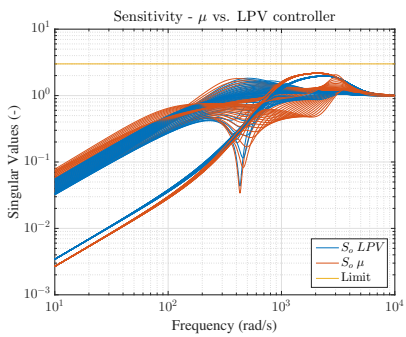

Fig. 12 Closed loop output sensitivity using LPV and μ controllers for plant variations due to change in operational speed in the range 20-300 Hz. The yellow line indicates the ISO14839-3 upper limit.

5. Conclusion

Robust control design is suggested for handling uncertain seal forces in AMB systems. Significant performance improvement is shown for robust control, incorporating model uncertainty, compared to nominal model based control. This clearly demonstrates the need for incorporating uncertainties into the model based con-

[DOI: 10.1299/mej.16-00618]

troller design process to obtain robust performance. The μ controller is minimally conservative to the known uncertainty structure.

In the case of significant frequency dependence of the dynamic seal characteristics, as for the hole pattern seal, combined with large variations in operational speed, it is more challenging to design a single robust LTI controller that provides satisfactory performance over the complete operational range. This paper demonstrates the performance improvement an LPV controller can deliver, compared to a single robust LTI controller, using the nominal plant model. The best robust controller that was designed for the whole rotational speed range used a nominal plant representation for the seal dynamics using the average speed of 140 Hz. While this controller actually meets the ISO requirements for the complete operating range, this controller shows a decreased performance, especially away from its operating point. For simplicity, robustness due to uncertainties is not considered when comparing the μ and LPV controller over the complete operational range. It would, however, be more challenging to design controllers which deliver satisfactory performance for plants that can change both due to the operational speed and uncertainties. The uncertainty representation can be integrated into the LPV synthesization, although this would make the synthesization computationally heavier and possibly more sensitive to numerical instabilities.

One of the advances by using the LPV framework for synthesizesing controllers is the possibility to guarantee stability due to fast changes in plant dynamics simultaneously with fast switching between controllers. The LPV controller in this paper is designed to guarantee stability due changes that can be infinitely fast. This typically introduces some conservativeness since the rotational speed changes in the physical plant are in reality limited due to the inertia of the shaft. Thus, the performance of the LPV controller can possibly be improved by imposing boundaries on the velocity. This can be done by making the Lyapunov function variables depended on the scheduling parameter. This would, however, increase the complexity of the synthesization.

References

Apkarian, P. and Adams, R. J., Advanced gain-scheduling techniques for uncertain systems, Control Systems Technology, IEEE Transactions on Vol.6, No.1 (1998), pp.21-32.

Balas, G. J. and Young, P. M., Control design for variations in structural natural frequencies, Journal of Guidance, Control and Dynamics Vol.18, No.2 (1995), pp.325-332.

Balini, H. M. N. K., Witte, J. and Scherer, C. W., Synthesis and implementation of gain-scheduling and LPV controllers for an AMB system, Automatica Vol.48, No.3 (2012), pp.521-527.

Bleuler, H., Cole, M., Keogh, P., Larsonneur, R., Maslen, E., Okada, Y. and Traxler, A., Magnetic bearings: theory, design, and application to rotating machinery (2009), Springer Science & Business Media.

Caple, M., Maslen, E., Nagel, J. and Wild, J., Control of an AMB to Zero Static Force, Proceedings of the 15th International Symposium on Magnetic Bearings (2016).

Cloud, C., Li, G., Maslen, E. H., Barrett, L. E. and Foiles, W. C., Practical applications of singular value decomposition in rotordynamics, Australian journal of mechanical engineering, Vol.2, No.1 (2005), pp.21-32.

Dawson, M., Childs, D., Holt, C., Phillips, S., Theory Versus Experiments for the Dynamic Impedances of Annular Gas Seals: Part 2 - Smooth and Honeycomb Seals, ASME J. Eng. Gas Turbines Power Vol.24 (2002), pp.963-970.

Hirschmanner, M., and Springer, H., Adaptive vibration and unbalance control of a rotor supported by active magnetic bearings, Proceedings of the 8th International Symposium on Magnetic Bearings (2002).

ISO 14839-3, Vibration of rotating machinery equipped with active magnetic bearings Part 3: Evaluation of stability margin, International Standards Organization (2006).

Jeong, S., Doyiung, J., Yongbok, L., Rotordynamic Behavior and Rigid Mode Vibration Control by Hybrid Foil-Magnetic Bearing System, Proceedings of the 15th International Symposium on Magnetic Bearings (2016).

Lang, O., Wassermann, J. and Springer, H., Adaptive vibration control of a rigid rotor supported by active magnetic bearings, Journal of engineering for gas turbines and power, Vol.118, No.4 (1996), pp.825-829.

Lauridsen, J. S., Sekunda, A. K., Santos, I. F. and Niemann, H., Identifying parameters in active magnetic bearing system using LFT formulation and Youla factorization, In: 2015 IEEE Conference on Control

[DOI: 10.1299/mej.16-00618]

Applications (2015), pp.430-435.

Maslen, E., Cloud, C., Hauge, T., Tarald, S. and Lie, J., Unbalance Response Assessment of a Subsea Compressor, Proceedings of the 13th International Symposium on Magnetic Bearings (2012).

Mushi, S. E., Lin, Z., Allaire, P. and Evans, S., Aerodynamic cross-coupling in a flexible rotor: Control design and implementation, Proceedings of the 11th International Symposium on Magnetic Bearings (2008).

Nelson, H. D., A finite rotating shaft element using Timoshenko beam theory, Journal of mechanical design, Vol.102, No.4 (1980), pp.793-803.

Nielsen, K. K., Joenck, K. and Underbakke, H., Hole-Pattern and Honeycomb Seal Rotordynamic Forces: Validation of CFD-Based Prediction Techniques, Journal of Engineering for Gas Turbines and Power Vol.134, No.12 (2012).

Pesch, A. H. and Sawicki, J. T., Stabilizing Hydrodynamic Bearing Oil Whip With mu-Synthesis Control of an Active Magnetic Bearing, In: ASME Turbo Expo 2015: Turbine Technical Conference and Exposition. American Society of Mechanical Engineers (2015), V07AT31A029-V07AT31A029.

Schonhoff, U., Luo, J., Li, G., Hilton, E. and Nordmann, R., Implementation results of mu-synthesis control for an energy storage flywheel test rig, Proceedings of the 8th International Symposium on Magnetic Bearings (2000).

Skogestad, S. and Postlethwaite, I., Multivariable feedback control: analysis and design, Vol. 2 (2007), New York: Wiley.

Wurmsdobler, P. and Springer, H., State space adaptive control for a rigid rotor suspended in active magnetic bearings, Proceedings to the 5th International Symposium on Magnetic Bearings (1996), pp.185-190.

Zhou, K., Doyle, J. C. and Glover, K., Robust and optimal control (1996), New Jersey: Prentice hall.

[DOI: 10.1299/mej.16-00618]

Chapter 5

On-site Identification of Dynamic Annular Seal Forces in Turbo Machinery Using Active Magnetic Bearings - An Experimental Investigation

Publication P4

This paper has by the 13th of March 2017 been submitted for journal publication in the ASME Journal of Engineering for Gas Turbines and Power.

On-site Identification of Dynamic Annular Seal Forces in Turbo Machinery Using Active Magnetic Bearings - An Experimental Investigation

Jonas S. Lauridsen*
PhD student
Department of Mechanical Engineering
Technical University of Denmark
Email: jonlau@mek.dtu.dk

Ilmar F. Santos†
Professor
Department of Mechanical Engineering
Technical University of Denmark
Email: ifs@mek.dtu.dk

Significant dynamic forces can be generated by annular seals in rotordynamics and can under certain conditions destabilize the system leading to a machine failure. Mathematical modelling of dynamic seal forces are still challenging, especially for multiphase fluids and for seals with complex geometries. This results in much uncertainty in the estimation of the dynamic seal forces which often leads to unexpected system behaviour.

This paper presents the results of a method suitable for on-site identification of uncertain dynamic annular seal forces in rotordynamic systems supported by Active Magnetic Bearings (AMB). An excitation current is applied through the AMBs to obtain perturbation forces and a system response, from which, the seal coefficients are extracted by utilizing optimization and a-priori information about the mathematical model structure and its known system dynamics. As a study case, the method is applied to a full-scale test-facility supported by two radial AMBs interacting with one annular center mounted test-seal. Specifically, the dynamic behaviour of a smooth annular seal with high preswirl and large clearance (worn seal) is investigated in this study for different excitation frequencies and differential pressures across the seal. The seal coefficients are extracted and a global model on reduced state-space modal form are obtained using the identification process. The global model can be used to update the model based controller to improve the performance of the overall system. This could potentially be implemented in all rotordynamic systems supported by AMBs and subjected to seal forces or other fluid film forces.

*Address all correspondence related to ASME style format and figures to this author.

†Address all correspondence related to ASME style format and figures to this author.

1 Introduction

Bulkflow and Computational Fluid Dynamics (CFD) methods are typically used to obtain the static and dynamic properties of seals. The development of the Bulkflow code goes back to the 1980s and is still in development [1–7]. This technique usually assumes that the flow through the seals can be represented using one-dimensional partial differential equations coupled to the equation describing the rotor lateral motion. In many cases, as for example for complex seal geometries, these simplified 1D assumptions do not hold and parameter adjustments and corrections are needed. Thus, the Bulkflow code is usually heavily linked to empirical parameters and lacks generality. The Bulkflow codes are however widespread in industrial rotordynamic software such as ISOTSEAL and XLTRC. The Bulkflow codes due to having a simple model structure are computationally inexpensive which, in that regard, makes them attractive compared to CFD. CFD models have on the other hand been shown to be able to find seal forces even with complex geometries without tuning empirical constants, which makes them more general than Bulkflow codes [8]. CFD simulations can be extremely time demanding and computationally heavy, since full 3D flow and pressure fields have to be calculated in time. That said, CFD methods are becoming increasingly popular as computational power in computers rapidly increases [9].

Modelling of seal forces can be very challenging. This is made clear by a survey conducted in 2007, where 20 survey participants from both industry and academia were asked to predict the dynamics of a gas labyrinth seal and consequently the rotordynamic behaviour [10]. The seals dynamics was predicted using Bulkflow and CFD methods. The survey showed large variations in the results and emphasises

the need for continuous efforts in modelling and uncertainty handling of seal forces, even for single phase flow condition, as presented in the article. Multiphase flows, i.e. where the fluid is a mixture of gas and liquid, add further complexity to the modelling and, consequently, higher uncertainties in the prediction of the seal dynamics are to be expected.

There are two usual ways of experimentally identifying dynamic force coefficients of seals: i) by keeping the lateral movements of the rotor constrained while shaking the seal housing or ii) by shaking the rotor laterally while keeping the seal housing constrained. Examples of method i are more common and thoroughly documented in the literature with testing performed at university laboratories [11–13]. Examples of method ii where AMBs are used to identify and characterize fluid film forces are reported in [9, 14–19]. The design of a full scale magnetic bearing test-facility to levitate and excite the rotor with an annular test-seal mounted in the center of the rotor is presented in [14]. This work also presents the identification results of dynamic force coefficients of a labyrinth seal for high pressure turbomachinery. The labyrinth seal forces are compared with CFD results in [9]. Identification of seal forces in a flexible rotor system using AMBs is shown in [19]. The AMB forces are measured using fiber-optic strain gauges that are bonded to the stator poles of the AMBs. Stiffness and damping coefficients are determined using a frequency domain identification method, utilizing an FE rotor model which is adjusted to match the characteristics of the test rotor in free-free conditions. The use of AMB for identification of fluid film forces of a journal bearing have been investigated among others in [15–18]. Here the forces are measured by use of hall sensors and the dynamics of the journal bearing is represented by mass, stiffness and damping matrices which are a function of the rotational speed and pocket pressure ratio.

This paper presents a force calibration free identification scheme for updating parameters in a global rotordynamic model with AMBs and seal forces. This method is applied to a test-facility and the results are shown. Thus, no force transducers or calibration equipment are needed to characterize magnetic forces like those suggested in [9, 14–16, 19]. The idea, though, is similar to the plausibility check, shown in [9], where the seal dynamics are identified as the residual dynamics between the global model and a baseline AMB-rotor model, assuming the baseline model is a-priori known. Hence, the approach in [9] still relies on traditional modelling and calibration of the AMB-rotor system. The method, presented in this paper is a general way to identify all uncertain/unknown parameters of an AMB-rotor-seal system systematically without changing the model structure or model order. This is particular useful in applications in which the seal forces are hard to model in advance, like for example in subsea applications in which the fluid can be a mixture between gas and liquid. In these cases it would be extremely useful to identify the forces in-situ to prevent system failure by improved model capabilities or to update the controller of the AMBs to improve stability and performance.

2 Experimental Facilities

The experimental facilities used for this work consists of a AMB-based rotordynamic test bench with a seal house presented in Fig. 1 and a cross-section view in Fig. 2. Two AMBs radially support a symmetric rigid rotor which is driven by an asynchronous motor through an intermediate shaft and a flexible coupling, as seen in Fig. 3. Angular contact ball bearings, supporting the intermediate shaft housed in the intermediate shaft pedestal, compensate for axial forces acting on the rotor. The radial AMBs are of the eight pole heteropolar type, see Fig. 4.

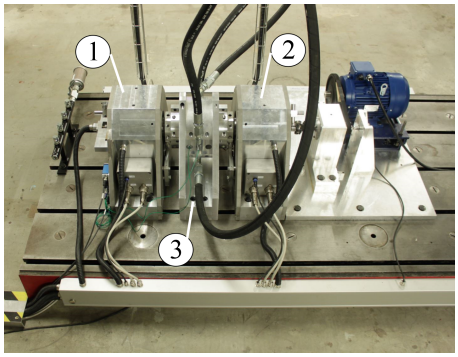

Fig. 1. Test facility overview. ① AMB A, ② Seal house, ③ AMB B. Figure adapted from [20].

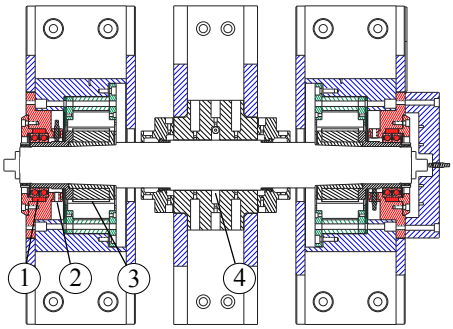

Fig. 2. Full section view of testrig with ① backup bearing, ② displacement sensor, ③ rotor and stator of the AMB,④ seal house. Figure adapted from [20].

In Fig. 4 both the global reference frame denoted by x, y and the actuator reference frame denoted by ζ, η are intro-

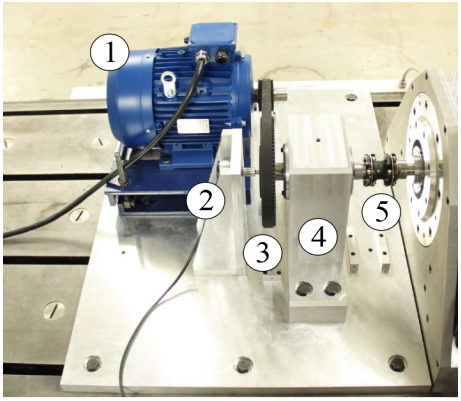

Fig. 3. Connecting the motor to the shaft. ① motor, ② Encoder, ③ Belt drive, ④, Intermediate shaft pedestal, ⑤ Flexible coupling. The figure is adapted from [20].

duced. The actuators are tilted 45° with respects to the global reference frame. Throughout the paper subscripts ζ, η are used to denote quantities belonging to the actuators aligned with the respective axes of the stator reference frame. The two AMB stators have been manufactured using two different production methods yielding different geometric tolerances for the AMBs. The AMBs are supplied by four commercially available 3 kW switch-mode laboratory amplifiers. The AMBs are controlled using a standard decentralized PID scheme, which would typically be used in industrial applications. The rotor is kept in the center of the seal, which is slightly offset from the magnetic/effective center of the AMBs.

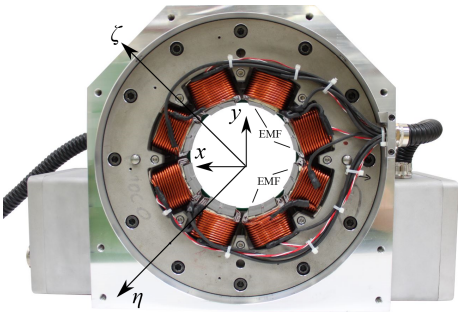

Fig. 4. Test bench AMB showing the AMB actuator and global reference frames. The figure is adapted from [21].

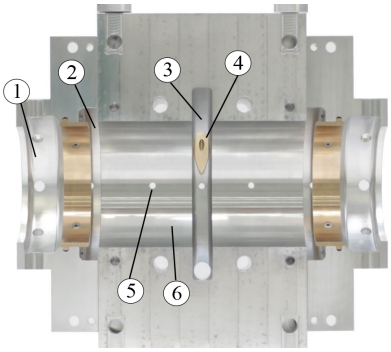

Fig. 5. Cross section of the seal house. ① secondary discharge cavity, ② discharge cavity,③ inlet injection cavity,④ inlet nozzle,⑤ pressure sensor,⑥ seal surface. The figure is adapted from [21].

The seal, mounted in the center of the shaft, is installed as a back-to-back configuration, hence two symmetrical seals are placed with the idea to cancel out possible axial fluid film forces. The seal housing and its features are illustrated in Fig. 5. It is designed with primary and secondary discharge seals to avoid any liquid entering the AMBs, since the test facility is designed to operate with both gas, liquid and mixtures between gas and liquid. The fluid used in this article is gas, though. The fluid is injected by four highly angled nozzles to obtain a high preswirl ratio, hence the fluid is already rotated at the inlet of the seal. A cross section of the injection system is shown in Fig. 6.

A full description of the test facility can be found in [20], which also presents the calibration of the complete system. Design parameters for the rotordynamic test bench can be found in Table 1.

3 Identification

The idea is to establish a precise global mathematical model of the test-facility consisting of an updated nominal model representation. Hence, a nominal model is constructed using conventional modelling methods and where the uncertain or unknown coefficients are identified in-situ.

Table 1. Design parameters for the rotordynamic test bench

Rotor length	860	mm
Rotor assembly mass	69	kg
1st rotor bending mode @	550	Hz
Stator inner diameter	151	mm
Nominal radial air gap	0.5	mm
Winding configuration	N-S-S-N-N-S-S-N	[-]
Number of windings	36	[-]

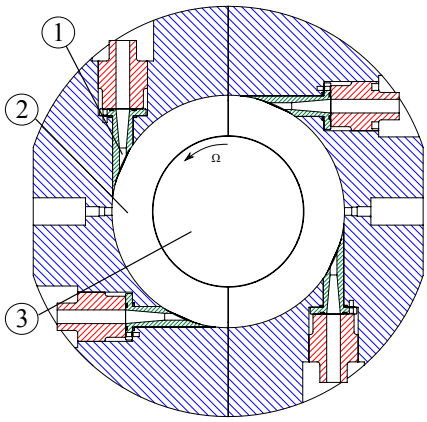

Fig. 6. Cross section of the seal house at the inlet cavity section. ① inlet injection nozzle, ② inlet cavity,③ shaft. The figure is adapted from [21]

Since the mathematical structure is kept intact and the identified parameters have physical meanings, this method is preferred over e.g blackbox modelling. The global model can for example be used to investigate the performance of the test-facility operating at other speeds or seal configurations than the one in-which the model was identified for. Also, analysis of robust stability and performance and the design of robust controllers can be carried out with respect to uncertain system parameters [22].

3.1 Mathematical representation of the nominal AMB-rotor-seal system

The nominal mathematical system representation of the test-facility consist of a finite element model of the rotor, dynamic model of AMB actuation forces, the coupling dynamics and the seal dynamics, described next.

3.1.1 Model of AMB Forces

The model of the magnetic bearing is simplified to describe the forces acting on the rotor as function of the rotor lateral displacements to AMB s_x and the control current i_x. The linearised expression of the forces for a given direction is given as [23]

$$f_b(i_x, s_x) = K_i i_x + K_s s_x \tag{1}$$

where K_i are K_s are constants. Initial estimates of K_i and K_s have been obtained using first principle methods. The dynamics of the electromechanical system, including the inductance of the coil and the amplifiers, is approximated as a second order system, denoted G_{act}

$$G_{act} = \frac{\omega_n^2}{s^2 + \zeta\omega_n s + \omega_n} \tag{2}$$

where the damping coefficient and natural frequency are empirically found to be $\zeta = 0.9$ and $\omega_n = 1360\,\mathrm{rad/s}$ (216 Hz).

3.1.2 Model of Dynamic Seal Forces

The dynamic seal forces are commonly descried by their linearised force coefficients: stiffness, damping and sometimes mass matrices. Mass coefficients are hereby neglected since the fluid used is air [1]

$$\begin{bmatrix} f_\zeta \\ f_\eta \end{bmatrix} = \begin{bmatrix} K & k \\ -k & K \end{bmatrix} \begin{bmatrix} \zeta \\ \eta \end{bmatrix} + \begin{bmatrix} C & c \\ -c & C \end{bmatrix} \begin{bmatrix} \dot{\zeta} \\ \dot{\eta} \end{bmatrix} \tag{3}$$

This model has a symmetric structure since the shaft is assumed to be in the center of the seal. The coefficients are generally a function of the rotational speed and the excitation frequency.

3.1.3 Model of Flexible Coupling Forces

The force of the flexible coupling, as shown in Fig. 3, is considered as a direct stiffness matrix for radial movements. Torsional stiffness is considered small and is neglected for simplicity.

$$\begin{bmatrix} f_\zeta \\ f_\eta \end{bmatrix} = \begin{bmatrix} K_{c_\zeta} & 0 \\ 0 & K_{c_\eta} \end{bmatrix} \begin{bmatrix} \zeta \\ \eta \end{bmatrix} \tag{4}$$

3.1.4 Model of Shaft

The dynamic behaviour of the rotating shaft is mathematically described using the Finite Element (FE) method and Bernoulli-Euler beam theory considering the gyroscopic effects of the shaft and discs [24]. The shaft model is built using 40 node points with 4 degrees of freedom each, i.e. x and y direction, and the rotation around the x and y axes. It yields 320 states in total. The rotational speed is kept at zero for this study to isolate the seal effects. The tangential fluid flow is induced by means of four injectors built as illustrated in Fig. 6, what leads to high preswhirl effect. The global rotordynamic system G_f consisting of the finite element model of the shaft, negative stiffness forces from the AMB, the stiffness and damping of the seal and the stiffness of the coupling can be written in state space form as

$$\dot{x}_f = A_f x_f + B_f u, \quad y = C_f x_f \tag{5}$$

Using modal truncation techniques, real left and right modal transformation matrices are obtained which transform the full order FE system to a reduced form

$$x = T_L{}^T x_f, \quad A = T_L{}^T A_f T_R, \quad B = T_L{}^T B_f, \quad C = C_f T_R \tag{6}$$

The first bending mode of the shaft lies at approximately 550 Hz. Since this is substantially above the frequency range of interest in this work, the shafts is assumed rigid and all bending modes have thus been removed in the reduced order model. The FE model is selected though for generality and for possibility of extending the model to include some of the bending modes if needed.

3.2 Changed Plant Representation

The nominal rotordynamic model consists of the reduced order shaft model, the negative stiffness from the AMBs and the nominal stiffness and damping from the seals. The updated model G_{fi} is constructed using the nominal model and the change of dynamics representation, which are combined and written in LFT form, illustrated in Fig. 7 [25]. Here θ is a diagonal matrix representing the normalized parameters to be identified. G_{fi} can be written in state space form, as shown in Eq. (7), where A, B and C are the nominal system matrices. Here the input and output matrices are extended from the nominal model to include the input and output mapping B_θ and C_θ. Note that no extra system dynamics is added since the LFT only changes the nominal system matrix A.

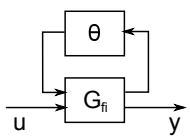

Fig. 7. Updated/changed plant representation using upper LFT, $G_{updated} = \mathcal{F}_u(G_{fi}, \theta)$

$$G_{fi} = \left[\begin{array}{c|cc} A & B_\theta & B \\ \hline C_\theta & 0 & 0 \\ C & 0 & 0 \end{array}\right] \tag{7}$$

B_θ and C_θ are selected to represent changes in the nominal plant caused by AMB bias stiffness, mechanical stiffness from coupling, stiffness and damping from the seal. The structures of e.g. B_θ and θ are given as

$$B_\theta = \left[B_{\theta K_s},\, B_{\theta K_{coupling}},\, B_{\theta K_{seal}},\, B_{\theta D_{seal}}\right]_{8\times 14} \tag{8}$$

$$\theta = diag\left(\left[\theta K_s,\, \theta K_{coupling},\, \theta K_{seal},\, \theta D_{seal}\right]\right)_{14\times 14} \tag{9}$$

B_θ and C_θ are constructed as follows and a thorough description of this process can be seen in [26]. It can be shown that changes in stiffness (or damping) in a single direction at e.g. A_x corresponds to a change in a single column of system matrix A, which corresponds to the node j where the stiffness (or damping) is altered.

$$A_{\Delta_f} = \begin{bmatrix} 0 \ldots 0 \; a_{1,j} \; 0 \ldots 0 \\ 0 \ldots 0 \; a_{2,j} \; 0 \ldots 0 \\ \vdots \; \ddots \; \vdots \; \vdots \; \vdots \; \ddots \; \vdots \\ 0 \ldots 0 \; a_{i,j} \; 0 \ldots 0 \end{bmatrix} \tag{10}$$

The change of the system matrix in reduced form A_Δ is found using the same modal truncation matrices as used to reduce the nominal system, as shown in Eq. (11). A_{Δ_f} in Eq. (10) can also be written as a column vector B_{θ_f} and a row vector C_{θ_f} and the change θ. The input mapping B_θ and output mapping C_θ of the uncertainties are thus given as shown in Eq. (13). Repeating this process 14 times (one for each stiffness and damping parameter) and assembling the coloums of B_θ and rows of C_θ and making θ a 14×14 diagonal matrix, yields the complete representation.

$$A_\Delta = T_L\, A_{\Delta_f}\, T_R \tag{11}$$
$$= T_L B_{\theta_f}\, \theta\, C_{\theta_f} T_R \tag{12}$$
$$= B_\theta\, \theta\, C_\theta \tag{13}$$

3.3 Estimation of Optimal Parameters

A current signal i_e can be imposed to perturb the system model and a time domain simulation can be employed to yield the displacement response y, which can be compared to a response quantified experimentally. To estimate the uncertain AMB parameters the identification scheme is formulated as a minimization problem that iterates through the uncertain parameters to decrease the discrepancy between the simulated response and the response experimentally acquired. The goal is to find the parameters that provide the best fit between simulation data and experimental data. This can be done by finding the global minimum of the cost function shown in Eq. (14) which is defined as the sum of squares of the discrepancy between simulation data and experimental data as

$$J(\theta) = \left\|y_{meas} - y)\right\|_2^2 \tag{14}$$

Minimization of the cost function seen in Eq. (14) has been implemented using MATLAB's `lsqnonlin` function. The method converges fast towards optimal parameters, even for the case where multiple parameters are simultaneously identified.

3.4 Identification of AMB-rotor Model Parameters

The first step in obtaining a global model which describes the complete test-facility and is able to separate the seal dynamics, is to update the mathematical model of the AMB-rotor system. The FE model of the rotor is considered sufficiently accurate and the uncertain parameters are

considered to be the AMB constants K_i and K_s, one for each degree-of-freedom (DOF), i.e. in all 2×4 parameters. Optimal parameters have been found using the representation of the changed system in Sec. 3.2 and optimization in Sec. 3.3. Two Pseudo-Random Binary Sequence (PRBS) identification signals have been simultaneously applied, one for each actuator direction, resulting in purely parallel displacements of the rotor. The AMB-rotor model shows a good performance, as shown in the time domain in Fig. 8, although the simulated time response shows slightly larger overshoot than the experimental, suggesting the model lacks a bit of damping to precisely represent the experimental response. The model has also been verified in frequency domain by using a linear chirp signal from 0-150 Hz. It is observed that the model represents experimental data up to approximately 100 Hz in magnitude and phase as shown for both AMB directions in Fig. 9 and 10. Furthermore, some cross coupling dynamics exist, which are plotted separately for the movement at bearing A and bearing B. These would ideally be zero, however in practice, these could arise from e.g. leakage in the magnetic flux path of the AMBs, the shaft being displaced from magnetic center, sensor measuring uncertainty, neglected base-frame movement etc. The displacements due to cross coupling are generally 10 times smaller when compared to the response in the excitation direction, and they are neglected in the mathematical model. However the cross coupled forces do seem to affect the response in the excitation direction as well, as for example around 30 Hz. The coherence is high from input to output in the excitation direction but lower in the cross coupled directions, probably due to lower displacement amplitude in the cross coupled directions. The correlation matrix in Tab. 2 shows high correlation between K_s and K_i for each DOF, for example at A_ζ, indicating that the dynamic effect of adjusting either K_i and K_s results in similar effects and their identified values might not be completely unique. τ_e, however, has a low correlation with the other parameters and is thus considered unique. K_i and K_s are theoretically expected to be unique to some degree since K_s only affects the bearing stiffness while K_i in addition to scaling the stiffness, through the proportional gain of the PID controller, also scales the integration and the derivative gain of the PID controller. Other identification experiments with other bias currents and other parameters of PID gains show that lower correlation between K_i and K_s can be obtained. Also, the correlation between K_s and K_i can possibly be lowered significantly by including the measured and simulated current signals in the optimization process. The uniqueness of K_i and K_s parameters are not considered an issue in this work since the main focus is to obtain an accurate

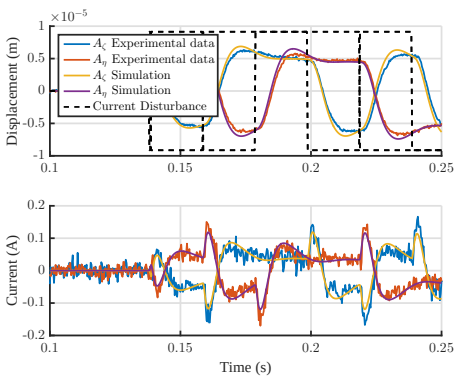

Fig. 8. AMB-rotor model versus experimental time response. Displacements are shown in upper and currents are shown in lower plot. The PRBS current perturbation signal are indicated with dashed lines and the amplitude is scaled to fit the plot. The results are shown for bearing A and are similar for bearing B.

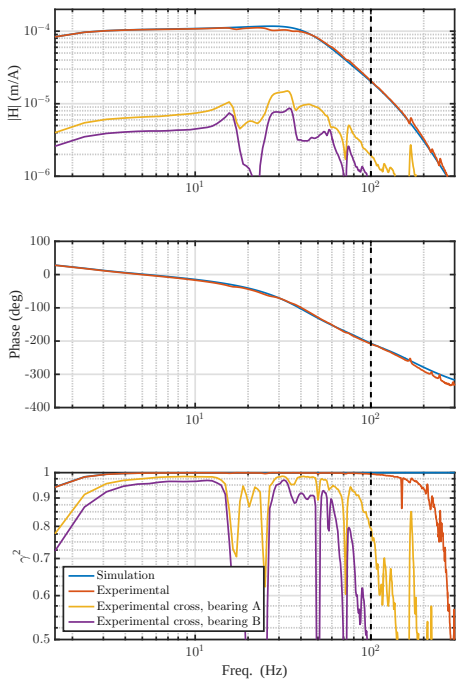

Fig. 9. FRFs of AMB-rotor model versus experimental for parallel excitation of rotor in ζ-direction using a 0-150 Hz chirp signal. The model fits experimental data well up to approximately 100 Hz indicated with the dashed line. "Simulation" and "Experimental" shows FRFs from simultaneously excitation on bearing A and bearing B to the center movement of the seal in the excitation direction. "Experimental cross, bearing A" and "Experimental cross, bearing B" shows FRFs from excitation on each bearing to the movement in the cross coupled direction - top: amplitude, middle: phase, bottom: coherence

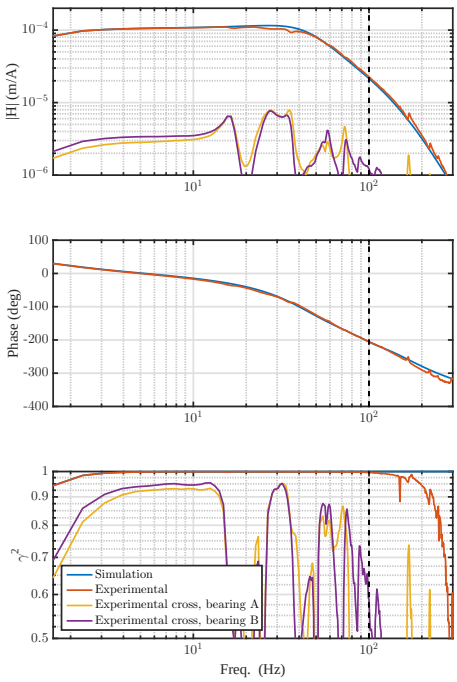

Fig. 10. FRFs of AMB-rotor model versus experimental for parallel excitation of rotor in η-direction using a 0-150 Hz chirp signal. The model fits experimental data well up to approximately 100 Hz indicated with the dashed line. "Simulation" and "Experimental" shows FRFs from simultaneously excitation on bearing A and bearing B to the center movement of the seal in the excitation direction. "Experimental cross, bearing A" and "Experimental cross, bearing B" shows FRFs from excitation on each bearing to the movement in the cross coupled direction - top: amplitude, middle: phase, bottom: coherence

AMB baseline model in order to precisely estimate the seal forces.

3.5 Identification of Flexible Coupling Dynamics

The flexible coupling is modelled as a direct stiffness in each actuator direction, which is identified in a separate experiment in order to obtain a unique solution. Again, two PRBS identification signals have been simultaneously applied, one for each actuator direction, resulting in purely parallel displacements of the rotor. The stiffness coefficients of flexible coupling are extracted and the results are shown in Table 3

	K_{i,A_ζ}	K_{i,A_η}	K_{i,B_ζ}	K_{i,B_η}	K_{s,A_ζ}	K_{s,A_η}	K_{s,B_ζ}	K_{s,B_η}
K_{i,A_ζ}	1.00	0.00	-0.08	0.00	-0.95	-0.00	0.08	-0.00
K_{i,A_η}	0.00	1.00	0.00	-0.08	-0.00	-0.96	-0.00	0.08
K_{i,B_ζ}	-0.08	0.00	1.00	0.00	0.08	-0.00	-0.96	-0.00
K_{i,B_η}	0.00	-0.08	0.00	1.00	-0.00	0.07	-0.00	-0.96
K_{s,A_ζ}	-0.95	-0.00	0.08	-0.00	1.00	0.00	-0.09	0.00
K_{s,A_η}	-0.00	-0.96	-0.00	0.07	0.00	1.00	0.00	-0.09
K_{s,B_ζ}	0.08	-0.00	-0.96	-0.00	-0.09	0.00	1.00	0.00
K_{s,B_η}	-0.00	0.08	-0.00	-0.96	0.00	-0.09	0.00	1.00

Table 2. Correlation matrix – calculated based on the Jacobian matrix. Values close to 1 or -1 indicates strong correlation between parameters.

Table 3. Identified stiffness coefficients of flexible coupling.

K_{c_ζ}	0.40×10^6 N/m
K_{c_η}	0.42×10^6 N/m

3.5.1 Identification of Seal Coefficients for Various Frequencies

The seal forces are identified with parallel movements of the rotor. This is to avoid axial forces being generated in the discharge system of the seal house. A stepped sine procedure in the range 5-200 Hz with steps of 10 Hz is applied as an excitation current signal to obtain seal force coefficients for different excitation frequencies - the same excitation signal that is used for extracting seal coefficients using CFD simulation as shown in [8]. The seal force coefficients for each excitation frequency are found using the representation of the changed system in Sec. 3.2 and optimization in Sec. 3.3. An example of the fit of seal force coefficients identified at 40 Hz excitation is shown in Fig. 11. Good agreement between the global model and experimental data is found, indicating the seal model structure and the found seal parameters describes the actual seal forces well. The cross coupled forces of the seal are clearly seen since the excitation is applied in the ζ-direction while a large response is also seen in the η-direction.

The stepped sine identification procedure has been repeated for differential pressures across the seal of 0.7 bar, 1.0 bar and 1.2 bar to investigate the influence of different pressures. The results, in terms of seal coefficients for different pressures across the seal, are shown in Fig. 12. As a reference, the identified seal coefficients, for when no pressure is applied, are plotted along with the other results. These reference coefficients indicates how biased the other coefficients might be due to residual dynamics that might not have been captured by the AMB-rotor-coupling model, such as the cross coupled effects of the AMB-rotor model. The following is observed from Fig. 12:

1. The direct stiffness values K around zero are expected since the seal clearance, simulating a worn seal, is large.
2. The cross coupled stiffness values k are large and change significantly with the pressure across the seal. This

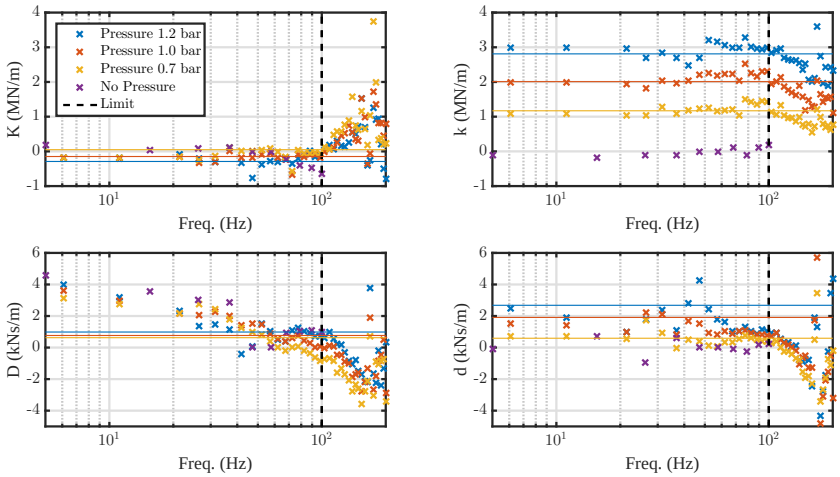

Fig. 12. Seal coefficients vs. excitation frequencies for different pressures across the seal. Coefficients are valid up to approximately 100 Hz as indicated with the dashed line. The solid lines indicates the constant seal coefficients chosen for model verification in Sec. 3.5.2.

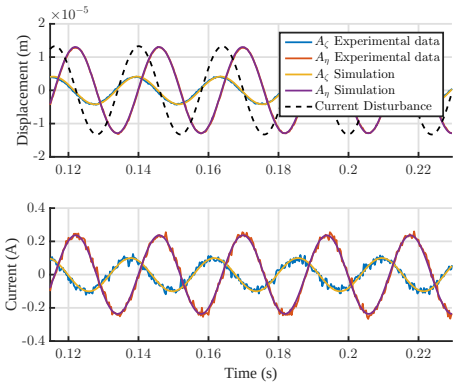

Fig. 11. Example of the fit of seal coefficients identified at 40 Hz excitation. The simulated and experimental time response are shown for displacement (upper) and for current (lower). A sinus excitation current is applied in the ζ-direction.

parameter does significantly effect the dynamic of the overall system. It is expected that the cross coupled stiffness is large due to high preswirl in the seal. Moreover k seems to be frequency-independent as also found using Bulkflow modelling for annular gas seals in [27].

3. The direct damping D decreases as the excitation frequency increases, however; this tendency must be disregarded since the tendency is also captured by coefficients found for no pressure. The direct damping is low and seems to depend on the applied pressure. High pressure yields high damping.
4. The cross coupled damping d is low and depends on the applied pressure. High pressure yields high cross coupled damping.

The uniqueness of the found seal coefficients is high, since all parameters are very weakly correlated, as shown in Table 4.

3.5.2 Verification of Global Model in Frequency Domain Including Fixed Frequency Seal Models

To verify the performance of the global model and the frequency independence of the identified test seal, a comparison is made between the frequency response functions of the simulated model responses with the experimental responses obtained from test-facility for different pressures.

	K	D	k	d
K	1.00	-0.00	0.01	-0.04
D	-0.00	1.00	0.04	0.01
k	0.01	0.04	1.00	-0.00
d	-0.04	0.01	-0.00	1.00

Table 4. Correlation matrix – calculated based on the Jacobian matrix. Values close to 1 or -1 indicates strong correlation between parameters. The values are shown for identification of seal coefficients with 40 Hz excitation frequency.

The global model includes a seal model with constant coefficients. These coefficients are highlighted as solid lines shown in Fig. 12. Datasets from the identifications of seal coefficients for different frequencies in Sec. 3.5.1 have been reused for the verification. The global model fits well up to approximately 100 Hz, which is the frequency range in which the AMB-rotor model is considered valid. This is shown for pressures 0.7 bar, 1.0 bar and 1.2 bar in Fig. 13, 14 and 15. Hence, the test seal with gas fluid seems to be independent of the excitation frequency for the investigated frequency range.

It is interesting that the frequency plot in Fig. 13 shows no significant resonance peak since the control system is able to suppress the rigid mode shapes of the system. However, as the pressure increases to 1.2 bar and the cross coupled stiffness increases, a resonance appears, as shown in Fig. 15. This indicates robustness and stability issues start to arise since the direct stiffness of the AMBs with their current controller configuration is not large enough for the cross coupled effects to be neglectable. Hence, to identify seal forces with higher pressures, the controller must either yield a larger direct stiffness or be designed to counteract the cross-coupled forces arising from the seal.

4 Conclusion

This paper demonstrates an elegant way of identifying the uncertain or unknown parameters with a focus on dynamic seal forces in rotordynamic AMB systems, step by step, without changing the system order of the global model. This is done by utilizing the structure of the model, the shaft model and closed loop system identification. This procedure is applied to a rotordynamic test-facility to identify the uncertain parameters of the dynamic AMB model, the flexible coupling forces and dynamic annular seal forces.

The identified seal coefficients of the tested seal with gas fluid shows practically no excitation frequency dependence. This fits well with previous results found using Bulk-flow modelling of annular seals using gas fluid in [27]. The most significant seal parameter is the cross-coupled stiffness which is highly dependent on the pressure across the seal. The test seal furthermore seems to yield some cross coupled damping. The direct stiffness and direct damping coefficients of the test seal are practically zero.

Precise identification of seal parameters, using the presented approach, relies on an accurate mathematical baseline model of the AMB-rotor-coupling system. However, this paper demonstrates that it is possible to obtain an indication of uncertainties and erroneous tendencies caused by imperfections of the mathematical baseline model. An erroneous tendency that should be disregarded is shown for the direct damping.

The excitation frequency-independence of the test seal is verified using a set of fixed seal coefficients to build a global model which fits experimental data well. This model is thus only dependent on the pressure across the seal.

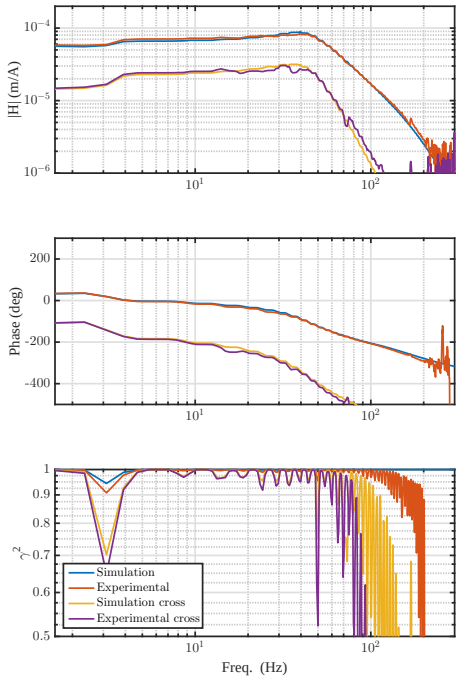

Fig. 13. FRFs of global model with constant seal coefficients versus experimental using 0.7 bar pressure across the seal - top: amplitude, middle: phase, bottom: coherence

References

[1] Childs, D. W., 1993. *Turbomachinery rotordynamics: phenomena, modeling, and analysis*. John Wiley & Sons.

[2] Picardo, A., and Childs, D. W., 2005. "Rotordynamic coefficients for a tooth-on-stator labyrinth seal at 70 bar supply pressures: measurements versus theory and comparisons to a hole-pattern stator seal". *Journal of engineering for gas turbines and power,* **127**(4), pp. 843–855.

[3] Soulas, T., and San Andres, L., 2007. "A bulk flow model for off-centered honeycomb gas seals". *Journal of Engineering for Gas Turbines and Power,* **129**(1), pp. 185–194.

[4] Scharrer, J. K., 1988. "Theory versus experiment for the rotordynamic coefficients of labyrinth gas seals: Part ia two control volume model". *Journal of Vibration, Acoustics, Stress, and Reliability in Design,* **110**(3), pp. 270–280.

[5] Iwatsubo, T., 1980. "Evaluation of instability forces of labyrinth seals in turbines or compressors".

[6] Millsaps, K. T., and Martinez-Sanchez, M., 1994. "Dy-

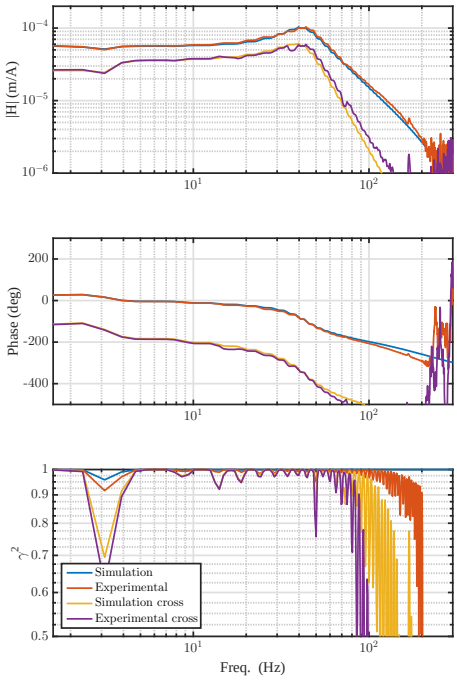

Fig. 14. FRFs of global model with constant seal coefficients versus experimental using 1.0 bar pressure across the seal - top: amplitude, middle: phase, bottom: coherence

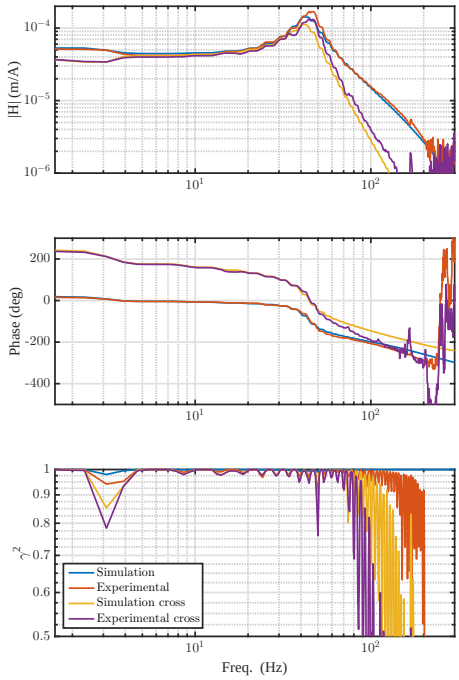

Fig. 15. FRFs of global model with constant seal coefficients versus experimental using 1.2 bar pressure across the seal - top: amplitude, middle: phase, bottom: coherence

namic forces from single gland labyrinth seals: Part iideal and viscous decomposition". *Journal of turbomachinery,* **116**(4), pp. 686–693.

[7] Childs, D. W., and Vance, J. M., 1997. "Annular gas seals and rotordynamics of compressors and turbines". In Proceedings of the 26th Turbomachinery Symposium, pp. 201–220.

[8] Nielsen, K. K., Jonck, K., and Underbakke, H., 2012. "Hole-pattern and honeycomb seal rotordynamic forces: Validation of cfd-based prediction techniques". *Journal of Engineering for Gas Turbines and Power,* **134**(12), p. 122505.

[9] Wagner, N. G., Steff, K., Gausmann, R., and Schmidt, M., 2009. "Investigations on the dynamic coefficients of impeller eye labyrinth seals". In Proceedings of the Thirty-Eighth Turbomachinery Symposium, Houston, TX, September, pp. 14–17.

[10] Kocur, J. A., Nicholas, J. C., and Lee, C. C., 2007. "Surveying tilting pad journal bearing and gas labyrinth seal coefficients and their effect on rotor stability". In 36th Turbomachinery Symposium, Turbomachinery Laboratory, Texas A&M University, College Station, TX, September, pp. 10–13.

[11] Ertas, B. H., Delgado, A., and Vannini, G., 2012. "Rotordynamic force coefficients for three types of annular gas seals with inlet preswirl and high differential pressure ratio". *Journal of Engineering for Gas Turbines and Power,* **134**(4), p. 042503.

[12] Elrod, D., Nicks, C., Childs, D., and Nelson, C., 1985. "A comparison of experimental and theoretical results for rotordynamic coefficients of four annular gas seals". *Progress Report NASA contract NAS8-33716 Texas A&M University, Turbomachinery Laboratories, Mechanical Engineering Department College Station, Texas,* **77843**.

[13] Brown, P. D., and Childs, D. W., 2012. "Measurement versus predictions of rotordynamic coefficients of a hole-pattern gas seal with negative preswirl". *Journal of Engineering for Gas Turbines and Power,* **134**(12), p. 122503.

[14] Wagner, N., and Steff, K., 1997. "Dynamic labyrinth coefficients from a high-pressure full-scale test rig using magnetic bearings". *Demag A. G, Rotordynamic Instability Problems in High-Performance Turbomachin-*

ery (SEE N 97-24525 01-37), pp. 95–111.

[15] Knopf, E., and Nordmann, R., 1998. "Active magnetic bearings for the identification of dynamic characteristics of fluid bearings". In Proceedings 6th International Symposium on Magnetic Bearings, Cambridge, MA, August, pp. 5–7.

[16] Matros, M., and Nordmann, R., 1997. "Dynamic characteristics of a hydrostatic bearing identified by active magnetic bearings". *Kaiserslautern Univ, Rotordynamic Instability Problems in High- Performance Turbomachinery 1996 p 23-28(SEE N 97-24525 01-37)*.

[17] Nordmann, R., and Aenis, M., 2004. "Fault diagnosis in a centrifugal pump using active magnetic bearings". *International Journal of Rotating Machinery,* **10**(3), pp. 183–191.

[18] Aenis, M., and Nordmann, R., 2002. "Fault diagnosis in rotating machinery using active magnetic bearings". In 8th International Symposium on Magnetic Bearing, p. 125.

[19] Zutavern, Z. S., and Childs, D. W., 2008. "Identification of rotordynamic forces in a flexible rotor system using magnetic bearings". *Journal of Engineering for Gas Turbines and Power,* **130**(2), p. 022504.

[20] Voigt, A. J., 2016. *Towards Identification of Rotordynamic Properties for Seals in Multiphase Flow Using Active Magnetic Bearings. Design and Commissioning of a Novel Test Facility*. Technical University of Denmark.

[21] Voigt, A. J., Mandrup-Poulsen, C., Nielsen, K. K., and Santos, I. F., 2017. "Design and calibration of a full scale active magnetic bearing based test facility for investigating rotordynamic properties of turbomachinery seals in multiphase flow". *Journal of Engineering for Gas Turbines and Power,* **139**(5), p. 052505.

[22] Lauridsen, J. S., and Santos, I. F., 2016. "Design of robust amb controllers for rotors subjected to varying and uncertain seal forces".

[23] Bleuler, H., Cole, M., Keogh, P., Larsonneur, R., Maslen, E., Okada, Y., Schweitzer, G., Traxler, A., Schweitzer, G., Maslen, E. H., et al., 2009. *Magnetic bearings: theory, design, and application to rotating machinery*. Springer Science & Business Media.

[24] Nelson, H., 1980. "A finite rotating shaft element using timoshenko beam theory". *Journal of mechanical design,* **102**(4), pp. 793–803.

[25] Skogestad, S., and Postlethwaite, I., 2007. *Multivariable feedback control: analysis and design*, Vol. 2. Wiley New York.

[26] Lauridsen, J. S., Sekunda, A. K., Santos, I. F., and Niemann, H., 2015. "Identifying parameters in active magnetic bearing system using lft formulation and youla factorization". In 2015 IEEE Conference on Control Applications (CCA), IEEE, pp. 430–435.

[27] San Andrés, L., 2012. "Rotordynamic force coefficients of bubbly mixture annular pressure seals". *Journal of Engineering for Gas Turbines and Power,* **134**(2), p. 022503.

Chapter 6

Design of Active Magnetic Bearing Controllers for Rotors Subjected to Seal Forces

Publication P5

This paper is recommended for journal publication in the ASME Journal of Dynamic Systems, Measurement, and Control, with revisions. The revised version of the paper is hereby included.

Design of Active Magnetic Bearing Controllers for Rotors Subjected to Gas Seal Forces

Jonas S. Lauridsen*
PhD student, Member of ASME
Department of Mechanical Engineering
Technical University of Denmark
Email: jonlau@mek.dtu.dk

Ilmar F. Santos†
Professor, Member of ASME
Department of Mechanical Engineering
Technical University of Denmark
Email: ifs@mek.dtu.dk

Proper design of feedback controllers is crucial for ensuring high performance of Active Magnetic Bearing (AMB) supported rotor dynamic systems. Annular seals in those systems can contribute with significant forces, which, in many cases, are hard to model in advance due to complex geometries of the seal and multiphase fluids. Hence, it can be challenging to design AMB controllers that will guarantee robust performance for these kinds of systems. This paper demonstrates the design, simulation and experimental results of model based controllers for AMB systems, subjected to dynamic seal forces. The controllers are found using $\mathcal{H}_\infty$- and μ synthesis and are based on a global rotor dynamic model in-which the seal coefficients are identified in-situ. The controllers are implemented in a rotor-dynamic test facility with two radial AMBs and one annular seal with an adjustable inlet pressure. The seal is a smooth annular type, with large clearance (worn seal) and with high pre-swirl, which generates significant cross-coupled forces. The $\mathcal{H}_\infty$ controller is designed to compensate for the seal forces and the μ controller is furthermore designed to be robust against a range of pressures across the seal. Experimental and simulation results shows that significant performance can be achieved using the model based controllers compared to a reference decentralised PID controller and robustness against large variations of pressure across the seal can be improved by use of robust synthesised controllers.

*Address all correspondence related to ASME style format and figures to this author.
†Address all correspondence related to ASME style format and figures to this author.

1 Introduction

Uncompressible and compressible fluid flowing through very narrow gaps in annular seals can generate large forces. The influence of such liquid and gas seal forces on the lateral dynamics of rotating machines has been intensively investigated over several decades, by Fritz [1], Black [2, 3], Childs [4] and Nordmann [5] among others. Under high pressure and high pre-swirl flow conditions such aerodynamic forces can destabilize the rotating shaft, leading to high levels of lateral vibration. In extreme cases of contact and rubbing between rotating shaft and seal stator catastrophic failures may occur.

In the last five decades the prediction of the dynamic behaviour of seals forces by means of mathematical models has been well documented in the literature, but it does not mean that an accurate prediction of seal forces is a solved problem. The publications have been focused on describing seal dynamics using either CFD [6–9] or Bulk-flow models [10, 11], and they have shown that for seals under well-defined single phase flow conditions a reasonable match between theoretical and experimental results can be achieved [12], especially in the case of incompressible fluids [13]. Once a Bulk-flow model is built based upon several simplifying assumptions which do not necessarily hold [14] in practical industrial applications, several ways of "tuning" uncertain model parameters based on experimental as well as theoretical approaches can be explored [15].

To illustrate the challenges associated with the modeling of dynamic seal forces and the accurate prediction of seal force coefficients a survey was conducted in 2007. Here 20 survey participants from both industry and academia were asked to predict the dynamics of a gas labyrinth seal and consequently the rotordynamic behaviour [16]. The seals dynamics was predicted using Bulkflow and CFD methods.

The survey showed large variations in results and emphasises the need for continuous efforts towards modelling and uncertainty handling of seal forces, even for the single phase flow condition, as presented in the article.

Seal forces under multiphase flow conditions, i.e. where the fluid is an inhomogeneous mixture of gas and liquid, are still an open and difficult modeling task [17]. In this framework, larger model uncertainties should be expected for seals under multiphase flow conditions due to a limited knowledge about the dynamic behaviour of fluid forces under such a condition, especially when combined with complex seal geometries, such as hole-pattern and labyrinth. Model uncertainties are thus unavoidable due to the complexity of the fluid-structure interaction and the limitations of mathematical modelling associated with simplifying assumptions.

In AMB supported rotordynamic systems, the effect of gas seal destabilizing forces can be significantly mitigated by employing feedback controllers, if these controllers are properly designed and tuned. Designing and implementing feedback controllers for AMB supported rotordynamic systems taking into account the destabilizing aerodynamic seal forces can be very challenging. The reasons are due to: i) the dependence of seal forces on the varying operating conditions such as rotational speed and pressure difference across the seal; ii) the changes in fluid (gas) properties; iii) changes in the process flow characteristics; and iv) model uncertainties. In this framework the necessity of designing robust controllers able to deal with uncertainties and parameter changes is clear. Several articles have focused on designing robust control for AMB systems. A popular choice for designing robust linear time-invariant (LTI) controllers for AMB systems is by using the $\mathcal{H}_\infty$ framework and an LFT formulation to represent the nominal system and uncertainty. Using $\mathcal{H}_\infty$ with an uncertainty representation of the plant allows for the direct synthetisation of the controller, ensuring the worst case performance. In many cases the conservativeness of the synthesised $\mathcal{H}_\infty$ controller can be reduced using DK-iteration, as done using the μ synthesis framework [18]. The robustness criteria for AMB systems are specified in ISO 14839-3 stating that the closed loop output sensitivity should be less than 3 for the system to be classified as Class A [19]. In the $\mathcal{H}_\infty$ framework such a requirement can be fulfilled by weighting the sensitivity function. Some articles report research efforts on fault-tolerant control methods. [20] shows that improved tolerance to specific external faults is achieved through $\mathcal{H}_\infty$ optimised disturbance rejection. Specifically, increased robustness is shown in the case of mass loss of rotor in a testrig with a flexible shaft and moveable baseframe. Improvement in performance of $\mathcal{H}_\infty$ controller based on nonlinear plant compared to $\mathcal{H}_\infty$ controller based on linear plant has been reported [21]. In [22] the authors show that robust controllers for uncertain rotational speed can be addressed using an LFT consisting of the nominal system and a representation of how the system changes due to gyroscopic effects using gyroscopic matrix scaled by a repeated uncertainty. The natural frequencies of the flexible shafts bending modes are the main uncertainties treated in [23] and a robust controller is designed using μ synthesis. Robust stability to additive and multiplicative uncertainties can directly be ensured by applying complex weighting functions to the transfer functions KS (controller sensitivity) and T (complementary sensitivity). The conservativeness of the robust controller design can be reduced in the case of a Linear Parameter Varying (LPV) controller design, where one or more parameters are measured in real time, and can represent changing dynamics, which otherwise would be considered uncertain. A measured parameter could be the rotation speed, which can be utilized to reduce synchronous vibrations as shown in [24]. A flexible rotor subjected to uncertain cross coupled stiffness (CCS) was considered in [25] and the CCS was generated by using an extra set of active magnetic bearings. It was found based on the experimental analysis that it is very hard to design robust controllers using μ synthesis able to compensate for uncertain cross coupled stiffness in flexible rotating systems. Adaptive controllers to detect and compensate for cross coupling forces have been reported in [26] where the authors numerically simulated a rotordynamic system supported by AMB and subjected to a time variant CCS. An observer was built and theoretically demonstrated the ability to track the changes of CSS parameter in time. Using pole placement technique a controller was designed to work along with the observer. In [27] the authors estimated on-line the unknown CSS parameter of a rotor by a recursive least square estimator. Simulation results of adaptive control in parallel with a baseline PID controller were considered in [28], where the controller was designed to compensate changes of CCS in time and periodic disturbance forces. The work shows that the adaptive controller could handle much larger amplitudes of CCS forces than a fixed LTI LQR compensator. However, only numerical studies have been carried out so far dealing with the adaptive controller problem. In general stability and robustness are hard to guarantee in adaptive control systems which is crucial for implementation in industrial applications.

The design and simulated results using $\mathcal{H}_\infty$, μ and LPV controllers to compensate for uncertain and varying seal forces in a turbocharger supported by AMBs are demonstrated in [29]. Specifically, a hole pattern seal is considered for a balance piston in a turbo-expander application. Performance improvements are shown when using robust control for handling model uncertainties in the dynamic force coefficients of the seal, compared to a controller based on a nominal model. Also, since the dynamic seal coefficients of the hole pattern seal are heavily dependent on the excitation frequency, a Linear Parameter Varying (LPV) controller is designed to deal with the frequency dependency using the rotational speed as the scheduling parameter. The performance enhancements compared to a μ controller are shown for delivering performance over the complete rotational speed range.

A method for identification of uncertain/unknown seal- and electromechanical parameters, to obtain a precise global model of an AMB-rotor-seal test facility is presented in [30]. The test facility is described in [31]. The method can be employed on-site without the use of any calibrated force measurement sensors - only the free-free model of the shaft is

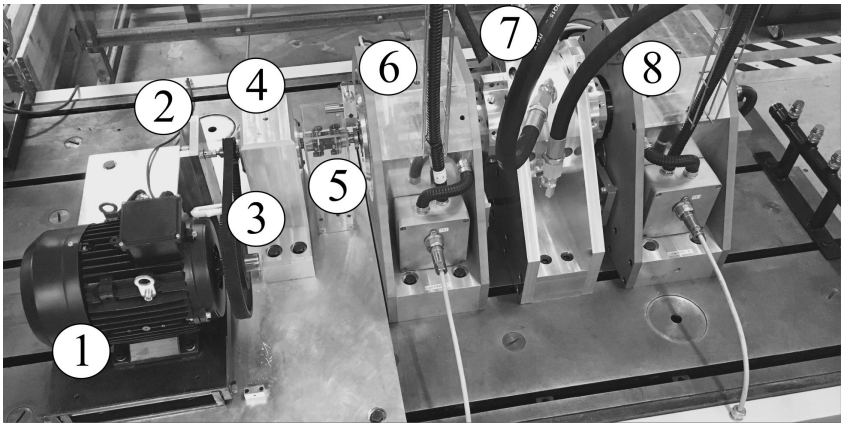

Fig. 1: Test facility overview. ① motor, ② Encoder, ③ Belt drive, ④, Intermediate shaft pedestal, ⑤ Flexible coupling. ⑥ AMB A, ⑦ Seal housing, ⑧ AMB B.

needed a-priori. The seal forces are characterized as direct stiffness and damping coefficients and cross coupled stiffness and damping coefficients as functions of pressure across the seal and excitation frequency. This method could potentially be implemented in all rotor dynamic systems supported by AMBs and subjected to seal forces.

This paper uses the rotor dynamic model with in-situ identified seal coefficients, presented in [30], to design model based controllers, for handling dynamic seal forces. The idea is to enhance the performance of the global system without increasing the direct stiffness or damping of the system.

This paper is structured as follows:

1. Description of the AMB-rotor-seal test facility.
2. Mathematical model representation of the nominal and perturbed plant.
3. Results of global model with identified seal coefficients.
4. Control design structure and weight function selection.
5. Simulated and experimental results of a PID reference controller and the synthesised $\mathcal{H}_\infty$- and μ controllers for handling seal forces at different pressures.

2 Experimental Facility

The experimental facilities used for this work consist of an AMB-based rotordynamic test bench with a seal housing presented in Fig. 1. Two AMBs radially support a symmetric rigid rotor which is driven by an asynchronous motor through an intermediate shaft and a flexible coupling, as seen in Fig. 1. Angular contact ball bearings, supporting the intermediate shaft housed in the intermediate shaft pedestal, compensate for axial forces acting on the rotor. The radial AMBs are of the eight pole heteropolar type.

The global reference frame is denoted by x, y and the actuator reference frame is denoted by ζ, η, which is tilted 45° with respects to the global reference frame. The two AMB stators have been manufactured using two different production methods yielding different geometric tolerances for the AMBs. The AMBs are supplied by four 3 kW laboratory amplifiers.

The seal, mounted in the center of the shaft, is installed as a back-to-back configuration, hence two symmetrical seals are placed with the idea to cancel out possible axial fluid film forces. It is designed with primary and secondary discharge seals to avoid any liquid entering the AMBs, since the test facility is designed to operate with both gas, liquid and mixtures between gas and liquid. The fluid used in this article is gas, though. The fluid is injected by four highly angled nozzles to obtain a high preswirl ratio, hence the fluid is already rotated at the inlet of the seal. A cross section of the injection system is shown in Fig. 2.

A full description of the test facility can be found in [32] and the design parameters for the rotor dynamic test bench can be found in Table 1.

Table 1: Design parameters for the rotordynamic test bench

Rotor length	860	mm
Rotor assembly mass	69	kg
1st rotor bending mode @	550	Hz
Stator inner diameter	151	mm
Nominal radial air gap	0.5	mm
Number of windings	36	[-]

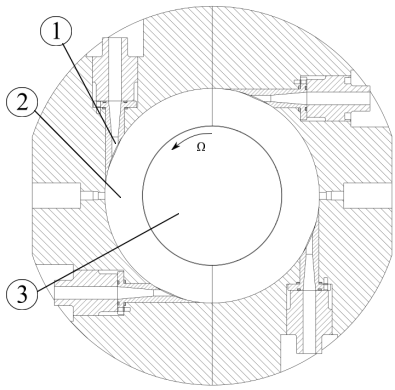

Fig. 2: Cross section of the seal house at the inlet cavity section. ① inlet injection nozzle, ② inlet cavity,③ shaft. The figure is adapted from [31]

3 Mathematical Modelling, Perturbed Plant and System Identification

This section presents details about the mathematical system, the perturbed system representation and the results of system identification - all related to the models used for control synthesis. The modelling and identification of uncertain/unknown parameters of the test facility are described in detail in [30].

3.1 Mathematical Model

The global mathematical model describes the dynamic interaction among all test rig components, namely rotor, AMB, motor-shaft flexible coupling and gas seal. An overview of the forces acting on the rotor and sensor positions is given in Fig. 3

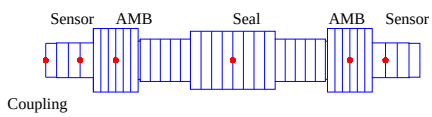

Fig. 3: Overview of the forces acting on the rotor and sensor positions. The red dots marks the input/output locations. The blue lines shows the finite elements of the shaft model.

3.1.1 Model of AMB Forces

The model of the magnetic bearing is simplified to describe the forces acting on the rotor as function of the rotor lateral displacements at the AMB location s_x and the control current i_x. The linearised expression of the forces is given as [33]

$$f_b(i_x, s_x) = K_i i_x + K_s s_x \tag{1}$$

where K_i are K_s are constants. Initial estimates of K_i and K_s have been obtained using first principle methods and identified as shown in [30]. The dynamics of the electromechanical system, including the inductance of the coil and the amplifiers, is approximated using a second order model, denoted G_{act}

$$G_{act} = \frac{\omega_n^2}{s^2 + \xi\omega_n s + \omega_n} \tag{2}$$

where the damping coefficient and natural frequency are found to be $\xi = 0.9$ and $\omega_n = 1360\,\mathrm{rad/s}$ (216 Hz).

3.1.2 Model of Dynamic Seal Forces

The dynamic seal forces are commonly described by their linearised force coefficients: stiffness, damping and sometimes mass matrices. Mass coefficients are hereby neglected since the fluid used is air [34]

$$\begin{bmatrix} f_\zeta \\ f_\eta \end{bmatrix} = \begin{bmatrix} K & k \\ -k & K \end{bmatrix} \begin{bmatrix} \zeta \\ \eta \end{bmatrix} + \begin{bmatrix} C & c \\ -c & C \end{bmatrix} \begin{bmatrix} \dot{\zeta} \\ \dot{\eta} \end{bmatrix} \tag{3}$$

This model has a symmetric structure since the shaft is assumed to be in the center of the seal. The coefficients are generally a function of the rotational speed and the excitation frequency.

3.1.3 Model of Flexible Coupling Forces

The force of the flexible coupling is modeled using linear stiffness associated with the lateral movements of the shaft. Angular stiffness associated with the tilting movements of the shaft is considered negligible, leading to:

$$\begin{bmatrix} f_\zeta \\ f_\eta \end{bmatrix} = \begin{bmatrix} K_{c_\zeta} & 0 \\ 0 & K_{c_\eta} \end{bmatrix} \begin{bmatrix} \zeta \\ \eta \end{bmatrix} \tag{4}$$

The stiffness matrix has been identified by shaking the rotor using the AMBs as shown in [30].

3.1.4 Model of Shaft

The dynamic behaviour of the rotating shaft is mathematically described using the Finite Element (FE) method and Bernoulli-Euler beam theory considering the gyroscopic effects of the shaft and discs [35]. The shaft model is built using 40 node points with 4 degrees of freedom each, i.e. x and y direction, and the rotation around the x and y axes.

It yields 320 states in total. The global rotordynamic system G_f consisting of the finite element model of the shaft, the linearised AMB force coefficients K_i and K_s, the stiffness and damping of the seal and the stiffness of the coupling can be written in state space form. Using modal truncation techniques, real left and right modal transformation matrices are obtained which transform the full order FE system to a reduced form. The first bending mode frequency lies at 550 Hz and the shaft is considered rigid for the work carried out in this paper. Thus, all bending modes have thus been removed in the reduced order model. The FE model is selected though for generality and for possibility of extending the model to include some of the bending modes if needed. The rotational speed is kept at zero for this study to isolate the seal effects. The tangential fluid flow is induced by means of four injectors built as illustrated in Fig. 2, what leads to high preswhirl effect. The state space matrices representing the nominal rotor dynamic system, A, B and C are given in Appendix A. These system matrices are normalised using scaling constants for simpler weight function selection in the control design, $D_e^{-1} G_f D_u$, using $D_e = 20 \times 10^{-6}$ m indicating the largest allowed control error and $D_u = 1$ A indicating the maximum allowed input change.

3.2 Perturbed Plant Representation

The nominal model can be extended to include changes or uncertainties in the plant dynamics. This is utilized for identification of uncertain AMB parameters K_i, K_s as well as unknown seal parameters K, k, D, d, as described in [30]. In this paper, Section 4, the perturbed system representation is utilised for the design of robust controllers. The perturbed plant G_{fi} is constructed using the nominal model (A, B and C) and the uncertain dynamics representation, which are combined and written in LFT form, as illustrated in Fig. 4 [36]. Here Δ is a diagonal matrix representing the uncertain parameters to be identified. G_{fi} can be written in state space form, as shown in Eq. (5), where A, B and C are the nominal system matrices. Here the input and output matrices are extended from the nominal model to include the input and output mapping B_Δ and C_Δ.

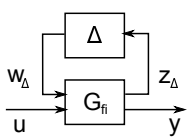

Fig. 4: Updated/changed plant representation using upper LFT, $G_{updated} = \mathcal{F}_u(G_{fi}, \Delta)$

$$G_{fi} = \left[\begin{array}{c|cc} A & B_\Delta & B \\ \hline C_\Delta & 0 & 0 \\ C & 0 & 0 \end{array}\right] \tag{5}$$

B_Δ and C_Δ represent changes in the nominal plant caused by deviations in stiffness and damping of the gas seal. B_Δ and C_Δ are built as shown in [29, 30] and given in Appendix A.

3.3 Identification of Seal Parameters for Different Pressures

The seal force parameters of the specific test seal have been identified in [30]. Here the seal coefficients are identified using sinusoidal disturbance forces at different frequencies to investigate their frequency dependency. The excitation force is generated using the AMBs by adding an excitation current on top of the control current used to stabilize and levitate the rotor. From the experiments, it is seen that the seal adds a significant amount of cross coupled stiffness which is dependent on the applied pressure and that the seal force coefficients have no frequency dependency in the frequency range of 0-200 Hz. Since the seal force coefficients are considered frequency independent and the stepped sinusoidal procedure is time-consuming, it is chosen to identify the seal force parameters for different pressures using impulse disturbances of 0.05 A with a duration of 10 ms for both bearings in ζ direction. Impulse responses showing the performance of the identified global model compared to experimental data are seen in Fig. 5 and 6, where the seal force coefficients have been identified at pressures of 0.95 bar and 1.90 bar, respectively. The decentralised PID controller with the gains given in Sec. 4.2 is used for the identification of the seal forces. The simulated and experimental responses match very well, indicating that the model captures the seal dynamics well. Moreover, the shaft lateral displacements at A_ζ are smaller than at B_ζ due to the coupling montage near bearing A and due to different K_i and K_s values of the two bearings. Identification results of K_i and K_s values can be found in [37] and coupling stiffness values can be found in [30]. Shaft lateral displacements are also detected in η direction due to the cross coupling gas seal forces. Nevertheless, the shaft lateral response in η direction is relatively low due to the low values of pressure drop along the seals, as depicted in Fig. 5 for pressure drops of 0.95 bar. The shaft lateral response in η direction becomes significantly larger when the pressure drop across the seal is increased by a factor 2, namely to 1.90 bar, as illustrated in Fig. 6.

The behaviour of the identified seal force coefficients as a function of the pressure drop along the seal is shown in Fig. 7. Linear regression lines are shown to highlight the trends and the estimation uncertainty of each coefficient. The direct stiffness K is low and weakly-dependent on the pressure drop along the (worn) seal with relatively large radial clearance. The cross coupled stiffness k is the most significant parameter and has a strong correlation with the applied pressure. It can be observed in Fig. 7 that the uncertainty of the estimated damping parameters, relative to their size, is large; though, it is normally expected that there is larger uncertainties in estimating damping than stiffness parameters. As shown in [30] direct damping D improves the global models accuracy. Nevertheless, such an identified parameter seems to compensate for some residual dynamics coming from the electro dynam-

ics rather than from the gas seal. The cross coupled damping decreases with increased pressure drop along the gas seal in the pressure range investigated.

Fig. 7 also shows the nominal pressure for the control design. Nominal gas seal force coefficients are found at the pressure of 2.15 bar using the values obtained from the linear regression lines.

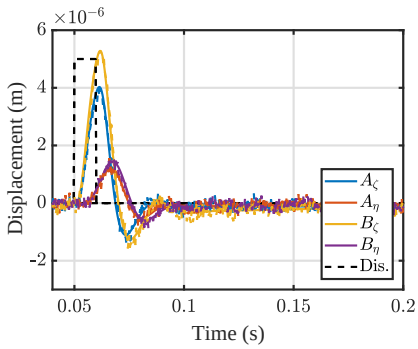

Fig. 5: Comparison of experimental (solid lines) and global model (dashed) impulse response using 0.95 bar inlet pressure. The global model includes the seal coefficients identified for the given pressure. Current impulse disturbance from 0.05 s to 0.06 s is scaled in amplitude and shown as the dashed line.

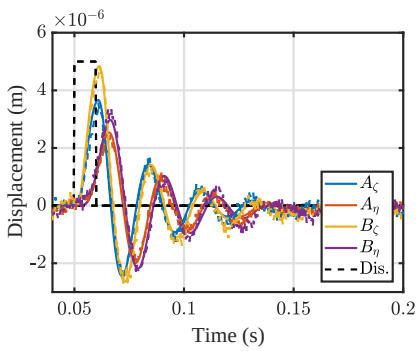

Fig. 6: Comparison of experimental (solid lines) and global model (dashed) impulse response using 1.90 bar inlet pressure. The global model includes the seal coefficients identified for the given pressure. Current disturbance from 0.05 s to 0.06 s is scaled in amplitude and shown as the dashed line.

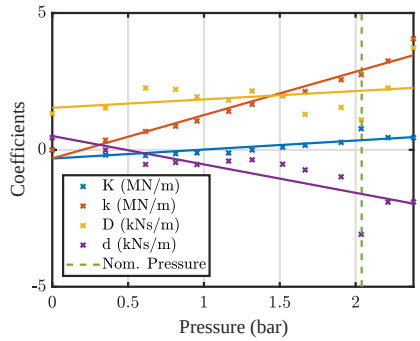

Fig. 7: Seal coefficients as function of the pressure drop across the seal inlet marked with 'x'. The solid lines show linear regression lines, estimated for each coefficient. The nominal pressure, used for the design of the model based controllers, is shown as the dashed line.

4 Design of Controllers

4.1 Control Design Objectives and Challenges

An $\mathcal{H}_\infty$ controller and μ controller are designed with the following objectives

1. The synthesised controllers should have similar gains of the direct terms in the frequency range of 0-200 Hz for them to be comparable. It is less challenging to find a controller that robustly stabilizes the plant for uncertain seal forces if the direct stiffness and damping gains are proportionally much higher than the cross coupled forces from the seals. Especially for the specific case where the rotor is considered rigid and thus no flexible modes will be excited.
2. Due to changes of the operational pressure across the seal, the controllers should deliver robust performance to plants with pressure drop changes within $\pm 100\,\%$ of the nominal pressure drop across the seal. The nominal pressure drop is chosen to be 2.04 bar, i.e. the controller must deliver robust performance in the range of 0-4.08 bar. Due to high preswhirl flow conditions associated to the gas seal under investigation, it is assumed that pressure changes only significantly alter the cross coupled stiffness k. Thus, changes in the seal coefficients K, D, d due to pressure change have been neglected when synthesizing the controllers and evaluating the compliance and sensitivity functions. It should however be noted that the nominal values of the coefficients are used in the nominal model. The identified values of K, D and d for two given pressures drop scenarios are directly used in the experimental validation of the controllers in Sec. 5.2 to show the exact controller performance.
3. The same parametric uncertainty δ_1 is used both for k, $-k$ to reduce the conservativeness in regard to synthesizing the robust controllers (See Appendix A).

4. The controller should satisfy ISO 14839-3, which states that the closed loop sensitivity (disturbance to error) should be less than 3 for all frequencies in order to be classified as Zone A [19]. This is to ensure a general robustness of the system due to unmodelled dynamics and gains in the system which can change over time. Although ISO 14839-3 only requires the sensitivity to be lower than 3 for each diagonal element, it is in this framework required that the maximum singular value of the full sensitivity function to be lower than 3 to ensure robustness due to cross coupled dynamics.
5. The compliance function should be as low as possible over the complete operational range to ensure small orbits and responses due to unbalance forces and other external disturbances.

4.2 Reference controller

A decentralised PID controller is chosen as a reference controller with an integral time T_i of 0.2 s and derivative time T_d of 3.5 ms with the transfer function

$$K_{PID} = K_p \left(1 + \frac{1}{T_i s} + \frac{T_d s}{\varepsilon T_d s + 1}\right) \tag{6}$$

The derivative action is limited for high frequencies using the term $\varepsilon T_d s + 1$ with $\varepsilon = 0.1$. K_p is the overall gain of the controller. This type of controller is the most commonly used controller in the industry for AMB systems due to its simple structure with only a few parameters to be tuned. This controller has shown to deliver good performance during an extensive experimental testing campaign. Nevertheless, due to its decentralised structure, it does not directly compensate for lateral cross coupling interaction coming from gyroscopic or seal forces.

4.3 Robust Control Design Interconnection and Weight Functions

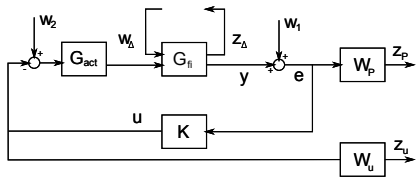

Fig. 8: Interconnection of actuator model G_{act}, rotordynamic model with uncertainty representation G_{fi}, performance weight functions W_P and W_u, and controller K.

The interconnection in Fig. 8 and 9 is used for robust controller synthesis. W_p shapes the sensitivity functions i.e. the relationship from input and output disturbances W_1 and

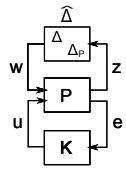

Fig. 9: Interconnection rearranged to the augmented system P, externally connected to the controller and $\hat{\Delta}$ containing Δ for uncertain plant representation and Δ_P as full complex perturbation for performance specification.

W_2 to the displacement error e. W_p is formulated with the structure

$$W_P = \frac{\frac{s}{M} + w_B}{s + w_B A_w} \tag{7}$$

The weighting function W_p has multiple purposes: I) Set a low sensitivity at low frequencies to obtain an integral effect, which eliminates steady state error in position reference. The constant A_w indicates the steady state error and is set to $\frac{1}{1000}$. II) The constant M indicates the maximum peak of the sensitivity functions and is tuned to obtain a peak value smaller than 3 (or 9.5 dB) for robustness [19]. III) The crossover frequency w_B indicates the desired bandwidth of the closed loop system [36]. This parameter is tuned to achieve an integral time close to the reference controller of 0.2 s.

The weight W_u has a function of adjusting the roll-off frequency of the controller and the amount of control effort. This weight is tuned to obtain similar gains as the PID reference controller in the mid range frequency range. The weight W_u is chosen as a constant and is independently tuned for the synthesis of the $\mathcal{H}_\infty$ and μ controllers to obtain similar gains of the direct terms, in order words, $K_{\mathcal{H}_\infty}(1,1) \approx K_\mu(1,1)$, $K_{\mathcal{H}_\infty}(2,2) \approx K_\mu(2,2)$, $K_{\mathcal{H}_\infty}(3,3) \approx K_\mu(3,3)$ and $K_{\mathcal{H}_\infty}(4,4) \approx K_\mu(4,4)$ as shown in Fig. 10.

4.4 Robust Control Synthesis

Fig. 8 shows the interconnection rearranged for controller synthesis such that P is the fixed augmented plant. Note that Δ is for the uncertain plant representation and Δ_P (full perturbation matrix representing the $\mathcal{H}_\infty$ performance specification) are collected into the diagonal elements of $\hat{\Delta}$. Hence synthesising a controller can be done by finding a controller that minimises the ∞ norm of the transfer function from w to z, formulated as a lower LFT

$$\gamma = ||F_l(P,K)||_\infty \tag{8}$$

An $\mathcal{H}_\infty$ controller of order 20 is synthesized using the nominal plant representation and a μ controller of order 24 is synthesized using the perturbed plant . The state space matrices of the synthesised controllers can be found in Appendix B.

The gain of the controller transfer functions is shown in Fig. 10. The shape of the direct terms of both the $\mathcal{H}_\infty$- and μ controller turns out to be very similar to the PID controller. While the direct gains of the three controllers are similar (up to 200 Hz), some of the cross coupling gains are quite different for the $\mathcal{H}_\infty$ and the μ controller, as shown for the term(1,3), representing the coupling between A_ζ and B_η, i.e. cross coupling gain linking the lateral movements of the shaft at bearing locations A and B in their orthogonal directions ζ and η (centralized controller).

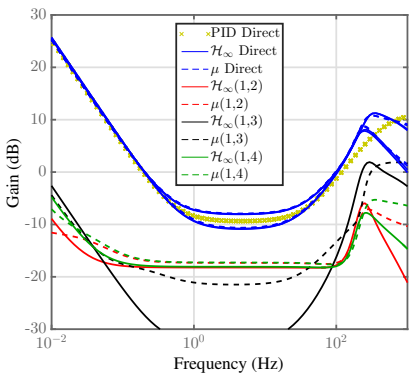

Fig. 10: Comparison of the direct and cross coupled gain of the controllers. Indices [1,2,3,4] represent node points [A_ζ, A_η, B_ζ, B_η]

4.4.1 Compliance Function

The compliance transfer function describes the relation between rotor lateral displacements at bearing locations A and B and external perturbation forces. This function must be as low as possible at all frequencies to ensure good force disturbance rejections and small orbits. An upper bound of the amplitude of the compliance function can be found by calculating maximum singular values of the compliance function, $\bar{\sigma}(G_f)$. These are shown for the system at nominal pressure (solid lines) and at nominal pressure with $\pm 100\,\%$ variation of nominal pressure in Fig. 11.

Not surprisingly, it is seen that $\mathcal{H}_\infty$ and μ controllers have their lowest amplitude over the frequency range for the nominal pressure (solid lines), since this corresponds to their design point, i.e. nominal operational pressure across the seal of 2.15 bar. Their amplitudes for the nominal pressure are only slightly higher than for the PID controller at low pressure condition. The rotor-bearing-seal system operating with the PID controller has a resonance peak at 40 Hz at nominal pressure. At a slightly higher frequency (50 Hz) the $\mathcal{H}_\infty$ has a peak which is the largest for the low pressure condition. Rotor-bearing-seal system operating with both the $\mathcal{H}_\infty$ and μ controllers have a resonance peak at a low frequency at approximately 2 Hz for low pressure conditions, showing their worst performance at low frequencies. This is evidenced by the highest compliance values at low frequencies in Fig. 11. The compliance function can be used as an indication of the worst case of unbalance response, if this function is multiplied by expected unbalance force, as shown in Fig. 12.

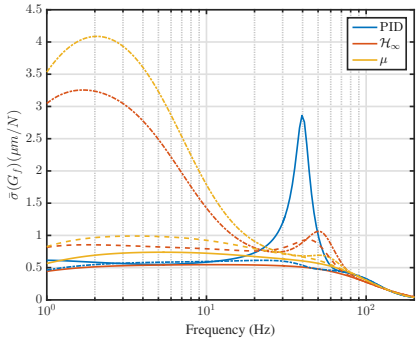

Fig. 11: The maximum amplitude of the compliance function using the three controllers. The solid lines indicate the performance of the controllers at nominal pressure. The lines marked with '- -' indicate high pressure i.e. +100 % of pressure compared to the nominal pressure and the lines marked with '-.' indicate low pressure i.e. $-100\,\%$ of pressure compared to the nominal pressure. The PID controller with high pressure is not shown since this makes the system unstable.

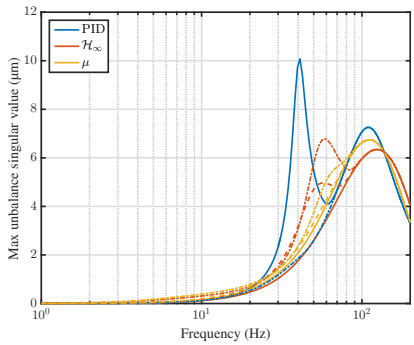

Fig. 12: The maximum singular value of the unbalance function for the three controllers. The solid lines indicate the performance of the controllers at nominal pressure. The lines marked with '- -' indicate high pressure i.e. +100 % of pressure compared to the nominal pressure and the lines marked with '-.' indicate low pressure i.e. $-100\,\%$ of pressure compared to the nominal pressure. The PID controller with high pressure is not shown since this makes the system unstable.

Assuming the shaft is balanced according to the G2.5 norm at 500 Hz results in a maximum unbalance force of 541 N at 500 Hz. Both the $\mathcal{H}_\infty$ and μ controllers ensure an orbit below 8 μm over the 200 Hz frequency range, which is considered acceptable. Gyroscopic effects are neglected for simplicity.

4.4.2 Sensitivity of Perturbed Plant Using Different Controllers

The closed-loop output sensitivity functions are shown in Fig. 13 using the perturbed plant with $\pm 100\,\%$ cross coupled stiffness variation and the PID, $\mathcal{H}_\infty$ and μ controllers. The μ controller nearly ensures the maximum peak of the singular values of the closed loop sensitivity function to be below 3 (or 9.5 dB), as recommended by ISO 14839-3. The $\mathcal{H}_\infty$ has higher sensitivity peaks than 3, but stabilises the plant for the whole pressure range. The PID controller has very high peaks and does not stabilise the system for high pressures. The input sensitivity is seen to be very similar to the output sensitivity and is not shown here.

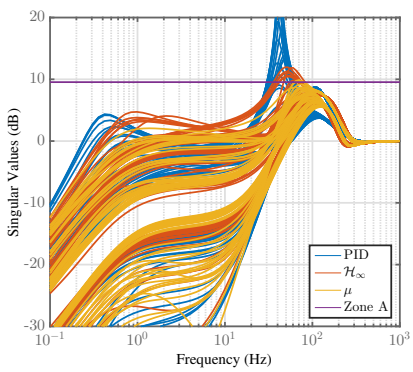

Fig. 13: Closed-loop output sensitivity of perturbed plant using PID, $\mathcal{H}_\infty$ and μ controllers.

5 Theoretical and Experimental Results

The performance of the designed controllers is demonstrated in this section using different disturbances and pressures. Simulation results show the performance of the perturbed plant in terms of the rotor lateral displacement and AMB current responses to current impulse disturbances. Experimental verification of the closed loop performance under different pressure conditions is shown for a pressure and a no pressure condition with two different current impulse disturbances.

5.1 Time Simulation of Perturbed Plant Operating With Different Controllers

Fig. 14 shows the simulated impulse response of the perturbed plant. Identical impulsive 10 ms disturbances of 0.05 A on both AMBs are simultaneously applied, exciting the rotor lateral movements orthogonally at positions A and B, i.e. directions A_ζ and B_η. There is a clear coincidence between the robustness issues in terms of the high peaks in sensitivity functions shown in Fig. 13 and the oscillations in the responses shown in 14. The μ controller leads to a rotor-bearing-seal system with lower sensitivity peaks and more stable (shorter settling time) than the system with the $\mathcal{H}_\infty$ controller. The rotor-bearing-seal system with PID controller turns unstable for high pressures across the gas seal. It is interesting to note that the μ controller handles the cross coupled forces differently to the $\mathcal{H}_\infty$ controller seen at the beginning of the impulse response. Here it can be seen that the two controllers requested currents start in opposite directions at A_η.

5.2 Experimental Validation of Controller Performance

The controller performance due to the impulse excitation current is verified experimentally, using a current disturbance simultaneously at the orthogonal directions and different bearing locations A_ζ and B_η, as shown in Fig. 15, and using a current disturbance simultaneously at the different bearing locations but in one single direction ζ, A_ζ and B_ζ, as shown in Fig. 16. It is chosen to benchmark the controllers at two conditions: 1) at a pressure drop of 2.04 bar which is the nominal design condition of the model based controllers. 2) at zero pressure drop which corresponds to a deviation of the cross coupled stiffness of $-100\,\%$ compared to the nominal design condition of the model based controllers. This is to test the robust performance of the model based controllers, i.e. how well they perform when operating far away from the nominal conditions. It is also to see the performance of the PID controller and how well the model performs, when applying different controllers. The top plots in Fig. 15 and Fig. 16 show the rotor lateral displacement responses for zero pressure drop across the gas seal while the lower pictures show the responses for the case of 2.04 bar across the gas seal. The experimental and simulated responses match well, indicating that the model fits well for different disturbances and the controllers act as expected. The seal force coefficients are identified based on responses using the PID reference controller as described ealier. From the plots, it can be observed that

1. The decentralized PID shows good performance when no pressure is applied as seen in e.g. Fig. 15a. The displacement in A_ζ and B_η directions are not equal despite the same sized current disturbance being applied in both AMBs. This is due to the flexible coupling that is mounted close to bearing A, and due to bearing A and B having different K_i and K_s values. No cross coupling is seen in the responses for the disturbance entering via A_ζ and B_ζ since no pressure is applied and no significant cross coupling exists in the decentralised PID controller.

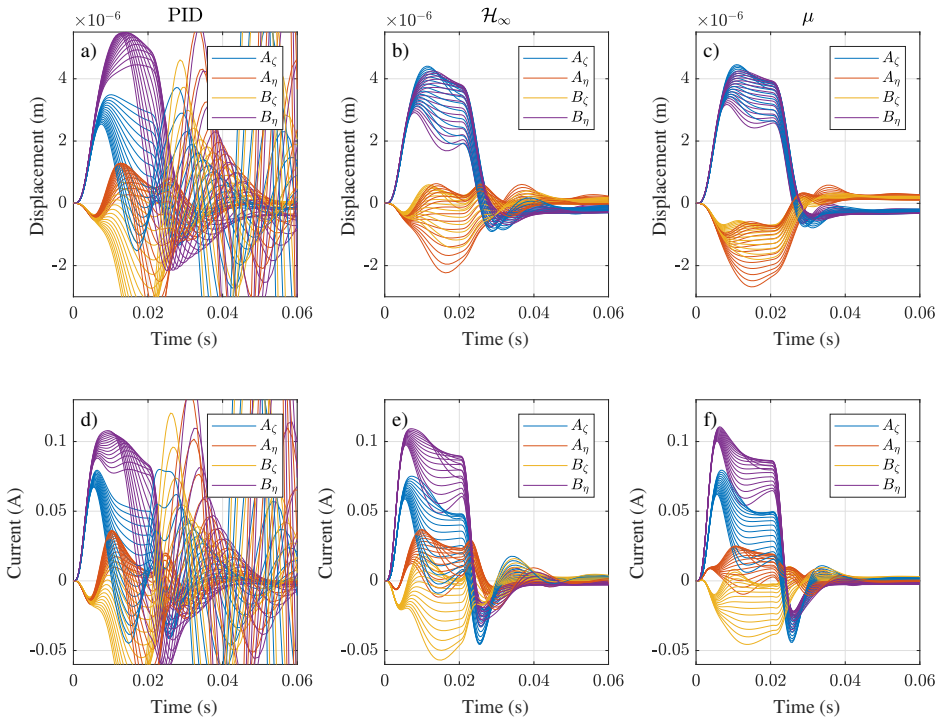

Fig. 14: Impulse response of perturbed plant using PID controller (left), $\mathcal{H}_\infty$ controller (middle) and μ controller (right). Lower plots show the control action in response to the impulse response.

This is seen in Fig. 16a. Stability and performance issues arise as the pressure is applied since this decentralized controller structure does not compensate for cross coupled seal forces. This is seen as oscillations in Fig. 15d.

2. The $\mathcal{H}_\infty$ shows good performance for the nominal design point where a fixed pressure across the seal is applied as seen in Fig. 15e. The settling time of approximately 0.03 s is very similar to the settling of the PID controller without pressure applied. The displacement in A_ζ and B_ζ is equal since the $\mathcal{H}_\infty$ controller synthesis accounts for the flexible coupling and the different K_i and K_s values of the two bearings. Stability problems can be detected when using this controller for the case of zero pressure across the seal. Such a claim can be reinforced by Fig. 15b.
3. The μ controller shows very similar performance as the $\mathcal{H}_\infty$ controller when the pressure drop across the gas seal is 2.04 bar. Such a similarity in terms of overshoot as well as settling time is depicted in Fig. 15e, even though the cross coupling effects due to the aerodynamic seal forces are handled slightly differently. For the case of no pressure drop across the seal, an improvement in terms of settling time, stabilization and reduction of oscillating behaviour is seen when using the μ compared to the $\mathcal{H}_\infty$ controller. Hence the μ controller is more robust to changes of pressures across the seal.

6 Conclusion

This paper demonstrates theoretically as well experimentally the capabilities of three types of controllers to deal and compensate rotor lateral vibrations induced by destabilising aerodynamic seal forces. Numerical simulations of rotor lateral dynamics are carried out using identified mathematical models. Experiments are conducted using the synthesised controllers applied to the test facility. Comparison between theoretical and experimental results agrees very well, allowing us to conclude that:

i) The designed $\mathcal{H}_\infty$ controller shows significant performance improvements when the rotor-bearing-seal system operates close to design pressure conditions, i.e. pressure drop across the gas seal around 2.04 bar. However, when the pressure drop across the seal changes from the nominal one, the

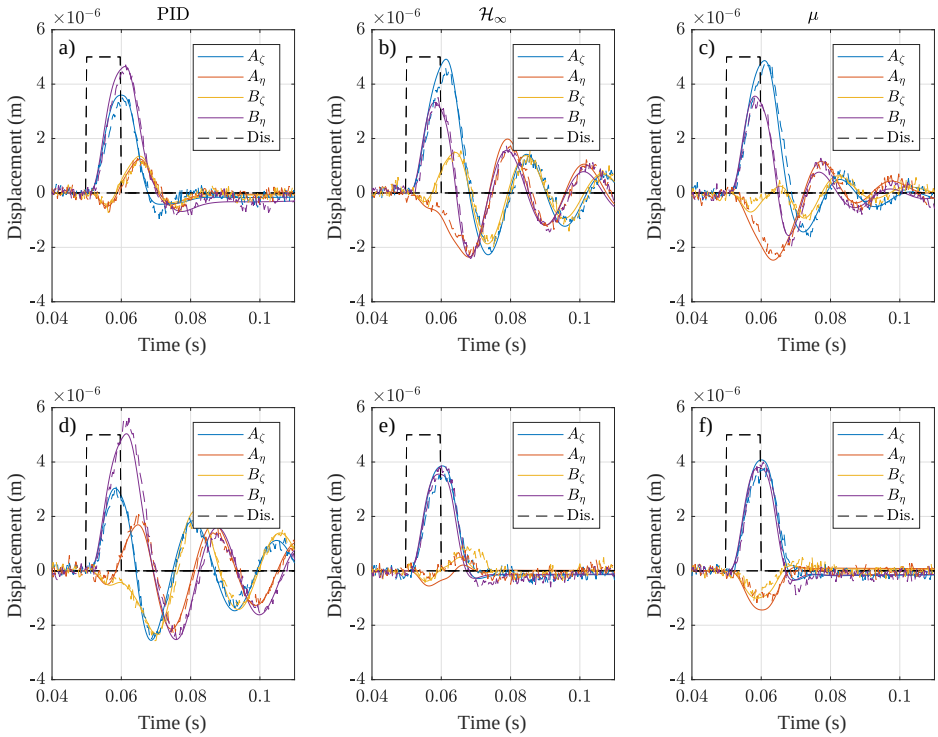

Fig. 15: Impulse response of plant in A_ζ and B_η direction using PID controller (left), $\mathcal{H}_\infty$ controller (middle) and μ controller (right). Upper plots show the response for when no pressure is applied and lower plots show the response when 2.04 bar pressure is applied. Simulated responses are shown as solid lines and experimental responses are marked with '- -'. Current setpoint disturbance from 0.05 s to 0.06 s is scaled in amplitude and shown as the dashed line 'Dis.'.

performance of the controller is reduced, once the identified model used to synthesize the controller is no longer able to accurately predict the dynamics of the rotor-bearing-seal system (plant). Specifically, a decreased performance is observed when the pressure drop across the seal is lower than the nominal condition. ii) Using the perturbed plant formulation and μ synthesis to design robust controllers, it is shown to be possible to optimize and improve the worst case performance over a larger pressure range. The synthesised μ controller is able to handle pressure variations better than the $\mathcal{H}_\infty$ controller.

iii) Since the controller gains, and thus the direct stiffness and damping coefficients of the AMBs are cost parameters, they are kept approximately constant for all three types of controllers, namely PID, $\mathcal{H}_\infty$ and μ. The parameters subjected to changes are only the gas seals force coefficients due to pressure drop variations. The seal force coefficients are quite high compared to the force coefficients of the AMBs. The theoretical and experimental investigations were carried out in such a way to emphasise the difference in performance of the controllers with similar gains. A slightly more realistic approach would be to increase the controller gain or the size of the AMBs to obtain larger values of direct stiffness and damping. This would immediately increase robustness and stability followed by significant improvement in system performance.

iv) Finalizing, this paper has presented a structured way to design robust controllers to deal with uncertain/varying seal forces, including the tuning of the weighting functions. It is shown that the robust controller synthesis deals with finding a non-conservative controller that will guarantee robust performance while at the same time keeping the controller gains moderate. The method could potentially be implemented in any AMB based systems subjected to seal or other fluid film forces.

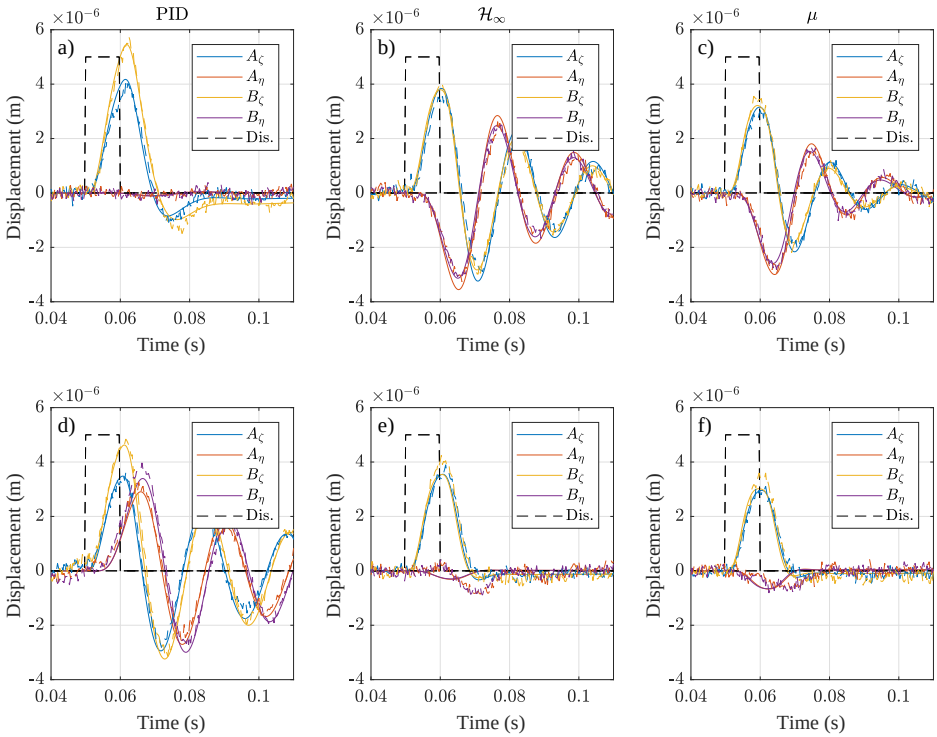

Fig. 16: Impulse response of plant in A_ζ and B_ζ direction using PID controller (left), $\mathcal{H}_\infty$ controller (middle) and μ controller (right). Upper plots show the response for when no pressure is applied and lower plots show the response when 2.04 bar pressure is applied. Simulated responses are shown as solid lines and experimental responses are marked with '- -'. Current setpoint disturbance from 0.05 s to 0.06 s is scaled in amplitude and shown as the dashed line 'Dis.'.

A The System Matrices

The system matrices for the nominal plant in section 3 and perturbed plant in 3.2 are given as

$$A = \begin{bmatrix} -111 & -166 & 130 & 84.6 & 8.07 & -8.07 & -2.81 & -2.81 \\ 155 & 100 & 130 & 84.6 & 8.07 & -8.07 & -2.81 & -2.81 \\ -132 & 86.2 & -261 & 67.7 & -3.56 & 3.55 & -4.62 & -4.62 \\ 132 & -86.2 & -4.56 & 198 & 3.56 & -3.55 & 4.62 & 4.62 \\ 86.7 & -86.7 & -52.5 & -52.6 & -180 & -117 & -0.11 & -0.108 \\ 86.8 & -86.8 & -52.6 & -52.6 & 118 & 180 & -0.108 & -0.106 \\ 64.1 & -64.1 & 148 & 148 & -0.934 & 0.861 & 182 & -116 \\ -64.1 & 64.1 & -148 & -148 & 0.86 & -0.787 & 116 & -182 \end{bmatrix}$$

$$B = \begin{bmatrix} -1.716\times10^{-2} & 5.470\times10^{-2} & -1.716\times10^{-2} & 5.470\times10^{-2} \\ -1.716\times10^{-2} & 5.469\times10^{-2} & -1.716\times10^{-2} & 5.469\times10^{-2} \\ -3.508\times10^{-2} & -4.534\times10^{-2} & -3.508\times10^{-2} & -4.534\times10^{-2} \\ 3.508\times10^{-2} & 4.533\times10^{-2} & 3.508\times10^{-2} & 4.533\times10^{-2} \\ 1.276\times10^{-2} & 2.533\times10^{-1} & -1.276\times10^{-2} & -2.533\times10^{-1} \\ 1.277\times10^{-2} & 2.534\times10^{-1} & -1.277\times10^{-2} & -2.534\times10^{-1} \\ -2.265\times10^{-1} & -1.142\times10^{-1} & 2.265\times10^{-1} & 1.142\times10^{-1} \\ 2.265\times10^{-1} & 1.140\times10^{-1} & -2.265\times10^{-1} & -1.140\times10^{-1} \end{bmatrix}$$

$$C^T = \begin{bmatrix} 4.654\times10^{-4} & -3.601\times10^{-4} & 4.654\times10^{-4} & -3.601\times10^{-4} \\ -4.653\times10^{-4} & 3.602\times10^{-4} & -4.653\times10^{-4} & 3.602\times10^{-4} \\ 5.615\times10^{-4} & 1.761\times10^{-4} & 5.615\times10^{-4} & 1.761\times10^{-4} \\ 5.614\times10^{-4} & 1.762\times10^{-4} & 5.614\times10^{-4} & 1.762\times10^{-4} \\ 8.229\times10^{-5} & -1.635\times10^{-4} & -8.229\times10^{-5} & 1.635\times10^{-4} \\ -8.238\times10^{-5} & 1.634\times10^{-4} & 8.238\times10^{-5} & -1.634\times10^{-4} \\ -1.828\times10^{-4} & 9.214\times10^{-6} & 1.828\times10^{-4} & -9.214\times10^{-6} \\ -1.828\times10^{-4} & 9.211\times10^{-6} & 1.828\times10^{-4} & -9.211\times10^{-6} \end{bmatrix}$$

$$D = \begin{bmatrix} 0 & 0 & 0 & 0 & 0 & 0 \\ 0 & 0 & 0 & 0 & 0 & 0 \\ 0 & 0 & 0 & 0 & 0 & 0 \\ 0 & 0 & 0 & 0 & 0 & 0 \\ 0 & 0 & 0 & 0 & 0 & 0 \\ 0 & 0 & 0 & 0 & 0 & 0 \end{bmatrix}$$

$$B_\Delta = \begin{bmatrix} 5.522\times10^{4} & 1.760\times10^{5} \\ 5.524\times10^{4} & 1.760\times10^{5} \\ 1.129\times10^{5} & -1.459\times10^{5} \\ -1.129\times10^{5} & 1.459\times10^{5} \\ -2.736\times10^{-3} & -8.407\times10^{-3} \\ -2.729\times10^{-3} & -8.418\times10^{-3} \\ -5.877\times10^{-3} & -1.426\times10^{-3} \\ 5.885\times10^{-3} & 1.438\times10^{-3} \end{bmatrix}$$

$$C_\Delta^T = \begin{bmatrix} -3.584\times10^{-4} & 4.632\times10^{-4} \\ 3.585\times10^{-4} & -4.631\times10^{-4} \\ 1.753\times10^{-4} & 5.588\times10^{-4} \\ 1.754\times10^{-4} & 5.588\times10^{-4} \\ 1.049\times10^{-12} & 1.432\times10^{-13} \\ -1.047\times10^{-12} & -1.446\times10^{-13} \\ -1.888\times10^{-13} & -3.178\times10^{-13} \\ -1.894\times10^{-13} & -3.160\times10^{-13} \end{bmatrix}$$

$$\Delta = \begin{bmatrix} \delta_1 & 0 \\ 0 & \delta_1 \end{bmatrix}, |\delta_1| < 1$$

B The Controller Statespace Matrices

C $\mathcal{H}_\infty$ Controller

$$B = \begin{bmatrix}
-3.705 & 7.297 & 4.803 & 9.525 \\
-6.587 & -9.528 & 3.470\times10^{-1} & 7.900 \\
7.240 & -3.190\times10^{-1} & -5.397 & 7.324 \\
-2.300\times10^{-1} & 9.377 & -9.378 & -7.295 \\
2.246 & -4.358 & 3.180\times10^{-1} & 3.946 \\
4.261 & 2.135 & -3.835 & 2.420\times10^{-1} \\
1.622 & -6.690\times10^{-1} & 1.318 & -1.769 \\
6.680\times10^{-1} & 1.634 & 1.733 & 1.285 \\
9.743 & -2.052\times10^{1} & 1.707 & 1.860\times10^{1} \\
2.029\times10^{1} & 9.249 & -1.812\times10^{1} & 1.437 \\
-7.117 & 1.320 & -6.848 & 6.251 \\
1.305 & 7.034 & 6.111 & 6.741 \\
1.140 & 1.800\times10^{-2} & -1.530 & 0.000 \\
0.000 & 1.070 & 1.400\times10^{-2} & -1.543 \\
-7.710\times10^{-1} & -2.930\times10^{-1} & -8.130\times10^{-1} & -1.990\times10^{-1} \\
-2.930\times10^{-1} & 7.640\times10^{-1} & -1.940\times10^{-1} & 7.690\times10^{-1} \\
5.460\times10^{-1} & 1.270\times10^{-1} & -6.900\times10^{-1} & 2.800\times10^{-1} \\
1.050\times10^{-1} & -4.990\times10^{-1} & 2.670\times10^{-1} & 7.020\times10^{-1} \\
-5.570\times10^{-1} & -1.560\times10^{-1} & -8.780\times10^{-1} & -1.410\times10^{-1} \\
-1.500\times10^{-1} & 5.430\times10^{-1} & -1.430\times10^{-1} & 8.640\times10^{-1}
\end{bmatrix}$$

$$C^T = \begin{bmatrix}
-4.587\times10^{2} & 2.548\times10^{2} & 7.269\times10^{2} & 5.248\times10^{2} \\
-3.563\times10^{2} & -5.871\times10^{2} & -6.740\times10^{2} & 9.188\times10^{2} \\
9.618\times10^{2} & -5.935\times10^{2} & -1.936\times10^{3} & 1.277\times10^{3} \\
1.820\times10^{2} & 2.838\times10^{2} & -1.450\times10^{3} & -6.449\times10^{2} \\
1.234\times10^{1} & 8.350\times10^{1} & 1.754\times10^{1} & -1.376\times10^{2} \\
-8.619\times10^{1} & 1.218\times10^{1} & 1.407\times10^{2} & 1.652\times10^{1} \\
3.338 & 4.289 & 6.950\times10^{-1} & 5.429\times10^{1} \\
-3.833 & 2.517 & -5.538\times10^{1} & 6.740\times10^{-1} \\
1.044\times10^{1} & 1.366\times10^{2} & 3.993\times10^{1} & -2.239\times10^{2} \\
-1.430\times10^{2} & 1.081\times10^{1} & 2.313\times10^{2} & 3.845\times10^{1} \\
1.189 & -1.673 & -6.310 & -9.959\times10^{1} \\
-7.620\times10^{-1} & -2.605 & -1.024\times10^{2} & 6.775 \\
4.032 & -6.230\times10^{-1} & -9.047 & -4.650\times10^{-1} \\
6.110\times10^{-1} & 3.613 & 3.650\times10^{-1} & -8.645 \\
-1.152 & -3.520\times10^{-1} & -4.106 & 3.040 \\
-3.320\times10^{-1} & 1.244 & 3.121 & 3.726 \\
2.648 & -1.450\times10^{-1} & -4.128 & 1.846 \\
-1.380\times10^{-1} & -2.493 & 1.818 & 4.064 \\
3.620\times10^{-1} & -2.000\times10^{-3} & 8.490\times10^{-1} & -3.036 \\
1.600\times10^{-2} & -4.020\times10^{-1} & -3.132 & -8.630\times10^{-1}
\end{bmatrix}$$

$$A = \begin{bmatrix}
-6849.3 & -2615.6 & 5494.9 & 3865.0 & 226.1 & -714.3 & -193.8 & 39.4 & 280.8 & -1436.1 & 627.0 & 183.8 & -52.3 & -18.0 & -9.7 & 108.3 & -1.9 & 3.9 & 17.0 & 47.9 \\
-2637.1 & -9661.1 & -4482.2 & 8558.9 & 1256.0 & -458.0 & -195.1 & 91.1 & 2437.9 & -1086.2 & 493.3 & 31.9 & -46.0 & -113.6 & 44.1 & -41.9 & -7.2 & 4.4 & 27.7 & 4.4 \\
2867.2 & -4908.1 & -18337.1 & -4021.2 & 565.8 & 848.9 & -230.3 & -205.0 & 1177.0 & 1637.4 & 492.4 & -444.8 & 83.0 & -52.7 & -45.0 & 44.3 & 3.7 & 8.7 & 19.6 & 6.4 \\
4995.9 & 4908.7 & 991.2 & -13554.0 & -1101.1 & 691.8 & 275.6 & -292.9 & -2116.7 & 1450.1 & -587.1 & -627.2 & 59.1 & 110.7 & 64.2 & 58.7 & 11.2 & -5.1 & 9.0 & -25.8 \\
-92.2 & -5453.7 & -10080.5 & 4238.0 & 884.4 & 139.5 & -213.7 & 31.0 & 1659.0 & 192.6 & 424.8 & 12.8 & 11.7 & -37.8 & -30.8 & -21.5 & -5.6 & -5.7 & 8.1 & 5.0 \\
4284.0 & 98.0 & -11323.7 & -7356.3 & -134.3 & 886.3 & -29.9 & -210.6 & -180.2 & 1672.6 & 13.4 & -421.6 & 34.3 & 10.7 & -20.7 & 29.6 & -5.9 & 5.2 & 4.8 & -8.5 \\
905.5 & 2846.6 & 2654.0 & 836.8 & -215.2 & -4.7 & 85.0 & 81.0 & -373.6 & 33.0 & -201.1 & 181.4 & 5.0 & -0.1 & -12.1 & -14.4 & 3.0 & 0.7 & -14.6 & -1.5 \\
-2152.2 & 1221.1 & 1966.8 & 2594.8 & -2.9 & -212.5 & -78.7 & 86.0 & -45.0 & -371.5 & 174.7 & 203.1 & 1.4 & 4.6 & -13.8 & 12.3 & 1.0 & -2.8 & -1.7 & 14.6 \\
-2336.0 & -39259.0 & -63477.4 & 30444.0 & 6279.7 & 558.8 & -1412.2 & 244.9 & 11134.6 & 537.4 & 2804.4 & 134.4 & 42.4 & 38.2 & -172.0 & -99.7 & -47.4 & -116.5 & 59.4 & 31.2 \\
31197.4 & -1519.0 & -82916.0 & -48458.1 & -526.9 & 6404.2 & -250.0 & -1413.3 & -455.8 & 11435.1 & 155.8 & -2828.0 & -68.6 & 35.8 & -102.6 & 168.8 & -122.3 & 45.7 & 30.1 & -61.8 \\
-8365.4 & -23570.8 & -33484.2 & -6320.3 & 2108.9 & 477.7 & -1070.3 & -714.2 & 3599.2 & 530.9 & 1856.3 & -1614.6 & -48.6 & 182.0 & -29.9 & -192.9 & -66.1 & -45.0 & 87.5 & -58.5 \\
-18080.3 & 11373.7 & 17840.4 & 31392.2 & 417.0 & -2094.2 & -704.3 & 1089.2 & 434.3 & -3602.4 & 1573.7 & 1896.0 & 181.2 & 42.5 & 206.0 & -30.5 & 42.8 & -63.3 & 58.7 & 88.1 \\
-15812.7 & 5248.6 & 39169.0 & 22619.4 & -108.1 & -3054.9 & 37.0 & 736.6 & -438.4 & -4869.9 & 129.2 & 1340.8 & -1180.7 & -6.6 & 105.3 & 20.4 & -1122.9 & 142.5 & -149.9 & 112.4 \\
-4656.2 & -20018.9 & -25149.6 & 12764.6 & 2976.6 & -108.1 & -734.7 & 27.2 & 4688.2 & -432.2 & 1312.4 & -154.2 & 8.9 & -1193.0 & 16.0 & -110.2 & 141.0 & 1125.3 & 119.7 & 160.4 \\
-1241.8 & 9728.3 & 6788.2 & 11018.4 & -272.9 & -311.0 & -31.0 & 541.3 & -452.3 & -516.6 & 133.4 & 738.4 & 66.7 & -91.2 & -1270.9 & -26.7 & 211.4 & 54.5 & -1177.5 & 282.7 \\
7136.1 & 972.2 & 4538.6 & -2527.4 & -236.9 & 252.1 & 514.6 & 23.5 & -399.6 & 419.6 & -688.3 & 119.7 & -94.5 & -60.1 & 21.8 & -1280.7 & -50.6 & 220.7 & -281.1 & -1178.6 \\
4139.6 & -1767.8 & -10424.0 & -5244.3 & 107.7 & 762.1 & -9.4 & -174.2 & 242.0 & 1251.5 & -14.6 & -335.0 & 1190.5 & -166.4 & -222.4 & -43.0 & -221.1 & 20.2 & -58.5 & -74.6 \\
-1499.6 & -5223.3 & -5212.1 & 3475.5 & 737.2 & -109.7 & -170.4 & 8.5 & 1196.1 & -245.8 & 324.2 & -18.3 & -166.1 & -1192.3 & 31.1 & -240.6 & -18.9 & -216.6 & 67.3 & -65.7 \\
759.1 & -3449.0 & -4503.6 & -3888.8 & 146.0 & 222.8 & -30.5 & -186.2 & 259.8 & 360.4 & 11.6 & -311.1 & 139.4 & -46.0 & 1168.3 & 229.4 & -27.0 & -76.6 & -276.6 & -44.2 \\
-2590.8 & -837.7 & -1626.1 & 2232.7 & 207.4 & -140.2 & -180.4 & 33.2 & 333.4 & -252.0 & 298.4 & 15.8 & -38.5 & -152.8 & -228.8 & 1169.4 & 80.1 & -24.6 & 46.9 & -272.6
\end{bmatrix}$$

$$D = \begin{bmatrix}
0 & 0 & 0 & 0 \\
0 & 0 & 0 & 0 \\
0 & 0 & 0 & 0 \\
0 & 0 & 0 & 0
\end{bmatrix}$$

D μ Controller

$$B = \begin{bmatrix}
0.000 & 0.000 & 0.000 & 1.000\times10^{-3} \\
0.000 & 0.000 & 0.000 & 0.000 \\
5.988\times10^{1} & 1.966\times10^{2} & 2.715\times10^{1} & 3.150\times10^{2} \\
-2.655\times10^{2} & 1.303\times10^{3} & -3.392\times10^{2} & 1.572\times10^{3} \\
-2.224\times10^{2} & -9.787\times10^{1} & -2.878\times10^{2} & -1.945\times10^{2} \\
9.787\times10^{2} & 1.046\times10^{3} & 1.129\times10^{3} & 1.264\times10^{3} \\
4.725\times10^{1} & 8.134\times10^{2} & -6.440\times10^{1} & -1.320\times10^{3} \\
2.685\times10^{2} & 5.001\times10^{3} & -2.938\times10^{2} & -5.984\times10^{3} \\
-4.589\times10^{3} & -2.247\times10^{3} & 5.369\times10^{3} & 2.704\times10^{3} \\
7.822\times10^{2} & 3.594\times10^{2} & -1.192\times10^{3} & -6.008\times10^{2} \\
2.000\times10^{-3} & 0.000 & 0.000 & 0.000 \\
0.000 & 2.000\times10^{-3} & 0.000 & 0.000 \\
0.000 & 0.000 & 2.000\times10^{-3} & 0.000 \\
0.000 & 0.000 & 0.000 & 2.000\times10^{-3} \\
-3.000\times10^{-3} & 0.000 & 1.000\times10^{-3} & 0.000 \\
1.000\times10^{-3} & 0.000 & 0.000 & 0.000 \\
0.000 & -3.000\times10^{-3} & 0.000 & 1.000\times10^{-3} \\
0.000 & 1.000\times10^{-3} & 0.000 & 0.000 \\
1.000\times10^{-3} & 0.000 & -3.000\times10^{-3} & 0.000 \\
0.000 & 0.000 & 2.000\times10^{-3} & 0.000 \\
0.000 & 1.000\times10^{-3} & 0.000 & -3.000\times10^{-3} \\
0.000 & 0.000 & 0.000 & 2.000\times10^{-3} \\
-1.000\times10^{-3} & 0.000 & -1.000\times10^{-3} & 0.000 \\
0.000 & 1.000\times10^{-3} & 0.000 & 1.000\times10^{-3}
\end{bmatrix}
\quad
C^T = \begin{bmatrix}
-2.325\times10^{1} & 1.843\times10^{3} & 2.700\times10^{2} & 3.132\times10^{3} \\
3.106\times10^{3} & 4.026\times10^{3} & 5.543\times10^{3} & 5.674\times10^{3} \\
1.884 & 2.001 & 3.313 & 2.589 \\
-4.456 & -1.377 & -7.122 & -1.309 \\
2.288 & 3.517 & 4.228 & 5.069 \\
1.013\times10^{1} & 1.220\times10^{1} & 1.735\times10^{1} & 1.716\times10^{1} \\
4.100\times10^{-2} & 5.200\times10^{-2} & 2.000\times10^{-2} & 1.780\times10^{-1} \\
-2.070\times10^{-1} & 2.180\times10^{-1} & 2.250\times10^{-1} & -7.790\times10^{-1} \\
-9.600\times10^{-2} & 3.960\times10^{-1} & 1.169 & 4.860\times10^{-1} \\
5.500\times10^{-2} & 8.800\times10^{-2} & 2.170\times10^{-1} & 1.150\times10^{-1} \\
1.781\times10^{4} & 1.346\times10^{4} & 1.936\times10^{4} & 1.858\times10^{4} \\
8.702\times10^{3} & 2.128\times10^{4} & 1.568\times10^{4} & 2.167\times10^{4} \\
1.587\times10^{4} & 1.912\times10^{4} & 3.661\times10^{4} & 2.642\times10^{4} \\
1.109\times10^{4} & 1.966\times10^{4} & 2.012\times10^{4} & 3.793\times10^{4} \\
5.502\times10^{4} & 3.234\times10^{4} & 4.778\times10^{4} & 4.374\times10^{4} \\
1.101\times10^{5} & 6.871\times10^{4} & 9.705\times10^{4} & 9.343\times10^{4} \\
3.234\times10^{4} & 7.508\times10^{4} & 5.753\times10^{4} & 7.053\times10^{4} \\
6.038\times10^{4} & 1.439\times10^{5} & 1.079\times10^{5} & 1.333\times10^{5} \\
4.778\times10^{4} & 5.753\times10^{4} & 1.241\times10^{5} & 7.861\times10^{4} \\
9.892\times10^{4} & 1.223\times10^{5} & 2.558\times10^{5} & 1.675\times10^{5} \\
4.374\times10^{4} & 7.053\times10^{4} & 7.861\times10^{4} & 1.439\times10^{5} \\
8.592\times10^{4} & 1.401\times10^{5} & 1.550\times10^{5} & 2.878\times10^{5} \\
5.056\times10^{3} & 4.553\times10^{3} & 8.049\times10^{3} & 6.224\times10^{3} \\
-3.550\times10^{3} & -6.490\times10^{3} & -6.235\times10^{3} & -9.079\times10^{3}
\end{bmatrix}$$

$$A = \left[\begin{array}{cccccccccccccccccccccccc}
-0 & 0 & 0 & 0 & 0 & 0 & 0 & 0 & 0 & 0 & 0 & 0 & 0 & 0 & 0 & 0 & 0 & 0 & 0 & 0 & 0 & 0 & 0 & 0 \\
0 & -0 & 0 & 0 & 0 & 0 & 0 & 0 & 0 & 0 & 0 & 0 & 0 & 0 & 0 & 0 & 0 & 0 & 0 & 0 & 0 & 0 & 0 & 0 \\
23688 & 7195 & -23 & -254 & 47 & 1 & -6 & 6 & 2 & 2 & 0 & 0 & 0 & 0 & 0 & -7001079 & 0 & 21573838 & 0 & -7934556 & 0 & 25293464 & -91276 & -516528 \\
128313 & -6766 & 964 & -710 & 34 & -12 & -23 & 23 & 7 & 7 & 0 & 0 & 0 & 0 & 0 & -7002457 & 0 & 21568214 & 0 & -7936117 & 0 & 25286871 & -91335 & -516385 \\
-15809 & -23777 & -51 & 5 & -56 & 273 & 3 & -3 & 2 & 2 & 0 & 0 & 0 & 0 & 0 & -14313495 & 0 & -17882589 & 0 & -16221961 & 0 & -20965794 & -443011 & 481953 \\
116164 & 105845 & 42 & 4 & -969 & -766 & -11 & 11 & -11 & -11 & 0 & 0 & 0 & 0 & 0 & 14313771 & 0 & 17876102 & 0 & 16222274 & 0 & 20958188 & 442991 & -481793 \\
-23280 & -4112 & -21 & 21 & 7 & 7 & 32 & -330 & 0 & 0 & 0 & 0 & 0 & 0 & 0 & 5207601 & 0 & 99887417 & 0 & -5901947 & 0 & -117109388 & 0 & 0 \\
-45096 & -7620 & -124 & 124 & 60 & 60 & 1211 & -912 & 1 & 1 & 0 & 0 & 0 & 0 & 0 & 5210942 & 0 & 99919285 & 0 & -5905734 & 0 & -117146750 & 0 & 0 \\
24898 & 36523 & -57 & 57 & -167 & -167 & 5 & -6 & -926 & -1224 & 0 & 0 & 0 & 0 & 0 & -92418242 & 0 & -45033594 & 0 & 104740676 & 0 & 52798006 & 0 & 0 \\
-13123 & -19218 & -1 & 1 & 18 & 18 & -3 & 3 & 336 & 38 & 0 & 0 & 0 & 0 & 0 & 92414117 & 0 & 44970403 & 0 & -104736001 & 0 & -52723920 & 0 & 0 \\
0 & 0 & 0 & 0 & 0 & 0 & 0 & 0 & 0 & 0 & 0 & 0 & 0 & 0 & 0 & 0 & 0 & 0 & 0 & 0 & 0 & 0 & 0 & 0 \\
0 & 0 & 0 & 0 & 0 & 0 & 0 & 0 & 0 & 0 & 0 & 0 & 0 & 0 & 0 & 0 & 0 & 0 & 0 & 0 & 0 & 0 & 0 & 0 \\
0 & 0 & 0 & 0 & 0 & 0 & 0 & 0 & 0 & 0 & 0 & 0 & 0 & 0 & 0 & 0 & 0 & 0 & 0 & 0 & 0 & 0 & 0 & 0 \\
0 & 0 & 0 & 0 & 0 & 0 & 0 & 0 & 0 & 0 & 0 & 0 & 0 & 0 & 0 & 0 & 0 & 0 & 0 & 0 & 0 & 0 & 0 & 0 \\
1 & -159 & -0 & 0 & -0 & -1 & 0 & 0 & 0 & 0 & -912 & -446 & -813 & -568 & -4410 & -7446 & -1656 & -3092 & -2447 & -5066 & -2240 & -4400 & -259 & 182 \\
0 & 0 & 0 & 0 & 0 & 0 & 0 & 0 & 0 & 0 & 0 & 0 & 0 & 0 & 1024 & 0 & 0 & 0 & 0 & 0 & 0 & 0 & 0 & 0 \\
-95 & -206 & -0 & 0 & -0 & -1 & 0 & 0 & 0 & 0 & -689 & -1090 & -979 & -1007 & -1656 & -3519 & -5437 & -9178 & -2946 & -6261 & -3612 & -7173 & -233 & 332 \\
0 & 0 & 0 & 0 & 0 & 0 & 0 & 0 & 0 & 0 & 0 & 0 & 0 & 0 & 0 & 0 & 1024 & 0 & 0 & 0 & 0 & 0 & 0 & 0 \\
-14 & -284 & -0 & 0 & -0 & -1 & 0 & 0 & -0 & 0 & -992 & -803 & -1875 & -1031 & -2447 & -4970 & -2946 & -5524 & -7948 & -14907 & -4026 & -7936 & -412 & 319 \\
0 & 0 & 0 & 0 & 0 & 0 & 0 & 0 & 0 & 0 & 0 & 0 & 0 & 0 & 0 & 0 & 0 & 0 & 1024 & 0 & 0 & 0 & 0 & 0 \\
-161 & -291 & -0 & 0 & -0 & -1 & 0 & 0 & 0 & 0 & -951 & -1110 & -1353 & -1943 & -2240 & -4785 & -3612 & -6826 & -4026 & -8578 & -8960 & -16546 & -319 & 465 \\
0 & 0 & 0 & 0 & 0 & 0 & 0 & 0 & 0 & 0 & 0 & 0 & 0 & 0 & 0 & 0 & 0 & 0 & 0 & 0 & 1024 & 0 & 0 & 0 \\
0 & 0 & 0 & 0 & 0 & 0 & 0 & 0 & 0 & 0 & 0 & 0 & 0 & 0 & 0 & 0 & 0 & 0 & 0 & 0 & 0 & 0 & -2 & 0 \\
0 & 0 & 0 & 0 & 0 & 0 & 0 & 0 & 0 & 0 & 0 & 0 & 0 & 0 & 0 & 0 & 0 & 0 & 0 & 0 & 0 & 0 & 0 & -2
\end{array}\right]$$

$$D = \begin{bmatrix}
0 & 0 & 0 & 0 \\
0 & 0 & 0 & 0 \\
0 & 0 & 0 & 0 \\
0 & 0 & 0 & 0
\end{bmatrix}$$

References

[1] Fritz, R., 1970. "The effects of an annular fluid on the vibrations of a long rotor, part 1theory". *ASME J. Basic Eng,* **92**, pp. 923–929.

[2] Black, H., 1969. "Effects of hydraulic forces in annular pressure seals on the vibrations of centrifugal pump rotors". *Journal of Mechanical Engineering Science,* **11**(2), pp. 206–213.

[3] Black, H., and Jenssen, D., 1970. "Dynamic hybrid properties of annular pressure seals". *Proc. J. Mech. Eng,* **184**, pp. 92–100.

[4] Childs, D. W., and Dressman, J. B., 1982. "Testing of turbulent seals for rotordynamic coefficients". In Proc. Workshop on Rotordynamic Instability Problems in High-Performance Turbomachinery, NASA Conf. Publ. 2250, pp. 157–171.

[5] Nordmann, R., and Massmann, H., 1984. "Identification of dynamic coefficients of annular turbulent seals". pp. 295–311.

[6] Baskharone, E., and Hensel, S., 1993. "Flow field in the secondary, seal-containing passages of centrifugal pumps". *ASME J. Fluids Eng.,* **115**, pp. 702–702.

[7] Schettel, J., and Nordmann, R., 2004. "Rotordynamics of turbine labyrinth seals-a comparison of cfd models to experiments". *IMechE paper C,* **623**, pp. 13–22.

[8] Ishii, E., Chisachi, K., Kikuchi, K., and Ueyama, Y., 1997. "Prediction of rotordynamic forces in a labyrinth seal based on three-dimensional turbulent flow computation". *JSME International Journal Series C Mechanical Systems, Machine Elements and Manufacturing,* **40**(4), pp. 743–748.

[9] Hensel, S., and Guidry, M., 1992. "Labyrinth seal rotordynamic forces using a three-dimensional navier-stokes code". *Journal of tribology,* **114**, p. 683.

[10] Hirs, G., 1973. "A bulk-flow theory for turbulence in lubricant films". *ASME J. Lubr. Technol*, pp. 137–146.

[11] Childs, D., 1989. "Fluid-structure interaction forces at pump-impeller-shroud surfaces for rotordynamic calculations". *ASME, Transactions, Journal of Vibration, Acoustics, Stress, and Reliability in Design,* **111**, pp. 216–225.

[12] Nielsen, K. K., Jønck, K., and Underbakke, H., 2012. "Hole-pattern and honeycomb seal rotordynamic forces: Validation of cfd-based prediction techniques". *Journal of Engineering for Gas Turbines and Power,* **134**(12), p. 122505.

[13] Childs, D., and San Andres, L., 1997. "Eccentricity effects on tiie rotordynamic coefficients of plain annular seals: Theory versus experiment". *Journal of Tribology,* **119**, p. 443.

[14] Hsu, Y., and Brennen, C., 2002. "Fluid flow equations for rotordynamic flows in seals and leakage paths". *Journal of fluids engineering,* **124**(1), pp. 176–181.

[15] Kirk, R., and Guo, Z., 2004. "Calibration of labyrinth seal bulk flow design analysis predictions to cfd simulation results". In Eighth International Conference on Vibrations in Rotating Machinery, pp. 3–12.

[16] Kocur, J. A., Nicholas, J. C., and Lee, C. C., 2007. "Surveying tilting pad journal bearing and gas labyrinth seal coefficients and their effect on rotor stability". In 36th Turbomachinery Symposium, Turbomachinery Laboratory, Texas A&M University, College Station, TX, September, pp. 10–13.

[17] San Andrés, L., 2012. "Rotordynamic force coefficients of bubbly mixture annular pressure seals". *Journal of Engineering for Gas Turbines and Power,* **134**(2), p. 022503.

[18] Zhou, K., Doyle, J. C., Glover, K., et al., 1996. *Robust and optimal control*, Vol. 40. Prentice hall New Jersey.

[19] ISO, S., 2004. "Mechanical vibration-vibration of rotating machinery equipped with active magnetic bearings-part 3: Evaluation of stability margin". *ISO 14839-3: 2006 (E)*.

[20] Cole, M. O., Keogh, P. S., Sahinkaya, M. N., and Burrows, C. R., 2004. "Towards fault-tolerant active control of rotor–magnetic bearing systems". *Control Engineering Practice,* **12**(4), pp. 491–501.

[21] Cole, M., Chamroon, C., and Keogh, P., 2016. "Hinfinity controller design for active magnetic bearings considering nonlinear vibrational rotordynamics". In Proceedings of ISMB15.

[22] Balas, G. J., and Young, P. M., 1995. "Control design for variations in structural natural frequencies". *Journal of Guidance, Control, and Dynamics,* **18**(2), pp. 325–332.

[23] Schonhoff, U., Luo, J., Li, G., Hilton, E., Nordmann, R., and Allaire, P., 2000. "Implementation results of mu-synthesis control for an energy storage flywheel test rig". In The Eight International Symposium on Magnetic Bearings (ISMB-8), Zurich, Switzerland.

[24] Balini, H., Witte, J., and Scherer, C. W., 2012. "Synthesis and implementation of gain-scheduling and lpv controllers for an amb system". *Automatica,* **48**(3), pp. 521–527.

[25] Mushi, S. E., Lin, Z., Allaire, P. E., and Evans, S., 2008. "Aerodynamic cross-coupling in a flexible rotor: Control design and implementation". In In proceeding of ISMB11.

[26] Wurmsdobler, P., 1997. *State space adaptive control for a rigid rotor suspended in active magnetic bearings*. na.

[27] Lang, O., Wassermann, J., and Springer, H., 1996. "Adaptive vibration control of a rigid rotor supported by active magnetic bearings". *Journal of engineering for gas turbines and power,* **118**(4), pp. 825–829.

[28] Hirschmanner, M., and Springer, H., 2002. *Adaptive vibration and unbalance control of a rotor supported by active magnetic bearings*. na.

[29] Lauridsen, J. S., and Santos, I. F., 2016. "Design of robust amb controllers for rotors subjected to varying and uncertain seal forces". *Accpeted for publishing in: Advances in Magnetic Bearing Technology*.

[30] Lauridsen, J. S., and Santos, I. F., 2017. "On-site identification of dynamic annular seal forces in turbo machinery using active magnetic bearings - an experimental investigation". *Submitted for publishing in Journal*

of Engineering for Gas Turbines and Power.

[31] Voigt, A. J., Mandrup-Poulsen, C., Nielsen, K. K., and Santos, I. F., 2017. "Design and calibration of a full scale active magnetic bearing based test facility for investigating rotordynamic properties of turbomachinery seals in multiphase flow". *Journal of Engineering for Gas Turbines and Power,* **139**(5), p. 052505.

[32] Voigt, A. J., 2016. *Towards Identification of Rotordynamic Properties for Seals in Multiphase Flow Using Active Magnetic Bearings. Design and Commissioning of a Novel Test Facility*. Technical University of Denmark.

[33] Bleuler, H., Cole, M., Keogh, P., Larsonneur, R., Maslen, E., Okada, Y., Schweitzer, G., Traxler, A., Schweitzer, G., Maslen, E. H., et al., 2009. *Magnetic bearings: theory, design, and application to rotating machinery*. Springer Science & Business Media.

[34] Childs, D. W., 1993. *Turbomachinery rotordynamics: phenomena, modeling, and analysis*. John Wiley & Sons.

[35] Nelson, H., 1980. "A finite rotating shaft element using timoshenko beam theory". *Journal of mechanical design,* **102**(4), pp. 793–803.

[36] Skogestad, S., and Postlethwaite, I., 2007. *Multivariable feedback control: analysis and design*, Vol. 2. Wiley New York.

[37] Voigt, A. J., Lauridsen, J. S., Poulsen, C. M., Nielsen, K. K., and Santos, I. F., 2016. "Identification of parameters in active magnetic bearing systems". In Proceedings of ISMB15.

Chapter 7

Conclusions and Future Aspects

A framework is presented for the design of model based controllers for AMB systems subjected to uncertain and changing dynamic seal forces. Based on the theoretical and experimental work carried out, the following can be concluded:

7.1 Identification of parameters in AMB systems

1. The paper [P2] aims at validating the performance of the identification scheme for identifying AMB parameters. The current-to-force parameter K_i is compared using the closed loop identification procedure and validated using a static loading procedure with calibrated force transducers. Good coherence between the results obtained by the two methods, allows us to conclude that the identifying method using LFT formulation and optimisation in time works well for identification of AMB parameters.

2. The paper [P4] demonstrates the use of the identification scheme for identifying dynamic seal forces. Using a stepped sine excitation current it is demonstrated that the dynamic seal coefficients can be extracted as a function of the excitation frequency. The identified seal coefficients of the tested gas (air) seal show practically no excitation frequency dependence. This fits well with previous results found using Bulkflow modelling of annular gas seals shown by San Andrés 2012.

3. Since the test seal characteristics shows practically no excitation frequency dependence, it is not necessary to use the time consuming stepped sine excitation procedure. Instead, it is found in [P5] that an impulse response can be used as an excitation signal, for identifying the dynamic seal coefficients. Using the identified models in model based control design results a system with well controlled performance.

4. The most significant seal parameter of the test gas seal is the cross-coupled stiffness which is highly dependent on the pressure across the seal [P4-P5].

5. The identification procedure presented in [P1-P2] has shown to work well not only for the cases mentioned above, i.e. items 1. to 4., but also for identification of parameters in a flexibly-mounted internal-stator magnetic bearings system,

as shown independently by Lusty 2016. Here multiple parameters were identified such as magnetic bearing negative stiffness, magnetic bearing current gain, damping of rotor, damping of secondary shafts, lateral stiffness of rolling element bearings among others. The identified model is shown to mimic the real system behaviour well. Additionally the identified model has been used in model based control design to synthesise a $\mathscr{H}_\infty$ controller, which can deliver substantial vibration reduction performance, compared to a tuned PD controller.

7.2 Model based controller design for compensation of seal forces

1. A designed $\mathscr{H}_\infty$ controller shows significant performance improvements over a decentralised PID controller, when the rotor-bearing-seal system operates close to the design pressure condition [P5].

2. Using the perturbed plant formulation and μ synthesis to design robust controllers, it is shown in [P5] to be possible to optimise and improve the worst case performance over a larger pressure range. The synthesised μ controller is able to handle pressure variations significantly better than the $\mathscr{H}_\infty$ controller. It is shown that the μ controller synthesis generates a non-conservative controller which guarantees robust performance and simultaneously keeps the controller gains moderate.

3. Increasing the controller gain to obtain larger values of direct stiffness and damping would, for the tested system, immediately increase robustness and stability followed by significant improvement in system performance.

4. In the case of significant frequency dependence of the dynamic seal forces, as for the hole pattern seal considered in [P3], combined with large variations in operational speed, it is more challenging to design a single robust LTI controller that provides satisfactory performance over the complete operational range. [P3] demonstrates the performance improvement which an LPV controller can deliver, compared to a single robust LTI controller, using the nominal plant model.

7.3 State of the art

The thesis aims to advance the state-of-the-art within the design of AMB controllers for rotors subjected to seal forces. The work might be beneficial for the optimisation of controllers on-site, i.e.

- Identifying dynamic seal coefficients on-site to obtain a precise mathematical model of the system and to access the changes in seal model parameters due to changes in operational conditions.

- Predicting stability and performance of the global system.

- Synthesizing model based controllers to guarantee robust stability and performance of rotordynamic systems when dealing with uncertain and changing seal forces.

The procedure might also be useable in the phase of designing new machines, for example, to reduce conservativeness when dimensioning the size and force capacity of AMBs. Here the control synthesis can be used to find the minimum control action required to guarantee robust performance.

7.4 Further aspects

1. The experimental tests were carried out on a test facility which needs a couple of modifications. Low slew rate of the amplifiers for larger amplitudes of current, and large runouts due to suboptimal sensor target material for the displacement sensors, resulted in a restricted operation envelope of the test-facility. Hence, amplifiers that are more suitable and a new shaft with better target material for the displacements sensors will results in the possibility for high speed operation and possibility applying higher pressure. This would allow for testing in realistic operational conditions, similar to those prevailing in industrial turbomachinery applications.

2. The dynamic seal forces have a known model structure and the coefficients typically are slow changing dependent on, for instance, speed and pressure. It could be interesting to investigate the performance and stability properties of using adaptive control techniques for handling uncertain and changing dynamic seal forces.

References

Aenis, M. and R. Nordmann (2002). 'Fault diagnosis in rotating machinery using active magnetic bearings'. *8th International Symposium on Magnetic Bearing*, p. 125.

Balas, G. J. and P. M. Young (1995). 'Control design for variations in structural natural frequencies'. *Journal of Guidance, Control, and Dynamics* **18**(2), pp. 325–332.

Balini, H., I. Houtzager, J. Witte and C. W. Scherer (2010). 'Subspace identification and robust control of an AMB system'. *American Control Conference (ACC), 2010*. IEEE, pp. 2200–2205.

Balini, H., J. Witte and C. W. Scherer (2012). 'Synthesis and implementation of gain-scheduling and LPV controllers for an AMB system'. *Automatica* **48**(3), pp. 521–527.

Baskharone, E. and S. Hensel (1993). 'Flow field in the secondary, seal-containing passages of centrifugal pumps'. *ASME J. Fluids Eng.* **115**, pp. 702–702.

Black, H. (1969). 'Effects of hydraulic forces in annular pressure seals on the vibrations of centrifugal pump rotors'. *Journal of Mechanical Engineering Science* **11**(2), pp. 206–213.

Black, H. and D. Jenssen (1970). 'Dynamic hybrid properties of annular pressure seals'. *Proc. J. Mech. Eng* **184**, pp. 92–100.

Brown, P. D. and D. W. Childs (2012). 'Measurement Versus Predictions of Rotordynamic Coefficients of a Hole-Pattern Gas Seal With Negative Preswirl'. *Journal of Engineering for Gas Turbines and Power* **134**(12), p. 122503.

Childs, D. W. and J. B. Dressman (1982). 'Testing of turbulent seals for rotordynamic coefficients'. *Proc. Workshop on Rotordynamic Instability Problems in High-Performance Turbomachinery, NASA Conf. Publ. 2250*, pp. 157–171.

Childs, D. (1989). 'Fluid-structure interaction forces at pump-impeller-shroud surfaces for rotordynamic calculations'. *ASME, Transactions, Journal of Vibration, Acoustics, Stress, and Reliability in Design* **111**, pp. 216–225.

Childs, D. and L. San Andres (1997). 'Eccentricity Effects on tiie Rotordynamic Coefficients of Plain Annular Seals: Theory Versus Experiment'. *Journal of Tribology* **119**, p. 443.

Cole, M., C. Chamroon and P. Keogh (2016). 'Hinfinity controller design for active magnetic bearings considering nonlinear vibrational rotordynamics'. *Proceedings of ISMB15*.

Cole, M. O., P. S. Keogh, M. N. Sahinkaya and C. R. Burrows (2004). 'Towards fault-tolerant active control of rotor–magnetic bearing systems'. *Control Engineering Practice* **12**(4), pp. 491–501.

Elrod, D., C. Nicks, D. Childs and C. Nelson (1985). 'A Comparison of Experimental and Theoretical Results for Rotordynamic Coefficients of Four Annular Gas Seals'.

Progress Report NASA contract NAS8-33716 Texas A&M University, Turbomachinery Laboratories, Mechanical Engineering Department College Station, Texas **77843**.

Ertas, B. H., A. Delgado and G. Vannini (2012). 'Rotordynamic force coefficients for three types of annular gas seals with inlet preswirl and high differential pressure ratio'. *Journal of Engineering for Gas Turbines and Power* **134**(4), p. 042503.

Fritz, R. (1970). 'The effects of an annular fluid on the vibrations of a long rotor, part 1—theory'. *ASME J. Basic Eng* **92**, pp. 923–929.

Gahler, C., M. Mohler and R. Herzog (1997). 'Multivariable identification of active magnetic bearing systems'. *JSME International Journal Series C Mechanical Systems, Machine Elements and Manufacturing* **40**(4), pp. 584–592.

Hensel, S. and M. Guidry (1992). 'Labyrinth seal rotordynamic forces using a three-dimensional Navier-Stokes code'. *Journal of tribology* **114**, p. 683.

Hirs, G. (1973). 'A bulk-flow theory for turbulence in lubricant films'. *ASME J. Lubr. Technol*, pp. 137–146.

Hirschmanner, M. and H. Springer (2002). *Adaptive vibration and unbalance control of a rotor supported by active magnetic bearings*. na.

Hsu, Y. and C. Brennen (2002). 'Fluid flow equations for rotordynamic flows in seals and leakage paths'. *Journal of fluids engineering* **124**(1), pp. 176–181.

Ishii, E., K. Chisachi, K. Kikuchi and Y. Ueyama (1997). 'Prediction of rotordynamic forces in a labyrinth seal based on three-dimensional turbulent flow computation'. *JSME International Journal Series C Mechanical Systems, Machine Elements and Manufacturing* **40**(4), pp. 743–748.

ISO, S. (2004). 'Mechanical vibration-Vibration of rotating machinery equipped with active magnetic bearings-part 3: Evaluation of stability margin'. *ISO 14839-3: 2006 (E)*.

Kirk, R. and Z. Guo (2004). 'Calibration of labyrinth seal bulk flow design analysis predictions to CFD simulation results'. *Eighth International Conference on Vibrations in Rotating Machinery*, pp. 3–12.

Knopf, E. and R. Nordmann (1998). 'Active magnetic bearings for the identification of dynamic characteristics of fluid bearings'. *Proceedings 6th International Symposium on Magnetic Bearings, Cambridge, MA, August*, pp. 5–7.

Kocur, J. A., J. C. Nicholas and C. C. Lee (2007). 'Surveying tilting pad journal bearing and gas labyrinth seal coefficients and their effect on rotor stability'. *36th Turbomachinery Symposium, Turbomachinery Laboratory, Texas A&M University, College Station, TX, September*, pp. 10–13.

Lang, O., J. Wassermann and H. Springer (1996). 'Adaptive vibration control of a rigid rotor supported by active magnetic bearings'. *Journal of engineering for gas turbines and power* **118**(4), pp. 825–829.

Lauridsen, J. S. and I. F. Santos (2017a). 'Design of Robust Active Magnetic Bearing Controllers for Rotors Subjected to Seal Forces'. *ASME Journal of Dynamic Systems, Measurement, and Control (accepted)*. (Publication P5, Chap. 6 at page 57).

Lauridsen, J. S. and I. F. Santos (2017b). 'Design of Robust AMB Controllers for Rotors Subjected to Varying and Uncertain Seal Forces'. *JSME Advances in Magnetic Bearing Technology (accepted)*. (Publication P3, Chap. 4 at page 31).

Lauridsen, J. S. and I. F. Santos (2017c). 'On-site Identification of Dynamic Annular Seal Forces in Turbo Machinery Using Active Magnetic Bearings - An Experimental Investigation'. *ASME Journal of Engineering for Gas Turbines and Power (submitted)*. (Publication P4, Chap. 5 at page 45).

Lauridsen, J. S., A. K. Sekunda, I. F. Santos and H. Niemann (2015). 'Identifying parameters in active magnetic bearing system using LFT formulation and Youla factorization'. *2015 IEEE Conference on Control Applications (CCA)*. IEEE, pp. 430–435. (Publication P1, Chap. 2 at page 13).

Li, G., Z. Lin, P. E. Allaire and J. Luo (2006). 'Modeling of a high speed rotor test rig with active magnetic bearings'. *Journal of Vibration and Acoustics* **128**(3), pp. 269–281.

Ljung, L. (1999). *System identification*. Wiley Online Library.

Lusty, C. (2016). 'Rotor Vibration Reduction and Control via Flexibly-Mounted Internal-Stator Magnetic Bearings'. Doctoral dissertation. University of Bath: University of Bath.

Matros, M. and R. Nordmann (1997). 'Dynamic characteristics of a hydrostatic bearing identified by active magnetic bearings'. *Kaiserslautern Univ, Rotordynamic Instability Problems in High- Performance Turbomachinery 1996 p 23-28(SEE N 97-24525 01-37)*.

Mushi, S. E., Z. Lin, P. E. Allaire and S. Evans (2008). 'Aerodynamic cross-coupling in a flexible rotor: Control design and implementation'. *Proceedings of the 1 hh International Symposium on Magnetic Bearings. Nara, Japan*.

Nielsen, K. K., K. Jønck and H. Underbakke (2012). 'Hole-Pattern and Honeycomb Seal Rotordynamic Forces: Validation of CFD-Based Prediction Techniques'. *Journal of Engineering for Gas Turbines and Power* **134**(12), p. 122505.

Nordmann, R. and M. Aenis (2004). 'Fault diagnosis in a centrifugal pump using active magnetic bearings'. *International Journal of Rotating Machinery* **10**(3), pp. 183–191.

Nordmann, R. and H. Massmann (1984). 'Identification of dynamic coefficients of annular turbulent seals', pp. 295–311.

San Andrés, L. (2012). 'Rotordynamic Force Coefficients of Bubbly Mixture Annular Pressure Seals'. *Journal of Engineering for Gas Turbines and Power* **134**(2), p. 022503.

Schettel, J. and R. Nordmann (2004). 'Rotordynamics of turbine labyrinth seals-a comparison of CFD models to experiments'. *IMechE paper C* **623**, pp. 13–22.

Schonhoff, U., J. Luo, G. Li, E. Hilton, R. Nordmann and P. Allaire (2000). 'Implementation results of mu-synthesis control for an energy storage flywheel test rig'. *The Eight International Symposium on Magnetic Bearings (ISMB-8), Zurich, Switzerland*.

Schweitzer, G., H. Bleuler, E. H. Maslen, M. Cole, P. Keogh, R. Larsonneur, E. Maslen, Y. Okada, G. Schweitzer, A. Traxler et al. (2009). *Magnetic bearings: theory, design, and application to rotating machinery*. Springer.

Söderström, T. and P. Stoica (1988). *System identification*. Prentice-Hall, Inc.

Vázquez, J. A., E. H. Maslen, H.-J. Ahn and D.-C. Han (2001). 'Model identification of a rotor with magnetic bearings'. *ASME Turbo Expo 2001: Power for Land, Sea, and Air*. American Society of Mechanical Engineers, V004T03A059–V004T03A059.

Voigt, A. J., J. S. Lauridsen, C. M. Poulsen, K. K. Nielsen and I. F. Santos (2016). 'Identification of Parameters in Active Magnetic Bearing Systems'. *Proceedings of ISMB15*. (Publication P2, Chap. 3 at page 21).

Voigt, A. J. (2016). *Towards Identification of Rotordynamic Properties for Seals in Multiphase Flow Using Active Magnetic Bearings. Design and Commissioning of a Novel Test Facility*. Technical University of Denmark.

Wagner, N. G., K. Steff, R. Gausmann and M. Schmidt (2009). 'Investigations on the dynamic coefficients of impeller eye labyrinth seals'. *Proceedings of the Thirty-Eighth Turbomachinery Symposium, Houston, TX, September*, pp. 14–17.

Wagner, N. and K. Steff (1997). 'Dynamic labyrinth coefficients from a high-pressure full-scale test rig using magnetic bearings'. *Demag A. G, Rotordynamic Instability Problems in High-Performance Turbomachinery 1996 p 95-111(SEE N 97-24525 01-37)*.

Wurmsdobler, P. (1997). *State space adaptive control for a rigid rotor suspended in active magnetic bearings*. na.

Zhou, K., J. C. Doyle, K. Glover et al. (1996). *Robust and optimal control*. Vol. 40. Prentice hall New Jersey.

Zutavern, Z. S. and D. W. Childs (2008). 'Identification of rotordynamic forces in a flexible rotor system using magnetic bearings'. *Journal of Engineering for Gas Turbines and Power* **130**(2), p. 022504.

Technical University of Denmark
Department of Mechanical Engineering
Section of Solid Mechanics
Nils Koppels Allé, Building 404
DK-2800 Kgs. Lyngby
Denmark
Phone: (+45) 45 25 25 25
Email: info@mek.dtu.dk
www.mek.dtu.dk

ISBN: 87–7475–490–4 978–87–7475–490–9